



**MULTISCALE HYDRO-ENVIRONMENTAL MODELLING OF MARINE
RENEWABLE ENERGY DEVICES, WITH PARTICULAR APPLICATION TO THE
SEVERN BARRAGE**

A thesis submitted to Cardiff University

in candidature for the degree of

Doctor of Philosophy

by

Samuel Bray

Hydro-environmental Research Centre

School of Engineering

Cardiff University

2017

Abstract

This research study presents enhancements to the hydro-environmental model Environmental Fluid Dynamics Code (EFDC), improving the predictive capabilities of the impacts of tidal range renewable proposals and dissolved phosphate concentrations in estuaries.

Refinements to the representation of turbines and sluice gates, including updates to the discharge relationships used and momentum conservation were applied to the Severn Tidal Power Group's Cardiff-Weston Barrage, providing an accurate assessment of the barrage's potential impacts and highlighting the importance of correct hydraulic structure representation. The Severn Barrage was found to have minor impacts on peak water levels as far-field as the west coast of Scotland. The refinements reduced predicted peak water levels by up to 1 m upstream of the barrage.

The applicability of the updated model in assisting with the design and optimisation of tidal lagoons was then tested by running a suite of different configurations of the Bridgwater Bay Lagoon, varying the turbine numbers from 60 to 360. It was demonstrated that additional turbines can negatively impact energy output, by reducing average generating time and generating over a lower head difference.

Previous laboratory and field studies demonstrated a link between salinity and phosphate sorption to sediments due to the competition for sorption sites between seawater anions and phosphate. Since sediment-associated

nutrients are not readily available for biological uptake, the dissolved proportion of phosphate is of particular importance when trying to predict the growth of phytoplankton and the potential for eutrophication.

The salinity-linked sorption relationship was incorporated into the EFDC model to improve the prediction for dissolved phosphate across the estuary by taking into account the salinity variation.

The refinement to the numerical calculation for the phosphate partition coefficient in the model caused a measurable change to the predicted dissolved phosphate levels, bringing them closer to measured data from the estuary.

Dedication

In loving memory of my grandmother and great-aunt, Granny and Betty, who sadly passed away over the course of this research study. Thank you for your encouragement and enthusiasm.

Acknowledgements

I would like to thank my supervisors, Dr Reza Ahmadian and Professor Roger Falconer for their guidance, patience and support throughout my PhD. I could not have completed this thesis without their technical expertise and experience.

Many thanks to Professors Shunqi Pan and Michael Hartnett for taking the time to examine the thesis and attend the viva. The changes and corrections that you suggested have greatly improved the work.

This research project was funded by Fujitsu and High-Performance Computing (HPC) Wales, whose contribution is gratefully acknowledged.

My thanks to Mudi and Amo, and to the 'Coffee Support Group' for keeping me sane at stressful moments!

Finally, I would like to express my gratitude to my family for all their support over the course of the PhD, and to Ella for getting me over the line.

Table of Contents

Abstract	i
Declaration.....	iii
Dedication.....	iv
Acknowledgements	v
Table of Contents	vi
List of Figures	xi
List of Tables	xvi
List of publications	xvii
1. Introduction	1
1.1 Background	2
1.2 Research objectives	5
1.3 Outline of thesis	5
2. Literature review	7
2.1 Introduction.....	8
2.2 Renewable energy	8
2.2.1 Drivers	8
2.2.2 Marine generation.....	9
2.2.3 Tidal range generation methods	13
2.2.4 Current schemes	15

2.2.5	Tidal lagoons.....	20
2.2.6	The Severn Barrage	23
2.3	Tide generation in the UK	25
2.3.1	Mechanisms resulting in exceptional tidal regime	26
2.3.2	Tidal stream resource	27
2.3.3	Tidal range resource.....	29
2.4	Extended domain modelling - Continental Shelf Model	30
2.5	Hydraulic structure representation in tidal range generating proposals	34
2.5.1	Internal boundary.....	34
2.5.2	Turbines	35
2.5.3	Sluices	38
2.5.4	Discharge coefficient.....	38
2.5.5	Discharge and momentum	39
2.5.6	Scheme optimisation	40
2.6	Eutrophication in estuaries and role of sediment.....	40
2.6.1	Phosphorus and the nutrient cycle	43
2.6.2	Phosphate partition coefficient.....	44
2.7	Chapter summary	46
3.	Governing equations.....	49
3.1	Introduction.....	50

3.1	Mass and momentum	50
3.1.1	Solute transport.....	52
3.2	Turbulence closure	53
3.3	Suspended sediment.....	55
3.3.1	Cohesive sediment	56
3.3.2	Adsorption and phosphate partition coefficient.....	56
3.4	Chapter summary	59
4.	Numerical model details.....	60
4.1	Introduction.....	61
4.2	Implementation of governing equations.....	61
4.3	EFDC	65
4.3.1	EFDC models	69
4.4	Refinement to hydraulic structure representation	74
4.4.1	Turbines and sluice operation.....	74
4.4.2	Momentum correction	76
4.5	Refinement to phosphate modelling	77
4.5.1	Salinity and phosphate	77
4.5.2	Sediment parameters.....	80
4.5.3	Implementation of updated partition coefficient.....	81
4.6	Use of High Performance Computing.....	82
4.7	Chapter summary	84

5. Model application 1 - Severn Barrage.....	86
5.1 Introduction.....	87
5.2 Impact of representation of turbines and sluices and far-field impacts of the Severn Barrage	87
5.2.1 Analysis.....	94
5.3 Sensitivity to discharge coefficient	97
5.3.1 Mitigation through increased sluice capacity	100
5.3.2 Analysis.....	101
5.4 Momentum representation in hydraulic structures	103
5.5 2D vs 3D barrage modelling	108
5.6 Chapter summary	109
6. Model application 2 - Bridgwater Bay Lagoon	111
6.1 Introduction.....	112
6.2 Refined mesh and model setup	113
6.3 Outputs and analysis	116
6.4 Chapter summary	121
7. Model application 3 - water quality modelling.....	123
7.1 Introduction.....	124
7.2 Salinity	124
7.3 Suspended sediment.....	126
7.4 Total phosphate	127

7.5	Dissolved and adsorbed phosphate	130
7.6	Chapter summary	135
8.	Conclusions and future work	138
8.1	Conclusions and limitations	139
8.1.1	Hydraulic structure representation and barrage impact assessment	140
8.1.2	2D models in lagoon scheme optimisation	142
8.1.3	Water quality modelling	144
8.2	Recommendations for future work	146
9.	References	150

List of Figures

Figure 2-1 - Technology Readiness Levels (reproduced from Southeast National Marine Renewable Energy Centre, 2017)	11
Figure 2-2 - Barrage operating modes (Xia <i>et al.</i> , 2010b)	15
Figure 2-3 - La Rance Barrage (public domain photograph)	16
Figure 2-4 - Lake Sihwa Tidal Power Plant (Electric-Power, 2015).....	18
Figure 2-5 - Annapolis Power Plant (CAA, 2017)	19
Figure 2-6- Kislaya Guba Power Plant (public domain image).....	20
Figure 2-7 - Swansea Bay tidal lagoon, location and key facts (public domain image)	21
Figure 2-8 - DECC shortlisted schemes for Severn Estuary tidal power	22
Figure 2-9 - Configuration of STPG Barrage (STPG, 1989)	24
Figure 2-10 - Amphidromic points (credit Dr R Ray, NASA - Goddard Space Flight Center)	26
Figure 2-11 - UK Tidal Stream Resource (credit DTI)	28
Figure 2-12- Maximum tidal range (credit SMARTtide)	30
Figure 2-13 - Computational domains used to test open boundary location effect (Zhou, Pan and Falconer, 2014a).....	32
Figure 2-14 - Impact of Severn Barrage on maximum water levels (Zhou, Pan and Falconer, 2014a)	33
Figure 2-15- Relationship between the water head, discharge and power output (STPG, 1989).....	36
Figure 2-16 - Discharge through a turbine as calculated from the hill chart and from the orifice equation	37

Figure 2-17 Fishkills linked to HABs, as of 2006, reproduced from Woods Hole Oceanographic Institution, 2008.....	41
Figure 2-18 - The phosphorus cycle, reproduced from Project Waterman, Hong Kong University, 2010	43
Figure 4-1 - EFDC modules (DSI, 2013).....	66
Figure 4-2 - Hydrodynamic modules (DSI, 2013)	66
Figure 4-3 - Vertical sigma coordinate system in EFDC (Craig, 2017)	67
Figure 4-4 - RGFGGrid screenshot - Severn Estuary grid creation.....	68
Figure 4-5 - Computational domain of the CSM, with black dots showing example validation sites and dotted lines to indicate open boundaries...	70
Figure 4-6 - Comparisons between observed (blue dots) and calculated (red lines) tidal stream current speeds and directions	71
Figure 4-7 - SEM domain, showing bathymetry of the Severn Estuary and Bristol Channel	73
Figure 4-8 - Turbine half-sinusoidal ramp function	76
Figure 4-9 - Major industrial discharges (Severn Estuary Partnership, 2001)	78
Figure 4-10 - Major sewage discharges (Severn Estuary Partnership, 2001)	79
Figure 4-11 - Predicted suspended sediment concentration at Minehead, plotted against survey data	80
Figure 4-12 - Predicted suspended sediment concentration at Southerndown, plotted against survey data	81
Figure 5-1 - Barrage location and Points A and B, used to demonstrate effects of refinements	89

Figure 5-2 - Upstream (green) and downstream (blue) water levels for Scenario 1	89
Figure 5-3 - Upstream (green) and downstream (blue) water levels for Scenario 2	90
Figure 5-4 - Impact of hydraulic structure refinements on water levels at Point A	91
Figure 5-5 - Domain-wide maximum water level changes caused by barrage Scenario 1	92
Figure 5-6 - Domain-wide maximum water level changes caused by barrage Scenario 2	93
Figure 5-7 - Impact of hydraulic structure refinements on maximum water levels in the Severn Estuary and Bristol Channel	94
Figure 5-8 - Maximum water level changes caused by a 10% reduction in the C_d	99
Figure 5-9 - Maximum water level changes caused by a 5% reduction in the C_d value	99
Figure 5-10 - Power generated by the barrage when varying C_d over one day	100
Figure 5-11 - Power generated by the barrage when varying C_d and sluice capacity	101
Figure 5-12 - Velocity magnitudes at mid-generating phase, pre-momentum adjustment	104
Figure 5-13 - Velocity magnitudes at mid-generating phase, post-momentum adjustment	105

Figure 5-14 - Velocity magnitudes and vectors at mid-generating phase, pre-momentum adjustment	106
Figure 5-15 - Velocity magnitudes and vectors at mid-generating phase, post-momentum adjustment	106
Figure 5-16 - Velocity profile through the water column 100m increments downstream of a turbine cell	107
Figure 5-17 - Water levels upstream and downstream of the barrage, in 2D and 3D	108
Figure 5-18 - Power output comparison for 2D and 3D STPG ebb-generating barrage simulations.....	109
Figure 6-1 - EA Flood Map for Planning - Bridgwater (Environment Agency, 2017).....	112
Figure 6-2 - Bridgwater Bay Lagoon within the refined SEM.....	114
Figure 6-3 - Locations of turbines (in red) along the Bridgwater Bay Lagoon wall	114
Figure 6-4 - Bed elevation profile (green), minimum water depth (blue) and potential turbine housing locations (yellow) along the Bridgwater Bay Lagoon line	115
Figure 6-5 - Bridgwater Bay Lagoon operational phases	116
Figure 6-6 - Peak power output of the Bridgwaer Bay Lagoon when varying the turbine number.....	117
Figure 6-7- Annual energy output of Bridgwater Bay Lagoon when varying the turbine number.....	119
Figure 6-8 - Hours of generation per tidal cycle when varying the turbine number	120

Figure 6-9 - Tidal range within the Bridgwater Bay Lagoon when varying the turbine number	121
Figure 7-1 - Snapshot of predicted salinity in the Severn Estuary and Bristol Channel.....	125
Figure 7-2 - Timeseries of salinity in the estuary between Minehead and Cardiff Airport.....	125
Figure 7-3 - Cohesive sediment parameters	126
Figure 7-4 - Snapshot of suspended sediment concentrations in the Severn Estuary midway through the ebb tide	127
Figure 7-5 - Locations of sample sites with phosphate concentration data	128
Figure 7-6 - Snapshot of the SEM's total phosphate predictions during the simulation.....	129
Figure 7-7 - Salinity-linked partition coefficient through the SEM	131
Figure 7-8 - Domain-wide dissolved PO ₄ levels when using a constant K _d	133
Figure 7-9 - Domain-wide dissolved PO ₄ levels when using a variable K _d	133
Figure 7-10 - Comparison of dissolved PO ₄ ranges at each sample point when varying the prediction method	134

List of Tables

Table 4-1 - Coefficients of $K_d = AS^{-b}$ for the suspended sediment concentrations used in the study, reproduced from (Kadiri and Bockelmann-Evans, 2012)	82
Table 5-1 - Scenarios for hydraulic structure representation	88
Table 5-2 - Scenarios 3-7 detailing the discharge coefficient sensitivity scenario setups.....	97
Table 5-3 - Scenarios 8-12 detailing difference sluice areas to mitigate for discharge coefficient changes	98
Table 5-4 - Power generation comparison for Scenarios 3-7	102
Table 5-5 - Power generation comparison for Scenarios 8-12.....	103
Table 6-1 - Peak power achieved as a percentage of installed capacity .	118
Table 7-1 - Phosphate field data for the Severn Estuary	128
Table 7-2 - Maximum and minimum total phosphate levels encountered at the 9 sample points, compared with field data	130
Table 7-3 - Comparison of field and model predicted dissolved phosphate levels	132
Table 7-4 - Comparison of field and model predicted dissolved levels, moving from constant to dynamic K_d	134

List of publications

Journal articles

Bray, S., Ahmadian, R. and Falconer, R. A. (2016) 'Impact of representation of hydraulic structures in modelling a Severn barrage', *Computers and Geosciences*. Elsevier, 89, pp. 96-106. doi: 10.1016/j.cageo.2016.01.010.

Angeloudis, A., Falconer, R. A., Bray, S. and Ahmadian, R. (2016) 'Representation and operation of tidal energy impoundments in a coastal hydrodynamic model', *Renewable Energy*. Elsevier Ltd, 99, pp. 1103-1115. doi: <http://dx.doi.org/10.1016/j.renene.2016.08.004>.

Conference proceedings

Bray, S., Ahmadian, R. and Falconer, R. A. (2014) 'Refinements to turbine representation in modelling the Severn Barrage', in. 3rd European IAHR Congress. Available at: <http://webpages.fe.up.pt/iahr2014/>.

Bray, S., Ahmadian, R. and Falconer, R. A. (2015) 'Sensitivity study of modelling of Severn Barrage performance', *Renewable Energies Offshore*. CRC Press, p. 147.

Chapter 1

Introduction

1.1 Background

Faced with the challenges of a growing population, climate change, and a continued reliance on fossil fuels for energy, research into renewable energy has caused the sector to develop rapidly in recent years. Solar and wind energy generation are now commonplace, from large-scale wind and solar farms to home wind turbines and solar roof tiles. The technology is advancing very quickly, becoming more efficient and affordable year after year; a result of intense commercial and academic study since the 1990s.

Despite these improvements, there are still questions over the longevity and environmental impacts of these renewable methods of generation, for example solar panels typically lose around 1% of their production every year, and there is frequent objection to the noise and visual impact of wind turbines.

Renewable energy is contributing an increasing amount to the UK's energy mix, with 8.3% of energy consumption coming from renewable sources in 2015. A diversified renewable energy portfolio provides the best energy security for a country, protecting against disruptions and outages to any one sector.

Tidal renewable energy generation has the large advantage over wind and solar in that it is entirely predictable; the tides can be forecast with high accuracy a long way into the future and hence the energy extraction can too. We are fortunate in the UK to have an enormous tidal energy resource on our doorstep, but doubts over the economic viability and environmental impacts of proposals to date have left the resource underexploited.

Tidal energy extraction can be divided into two main categories: tidal stream generation, where the kinetic energy of tidal currents is extracted; and tidal range generation where the potential energy created by the rising and falling tides is captured. The UK's tidal stream resource is located mainly in waters near Anglesey, Pembrokeshire, the Severn Estuary, Pentland Firth and Northern Ireland. Tidal range resource is mostly concentrated in the Severn Estuary, which has the second largest tidal range in the world, and a funnel shape providing the potential to impound 500 km² of water with a 16 km long structure.

As a result of the suitability of the Severn Estuary for tidal range energy extraction, it has attracted much commercial, government and academic interest. The best known of the proposals for harnessing the tidal range in the Severn Estuary is the Severn Barrage. Several configurations have been proposed over the last few decades, at different locations and with different energy extraction methods.

A proposal from the Severn Tidal Power Group (1989) suggested an ebb-generating barrage from Cardiff to Weston. This is the configuration that has received the most study, and is referred to as The Severn Barrage. With an energy output of around 17 TWh per year, the Severn Barrage could supply around 5% of the UK's energy requirements.

More recently, there have been several proposals for tidal lagoons in the Severn Estuary. Tidal lagoons aim to take advantage of the huge tidal range while reducing some of the hydro-environmental concerns associated with the Severn Barrage. The Swansea Bay Tidal Lagoon is the most advanced of

the proposals, with a suggested capacity of 320 MW, powering around 150,000 Welsh homes.

Tidal renewable proposals such as the Severn Barrage and the Swansea Bay Tidal Lagoon cannot be granted development consent until all potential hydro-environmental impacts have been considered. Hydraulic models play a key part in the environmental impact assessments of tidal renewable energy schemes, and so the sophistication, accuracy and confidence in the hydraulic model is of paramount importance.

There are a huge range of environmental factors that must be taken into consideration in the design and potential approval of a large-scale tidal renewable energy plant. Hydraulic models can help with the assessment of a number of these, including impacts on: water levels; current velocities; suspended sediment; and water quality, as well as assisting in the optimisation of a proposal to maximise efficiency and energy output.

Accurate assessment of the potential impacts of a proposal is one of the first steps to ensuring the correct decision is made about whether to proceed. This research study aims to improve the hydro-environmental modelling of marine renewable energy devices through refinements to an existing model, removing uncertainty around impact assessment and increasing confidence by improving techniques and hydraulic structure and water quality representation.

1.2 Research objectives

The aim of improving the hydro-environmental modelling of marine renewable energy devices is divided into the following key objectives:

- assess current techniques and understanding of the numerical representation of tidal range renewable devices within hydraulic models;
- improve the representation of hydraulic structures such as turbines and sluices;
- assess the applicability of 2D hydraulic models in assisting with the design and optimisation of tidal lagoons; and
- improve the water quality modelling capabilities of the hydraulic model.

Achieving these objectives will provide new insight into the hydro-environmental modelling of tidal range proposals, ensuring accurate appraisal of their potential impacts.

1.3 Outline of thesis

The thesis is organised into a further seven chapters following this introduction:

Chapter 2: Literature review, which presents an overview of the literature relevant to this study, to identify the objectives set out above;

Chapter 3: Governing equations, which presents details of the governing equations which underpin hydraulic models;

Chapter 4: Numerical model details, which describes the numerical model EFDC in detail: the implementation of the governing equations; the models developed as part of this research study; and the refinements to the EFDC source code to improve hydro-environmental modelling;

Chapter 5: Severn Barrage, which uses the Severn Barrage as a case study to demonstrate the improvements made as part of this study to the representation of hydraulic structures in EFDC;

Chapter 6: Bridgwater Bay Lagoon, which uses the Bridgwater Bay Lagoon as a case study to demonstrate the role of 2D hydraulic models in the design and optimisation of tidal lagoon proposals;

Chapter 7: Water quality modelling, which uses the Severn Estuary as a case study to demonstrate improvements to the prediction of dissolved phosphate concentrations; and

Chapter 8: Conclusions and future work, which presents the main findings of this research study and provides suggestions for future research building on the thesis conclusions.

Chapter 2

Literature review

2.1 Introduction

This chapter presents an overview of the currently available literature relevant to this thesis. Research on renewable energy, tide generation, hydraulic modelling and water quality is reviewed to determine the key uncertainties in tidal renewable energy modelling.

2.2 Renewable energy

This section reviews the currently available literature on the drivers behind marine renewable energy generation, the method for tidal range generation and the schemes currently in operation. Tidal lagoons and The Severn Barrage are discussed to provide a background for the proposals modelled as part of this research study.

2.2.1 Drivers

Enthusiasm for renewable energy has continued to grow in recent years in the UK, driven by several factors. An increasingly informed, environmentally-conscious general public, along with a continued reliance on ever more expensive and depleting fossil fuels has caused a change in mindset at demand level, while government schemes such as the Low Carbon Innovation Co-ordination Group (LCICG) aim to tackle supply issues (DECC, 2012). The Government's aims include making sure that the UK has a secure supply, reducing greenhouse gas emissions to slow down climate change, and to stimulate investment in new jobs and businesses. Alongside this the UK has EU-set targets to deliver 15% of its energy consumption from renewable sources by 2020, and an 80% decrease in carbon emissions by 2050, compared with levels in 1990 (DECC, 2011). February 2003 saw the

publication of a UK Government White Paper, setting out a plan for a different and green UK energy mix that would deliver 60% cuts in carbon dioxide emissions by 2050 and 10% of electricity coming from renewables by 2010 (DTI, 2003). Amid concerns about the feasibility of the policy the Government extended the target year to 2015 (Mitchell and Connor, 2004), and indeed this did enable the electricity generation from renewables target to be met with 19.1% in 2014 (DECC, 2015a). For the energy targets to be met, however, there will need to be a significant increase in capacity in the next few years, and one area with enormous scope for increased capacity is tidal power, with hydro and wave/tidal electricity generation accounting for just 3.7% of renewable generation in 2014 (DECC, 2015b).

2.2.2 Marine generation

Energy can be extracted from the marine environment from either the tides or from waves. Tidal energy, in particular, has the important advantage of predictability over other renewable energy sources; discounting surges and other meteorological effects, tide times and levels can be predicted long into the future, and hence the energy generating potential can also be accurately assessed. Generating energy from the tides requires harnessing either the potential energy of rising and falling tides, or the kinetic energy from tidal currents (Rourke *et al.*, 2010).

Marine sources globally produced approximately 530 MW of electricity in 2015, a figure expected to increase in the coming years with technological advancements (Renewable Energy Policy Network for the 21st Century (REN21), 2016). The global marine resource is difficult to accurately

establish (Demirbaş, 2006); however, there is significant wave and tidal power resource available in the UK; with wave capacity estimated at 27 GW and tidal at approximately 90 GW (The Crown Estate, 2012), accounting for as much as 50% of the total available resource in Europe (Hammons, 2008).

Wave and tidal generating technology is considered to be behind other renewables such as wind and solar (Mueller and Wallace, 2008), beginning now to move from innovation and development into pre-commercial phases. It is thought that intellectual property issues in research and development have hindered progress in the past, but significant progress is now being made with wave and tidal stream technology, and the UK is considered amongst the world leaders in the technological development (Foxon *et al.*, 2005). Initial research focused on the proven tidal range generating schemes; however, in more recent years, development attempts have been equally directed towards tidal stream generation (Bryden and Couch, 2006; Khan *et al.*, 2009). Figure 2-1 below shows a scale for the readiness of a technology, adopted by the U.S. Department of Energy to assess the maturity of energy generating innovations.

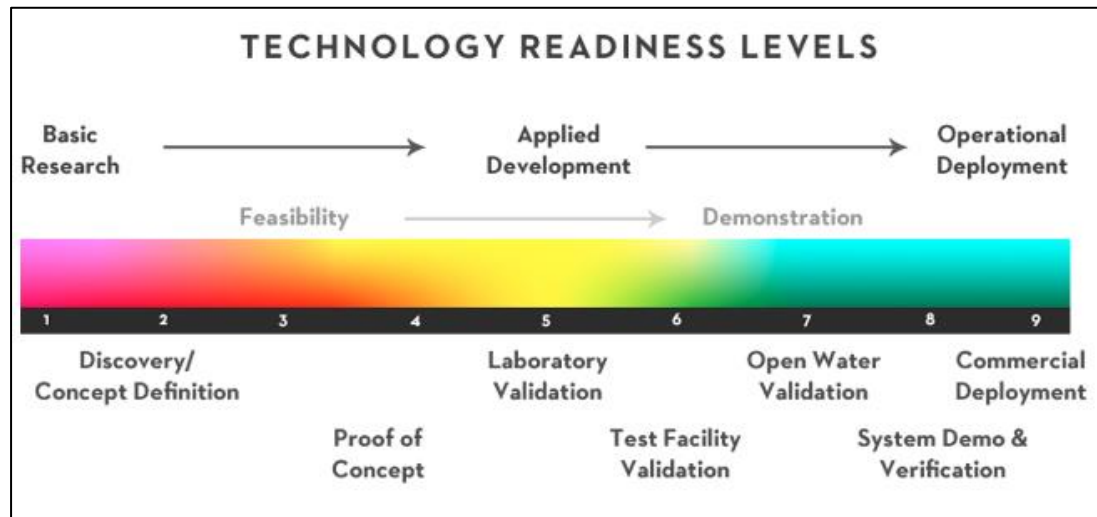


Figure 2-1 - Technology Readiness Levels (reproduced from Southeast National Marine Renewable Energy Centre, 2017)

The key scientific advances required to bring marine renewable energy generation to a technological level that it can be a viable component in the renewable energy mix include “resource assessment and predictability, engineering design and manufacturability, installation, operation and maintenance, survivability, reliability and cost reduction” (Mueller and Wallace, 2008). Having started later, research and development in marine generating technology has gained ground on other renewable sectors.

To ensure continued investment into development, it must be demonstrated that there are sufficient viable locations for marine generation. For tidal stream generation where the energy is generated from the velocity head, the maximum potential power (P) in a free stream is defined by Equation 2.1:

$$P = \frac{1}{2} \rho A V^3 \quad 2.1$$

where ρ is the fluid density, A is the turbine area, and V the free stream velocity of the current. Being proportional to the cube of the velocity, the power and hence energy capture is very sensitive to velocity (Fraenkel, 2002). Once areas with high tidal stream velocities have been identified, more sophisticated modelling can be applied to accurately assess the energy yield from various array configurations (Walkington and Burrows, 2009; Ahmadian and Falconer, 2012; Fairley *et al.*, 2013).

For tidal range generation, where the energy is generated from the potential head, the maximum potential power is directly proportional to the difference in water levels either side of an impoundment (h), as given by Equation 2.2:

$$P = \rho g Q h \quad 2.2$$

where g and Q have their usual meaning, i.e. gravity and discharge in cumecs respectively. Energy yield is proportional to the plan surface area impounded, and the square of the water level difference, shown in Equation 2.3:

$$E \propto A_p h^2 \quad 2.3$$

where E is Energy, and A_p is the plan area impounded. The equation demonstrates that for high energy yield, a large surface area with a high tidal range must be enclosed. Similarly to tidal stream resource, sites identified as having potential for tidal range generation can then be hydrodynamically modelled to investigate yield, explore optimisation

options and assess potential environmental impacts (Xia *et al.*, 2012; Ahmadian *et al.*, 2014; Zhou, *et al.*, 2014b; Angeloudis *et al.*, 2016).

There are inevitable environmental implications of any energy generating development, marine or otherwise, and it is vital that these are as accurately established as possible to give each proposal the best possible chance of acquiring development consent order and minimising any adverse effects. The high-priority areas of concern for tidal stream generation are broadly the interaction with marine mammals and fish, and the effects on physical systems as a result of removing energy from the water column (Copping *et al.*, 2014). Tidal stream renewable technology can now be considered at the commercial scale, led by Atlantis Resources' 6MW MeyGen Phase 1A in Pentland Firth, Scotland (Atlantis Resources, 2017). For tidal range generation, the same environmental associations apply, along with others that are associated with introducing an impoundment, specifically loss of intertidal habitat areas, siltation, changes to water quality and effects of construction (Wolf *et al.*, 2009; Rourke *et al.*, 2010; Frid *et al.*, 2012; Kadiri *et al.*, 2012, 2014). There are examples of tidal barrages in operation, in Sihwa, Korea (Bae *et al.*, 2010; Choi *et al.*, 2010), and the La Rance barrage in Brittany (Retiere, 1994; Kirby and Retiere, 2009; Rourke *et al.*, 2010).

2.2.3 Tidal range generation methods

Electricity can be generated from the incoming tide, the outgoing tide, or both (Baker, 1991). Ebb generation includes the four stages of filling, holding, generating and then holding, as shown in Figure 2-2a. Here, the

basin upstream of a barrage or lagoon is filled through sluices until high tide, at which point the sluice gates are closed, holding the water at high tide level while the sea level falls on the downstream side. When sufficient head is created for electricity generation, the turbines are opened and generate power until the minimum head for generation is reached. When the downstream water level begins to rise again with the tide, the sluice gates are opened once again and the basin re-fills. This has the effect of raising the minimum water level in the basin.

Flood generation is achieved in the reverse fashion, by generating power when the upstream basin fills from the sea, as per Figure 2-2b. The maximum water level in the basin is significantly reduced.

Two-way generation requires further stages, shown in Figure 2-2c. Ebb generation begins the cycle, starting from a lower head difference than in ebb-only generation. Once the minimum head for generation is reached, turbines or sluices continue to empty the basin, enabling it to reach the lowest water level possible. At this point, turbines and sluices are closed, until the tide has risen on the seaward side of the barrage to a sufficient height to enable flood direction generation. The basin then fills through the turbines and generates power, until the minimum head for generation is reached. Sluices and turbines fill the basin until the maximum water level is reached. The water is then held again until the required head for ebb generation. Two-way generation preserves a more natural tidal cycle in the basin, but requires a more complex operating mode and turbines that can produce power bi-directionally with high efficiency (Xia *et al.*, 2010b).

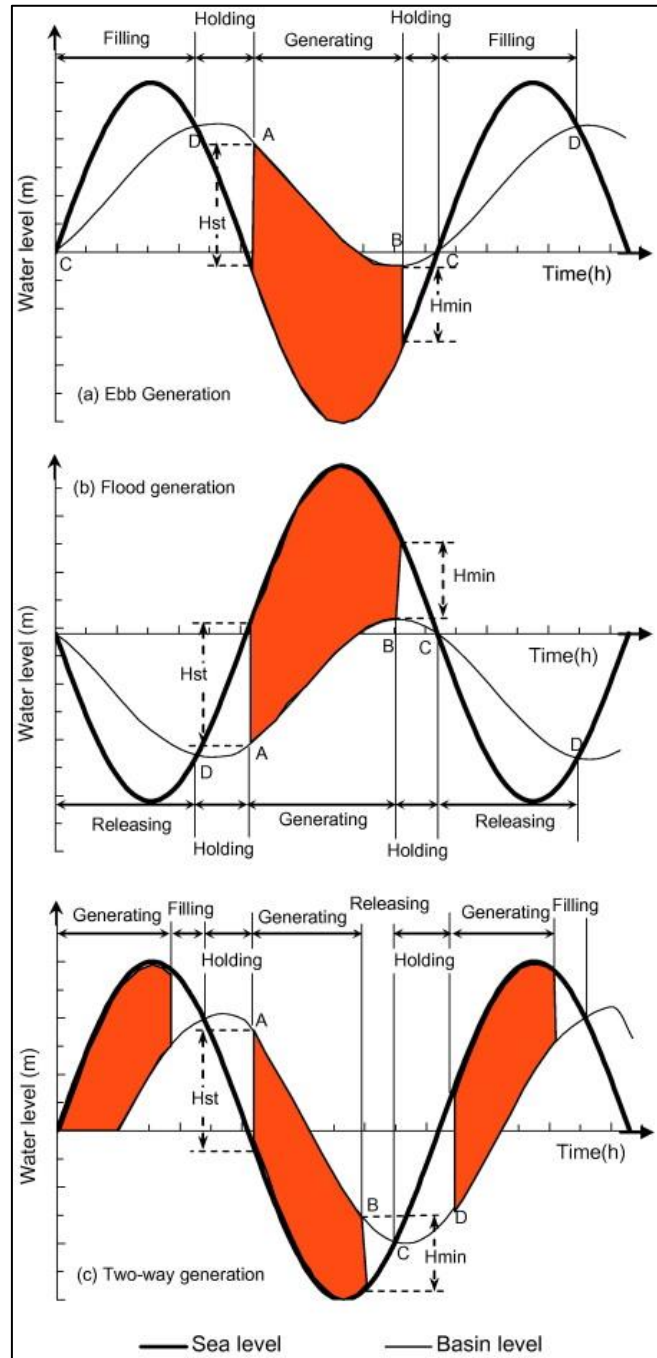


Figure 2-2 - Barrage operating modes (Xia et al., 2010b)

2.2.4 Current schemes

A review of the limited number of tidal range projects currently in operation is presented by Waters & Aggidis (2016). The La Rance tidal barrage in Brittany, shown in Figure 2-3, was the first tidal range project to be

operational (Andre, 1978; Charlier, 2007), built between 1961 and 1967. The 720 m long barrage impounds a 22 km² area of water, producing 480 GWh per year (Rourke *et al.*, 2010).



Figure 2-3 - La Rance Barrage (public domain photograph)

The barrage was initially intended to produce power on both the ebb and flood tides, however, usually now only produces power on the ebb, with the exception of large spring flood tides (author visit to La Rance barrage 2014). As the 24, 10 MW Kaplan bulb turbines are bidirectional, they are able to be used as pumps to increase the head difference and energy yield, and hence can also be used as a means of energy storage (Kerr, 2007).

The barrage has produced electricity reliably and productively for over 50 years, with minimal downtime (less than 6.5%) and without the requirement for any major works on the turbines (Charlier, 2007). The tidal barrage also provides a road link across the river and is a valuable tourist attraction, enhancing the local economy (Frau, 1993). Despite its success, there

continue to be reservations about tidal range electricity generation through a barrage, due to the associated environmental impacts.

Much of the damage to the environment was caused during the construction of the barrage. With the exception of small amplitude discharges (1 m) at 2-week intervals for flushing purposes, the estuary was isolated from the open sea for 3 years. The changes to the estuarine regime virtually eradicated the marine flora and fauna (Retiere, 1994), apart from some particularly hardy species. Since then, the estuary has recovered and hosts a diverse, prolific ecosystem, albeit one that has changed due to the barrage (Kirby and Retiere, 2009). There is no reason that the construction of a new barrage would have to have the same catastrophic effect on the ecosystem, with the advancement of construction techniques and a better understanding of the requirements and baseline of the biological community (British Hydro, 2009; Kirby and Retiere, 2009).

The Sihwa Tidal Power Plant in Korea (Figure 2-4) is the world's largest, with a total capacity of 254 MW, surpassing La Rance's 240 MW (Choi *et al.*, 2010). The dam for the Lake Sihwa barrage was originally built to hold irrigation water for agricultural land (Bae *et al.*, 2010). Significant industrial pollution rendered the freshwater unusable for irrigation, leading to the modification of the dam to a tidal barrage (Kim *et al.*, 2012).



Figure 2-4 - Lake Sihwa Tidal Power Plant (Electric-Power, 2015)

After seven years of modifications, the power plant was connected to the grid and the Lake Sihwa tidal power plant began producing electricity. Since then it has produced around 0.5 TWh per annum (Electric-Power, 2015). This barrage produces power on the flood tide only, and is limited by the water level permitted in the lake. Water quality has been considerably improved by the regular flushing and seawater influx, and the plant is regarded as a great success from a power, tourism and environmental perspective, and has led to the South Korean government exploring the option of adding further tidal barrages at the bays of Gerolim and Incheon (British Hydro, 2008; Cho *et al.*, 2012; IHA, 2016).

Except for La Rance and Sihwa, the only industrial-scale tidal power barrages to date, other current schemes are pilot installations set up as precursors to potentially pave the way for future large-scale projects (Frau, 1993). The Annapolis power plant in Canada, shown in Figure 2-5, takes

advantage of the largest tidal range in the world (NOAA, 2017), with a spring tidal range of 16 m. A single 20 MW turbine produces up to 50 GWh per year on the ebb tide, and is also used as a flood defence system and transport link (Pelc and Fujita, 2002).

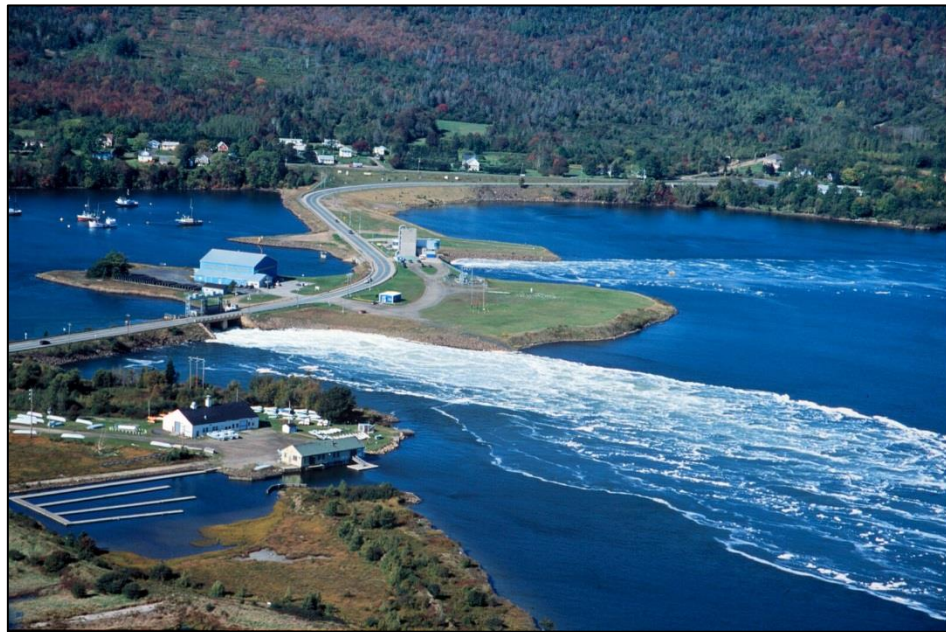


Figure 2-5 - Annapolis Power Plant (CAA, 2017)

The Kislaya Guba tidal power plant (Figure 2-6) was Russia's first, and was seen as an exploration of alternative energy (Bernshtein, 1972), as indicated by the capacity of just 1.5 MW. Geographical constraints and a harsher aquatic environment posed a complex engineering challenge (Charlier *et al.*, 2012), but nevertheless, celebrated 40 years of successful electricity generation in 2008 (Chaineux and Charlier, 2008).



Figure 2-6- Kislaya Guba Power Plant (public domain image)

Jiangxia power plant in China is the only other tidal range power plant currently in operation (Wang *et al.*, 2011). There have been seven other tidal range plants constructed in China, but none still in operation due to issues with locations and turbine designs (Chaunkun, 2009), and the focus has more recently switched to tidal current generation (Li *et al.*, 2010; Liu *et al.*, 2011). The turbines at Jiangxia produce power bi-directionally, with a capacity of 3.9 MW.

2.2.5 Tidal lagoons

The tidal lagoon is a more recent approach to tidal power generation that attempts to mitigate some of the environmental concerns associated with a barrage that blocks off an entire bay or estuary. Similarly to a barrage, a lagoon requires the construction of a wall to impound water and create a head difference, before allowing water to pass through turbines and generate electricity. A lagoon can be either attached to the coast (onshore),

or a circular dam (offshore). Onshore lagoons have attracted the most attention from a research and commercial perspective, due to the simpler grid connection and lower wall length requirements.

The Swansea Bay Tidal Lagoon, shown in Figure 2-7, is the most advanced proposal for a tidal lagoon, having been granted development consent order in 2015 (DECC, 2015c). The Severn Estuary has been the subject of continued study with regards to tidal power, due to very high tidal range and ease of grid connection.



Figure 2-7 - Swansea Bay tidal lagoon, location and key facts (public domain image)

The Swansea Bay tidal lagoon would surpass the Lake Sihwa tidal plant to become the largest tidal range generating plant in the world, with a capacity of 320 MW from the 16 x 20 MW bulb turbines (Baker and Leach, 2006; DECC, 2015c; Tidal Lagoon Power, 2015). In spite of this, it is perceived as a pilot scheme for larger projects that would be either within the Severn Estuary or beyond, such as along the North Wales coast (Falconer *et al.*, 2009; Hendry, 2016). Hydrodynamic modelling studies have indicated that the

Swansea Bay tidal lagoon is likely to generate around 0.5 TWh per year of electricity (Angeloudis *et al.*, 2016; Petley and Aggidis, 2016), at a cost of approximately £1.3 billion (WalesOnline, 2016).

It is the hope of Tidal Lagoon Power PLC that approval and subsequent successful operation of the Swansea Bay lagoon will be the catalyst for a network of tidal lagoons in the Severn Estuary and North Wales coast. Concerns still remain about the hydro-environmental impact of lagoons (Cornett *et al.*, 2013; Angeloudis and Falconer, 2016), and whether they make a cost-effective contribution to the UK energy mix. 2D modelling is a tool that can mitigate these concerns, helping to thoroughly assess potential impacts and optimise lagoons for maximum electricity production at minimal environmental cost. This is explored further as part of this thesis, through looking at another of the UK government's shortlisted tidal power schemes, the Bridgwater Bay lagoon (DECC, 2010a).

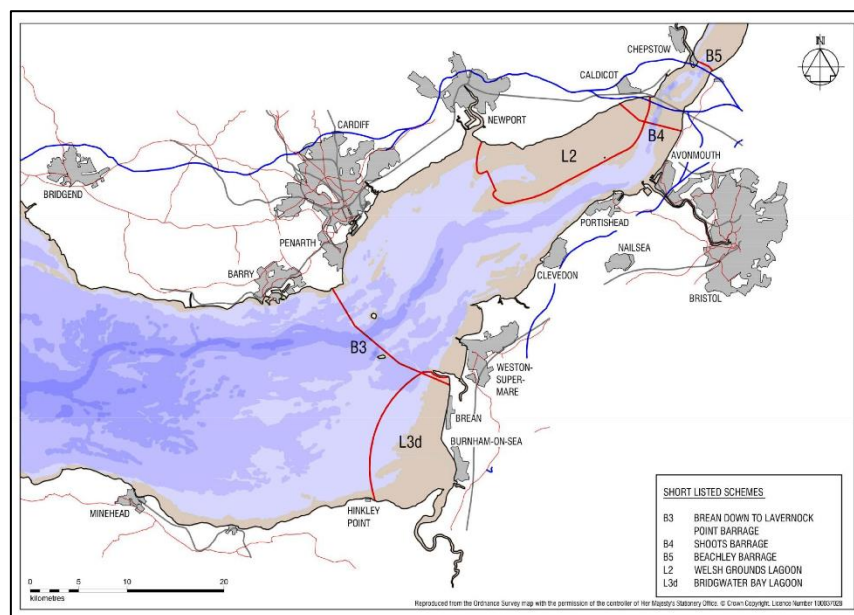


Figure 2-8 - DECC shortlisted schemes for Severn Estuary tidal power

2.2.6 The Severn Barrage

The proposal with the longest history of research and government and commercial consideration for tidal range generation in the Severn Estuary is the Severn Barrage. Several options for barrages in the Severn Estuary have been appraised by the UK government (DECC, 2010b), including an “Outer Barrage” from Minehead to Aberthaw, and a “Shoots Barrage”, a smaller barrage located just downstream of the Second Severn Crossing (as seen in Figure 2-8); however, the Severn Barrage refers to that which has received the most study, the barrage from Cardiff to Weston.

The Severn Barrage was proposed by the Severn Barrage Committee in 1981 (SBC, 1981), and developed further by the Severn Tidal Power Group (STPG, 1989). The proposal presented a 16.2 km long barrage from Cardiff to Weston, housing 216 x 40 MW 9m bulb turbines, shown in Figure 2-9 - Configuration of STPG Barrage (STPG, 1989), for a total capacity of 8640 MW (DECC, 2010a). This version of the Severn Barrage was designed to generate on the ebb-tide only, using 166 sluices to fill the basin on the flood tide.

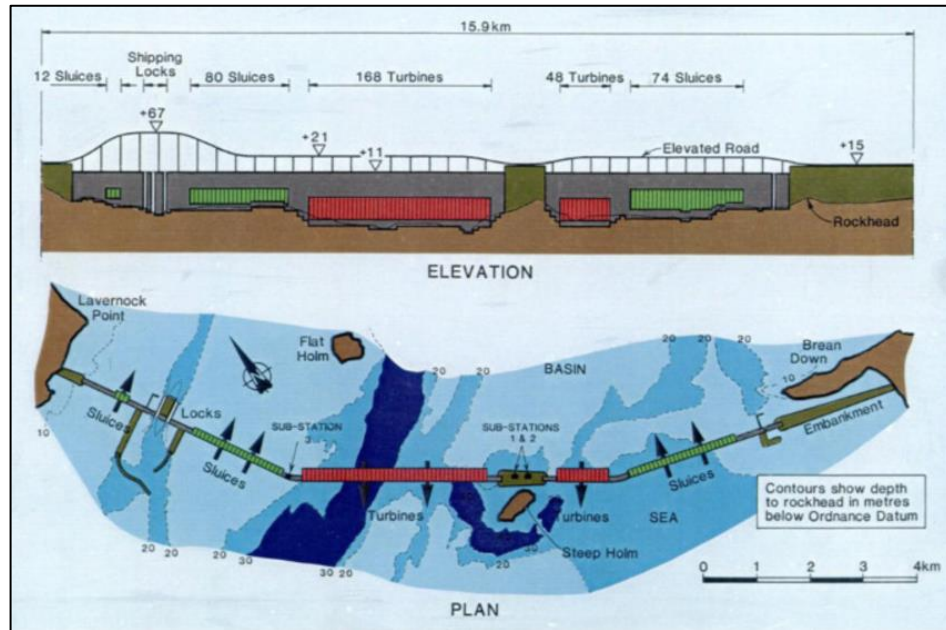


Figure 2-9 - Configuration of STPG Barrage (STPG, 1989)

The energy yield predicted in the proposals, government reports and from hydrodynamic modelling ranges from 14 - 17 TWh per year (DECC, 2010b; Xia *et al.*, 2012; Angeloudis and Falconer, 2016; Bray *et al.*, 2016), roughly equivalent to 4-5% of the UK's electricity needs. A decision to build the STPG barrage was not considered economically viable by the UK government, given the then present energy and economic situation, but a subsequent Energy White Paper did not rule out future consideration of a Severn Barrage, if environmental concerns could be mitigated (DEFRA, 2003).

The main environmental concerns regarding the Severn Barrage are the reduction in intertidal habitat areas, the risk to fish in terms of interruption to migration and injury from turbines, and the effect on the ecosystem as a result of lowering the suspended sediment levels and affecting currents (Ahmadian *et al.*, 2010). There are, however, significant non-energy benefits to the barrage, including a reduction in flood risk and protection

against future sea level rise (Ahmadian *et al.*, 2014) and increased productivity of the benthic flora and fauna due to increased light penetration.

More recent proposals, such as the Hafren Power two-way generating Severn Barrage, have claimed to reduce environmental damage at minimal cost to electricity generation (Xia *et al.*, 2010c; Ahmadian *et al.*, 2014a; Ahmadian *et al.*, 2014b; Zhou *et al.*, 2014). Although limited information was made publicly available on design specifics of the Hafren Power Barrage, it was reported to be 18 km in length, with 1026 very low head (VLH) turbines, no sluices and generating 16.5 TWh per year (DECC, 2013a). It was again decided at the House of Commons that there was insufficient evidence that the environmental concerns had been completely mitigated, in particular flood risk, intertidal habitat loss and fish mortality. It was suggested that further investigation and modelling was required, and that all options for exploiting Severn tidal resources should be explored. Continued development and improvement to hydrodynamic modelling could improve the chances of such proposals being granted permission, through increasing confidence in the results and impacts and aiding optimisation and environmental damage mitigation, explored further within this thesis.

2.3 Tide generation in the UK

This section discusses the exceptional tides in the UK, and hence the enormous tidal stream and range resource available.

2.3.1 Mechanisms resulting in exceptional tidal regime

A great number of factors influence the tides, with the best known being the moon, the sun and the Coriolis Effect. Other factors, including distance from amphidromic points (tidal nodes at which the tidal range is zero), shown in Figure 2-10, ocean depth, basin size, shoreline configuration and local topography can combine to significantly affect the tidal range, as is the case with the Severn Estuary (Baker, 1991; Uncles, 2010).

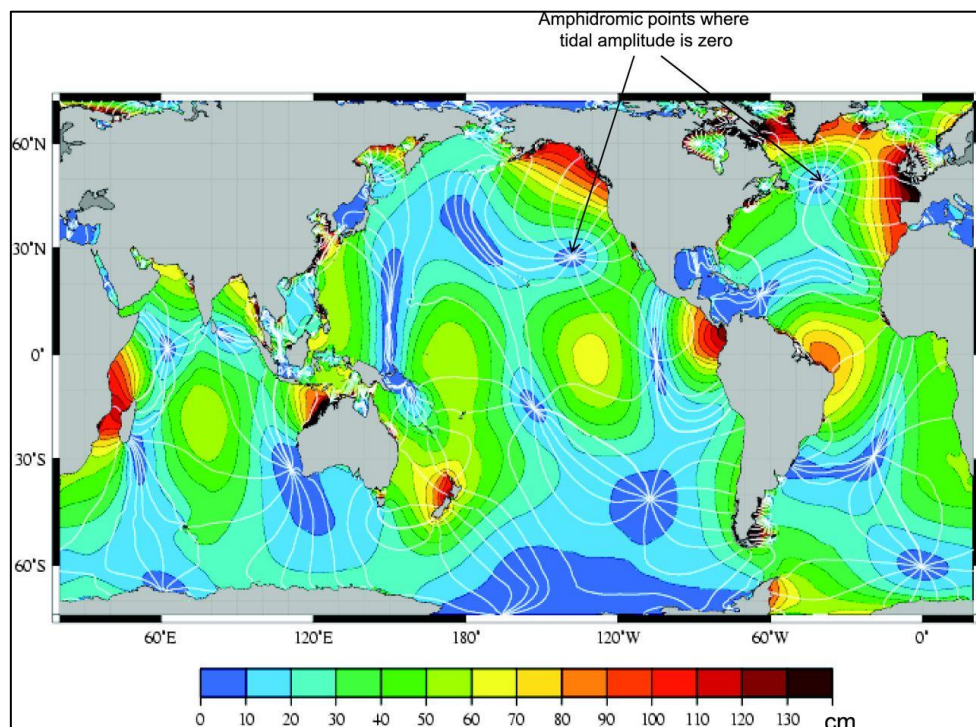


Figure 2-10 - Amphidromic points (credit Dr R Ray, NASA - Goddard Space Flight Center)

The huge, deep basin of the Atlantic Ocean has a tidal force accentuated by the funnel shape of the Severn Estuary, creating a tidal range second only to that in the Bay of Fundy, Canada. The unique characteristics of the Severn Estuary that produce this large tidal range can make the estuary a challenge to represent in a hydrodynamic model, and so further investigation is important to ensure potential tidal range generating proposals do not have

unforeseen effects on the tidal regime, as explored in section 2.4, and further in the modelling undertaken as part of this thesis.

2.3.2 Tidal stream resource

A large tidal range induces tidal currents, from which energy can be extracted via tidal stream turbines. Few sites are appropriate for tidal stream energy extraction, as the turbines require high current velocities and sufficient water depth (Black & Veatch, 2005). The theoretical tidal stream resource in the UK is estimated to be 95 TWh per year (The Crown Estate, 2012), of which 18 TWh per year is extractable (Black & Veatch, 2005).

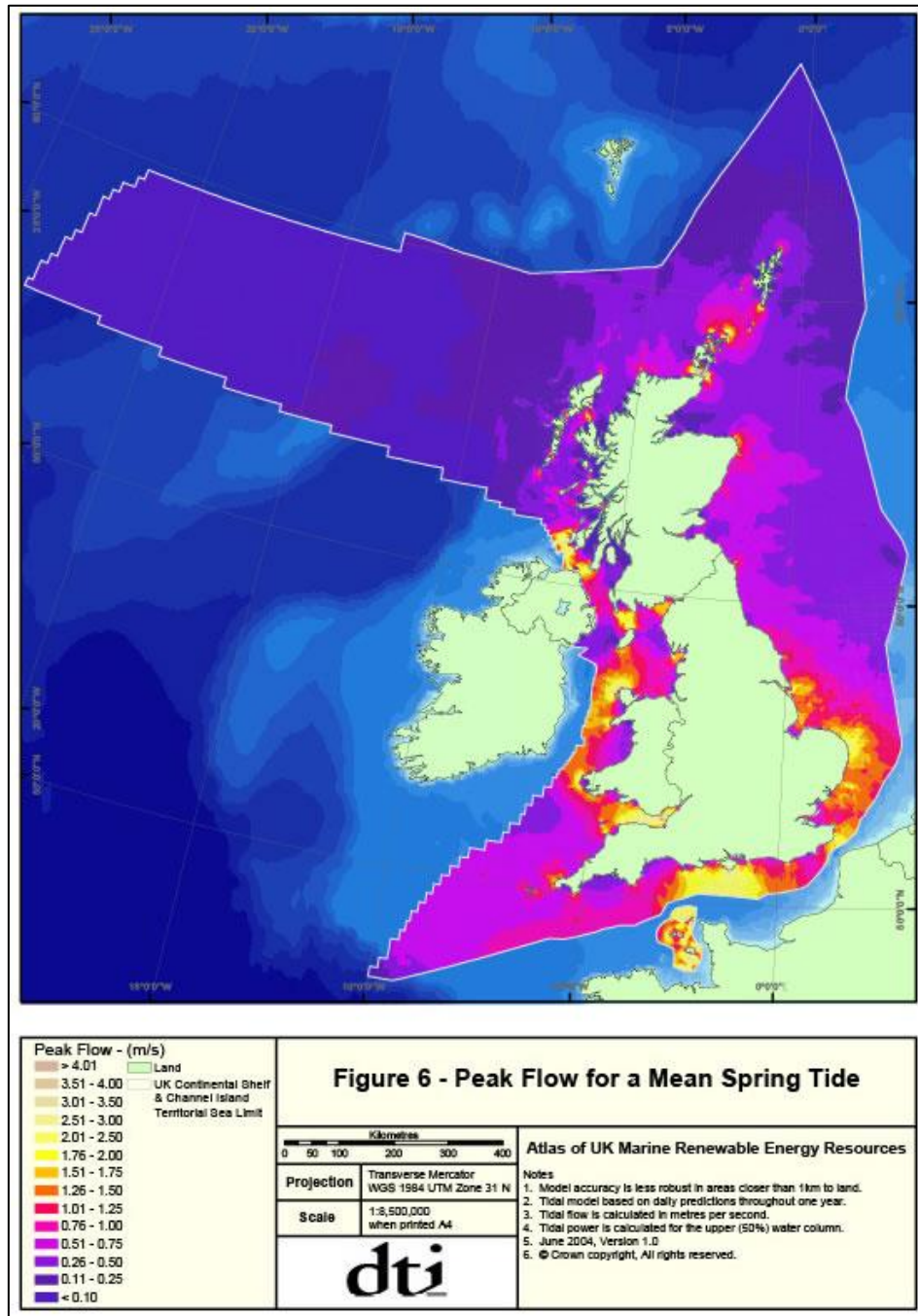


Figure 2-11 - UK Tidal Stream Resource (credit DTI)

Although in comparatively early stages of development compared to wind or solar energy technology, marine current turbines have progressed quickly (Fraenkel, 2006; Ben Elghali *et al.*, 2007; Khan *et al.*, 2009), and at the time of writing are at the first stages of commercial scale deployment.

Several modelling studies have investigated the potential energy yield from tidal stream turbines at various sites in the UK, and assessed their likely impact on the hydro-environment (Blunden and Bahaj, 2006; Neill *et al.*, 2009; Walkington and Burrows, 2009; Xia, *et al.*, 2010; Ahmadian, *et al.*, 2012; Gao, *et al.*, 2013; Fallon *et al.*, 2014; Nash *et al.*, 2014; Nash, *et al.*, 2015), demonstrating significant potential for tidal stream generation in the Severn Estuary, Portland Bill, Pentland Firth, and Anglesey, but that further consideration needs to be given to the interaction between turbines, and their impact on sediment dynamics and marine wildlife (Nash and Phoenix, 2017).

2.3.3 Tidal range resource

To put the Severn Estuary's huge tidal range into context, it is estimated that Europe's tidal energy resource is around 64 GW (Hammons, 2008), of which up to 30 GW is UK tidal range resource, with 12 GW within the Severn Estuary (DECC, 2013b). It is also uniquely extractable, as the large basin of around 500 km² can be impounded by a comparatively short wall of 16 km in the case of the Severn Barrage, and the Estuary is host to several large cities that could make use of the electricity.

The Energy Technologies Institute (ETI) funded the SMARTtide project to develop a UK Continental Shelf Model to help with the assessment of tidal energy resource in the UK (SMARTtide, 2013). The model produced a maximum tidal range map, seen in Figure 2-12 below.

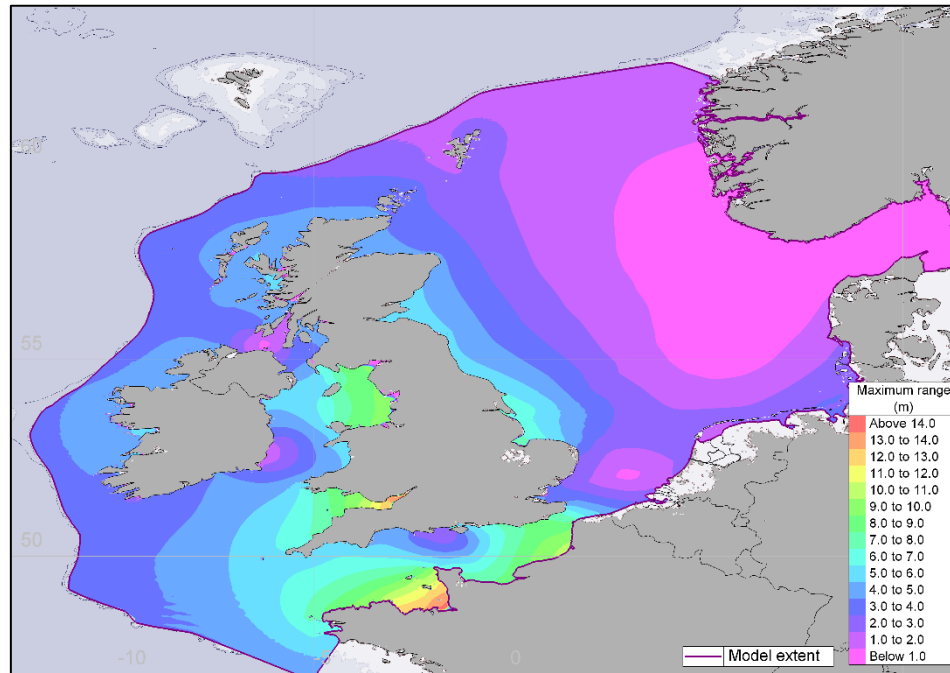


Figure 2-12- Maximum tidal range (credit SMARTtide)

The model further demonstrates the resource available in the Severn Estuary, but requires a three-tiered approach to assessing potential tidal range generation schemes: initial evaluation using the coarse continental shelf model; feasibility assessment using the detailed continental shelf model; and detailed assessment using the high-resolution Severn Estuary model (IRF, 2013). A combined solution would enable more straightforward and detailed assessment of hydro-environmental impacts of tidal range generating proposals, as developed as part of this research study, with a large domain, resolution-varying model: the Continental Shelf Model.

2.4 Extended domain modelling - Continental Shelf Model

Proposals for tidal range generation in the Severn Estuary have traditionally been modelled using a domain extending to the end of the Bristol Channel (Ahmadian, *et al.*, 2010; Xia, *et al.*, 2010b, 2010c; Zhou, *et al.*, 2014;

Angeloudis and Falconer, 2016). When modelling a Severn Barrage, these models all predict changes to water levels at the open boundary at the Bristol Channel, and hence it was hypothesised within the Cardiff University Hydro-environmental Research Centre (HRC) that the domain should be extended to ensure that the model predictions are accurate, and that the effects of a barrage may reach further than initially expected. This led to the development of the HRC's own Continental Shelf Model (CSM), built using the hydrodynamic modelling package EFDC - Environmental Fluid Dynamics Code. This was presented by Zhou *et al.* (2014a), where the Severn Barrage was modelled with two different computational domains (as seen in Figure 2-13), and the results compared to test the effect of the open boundary locations.

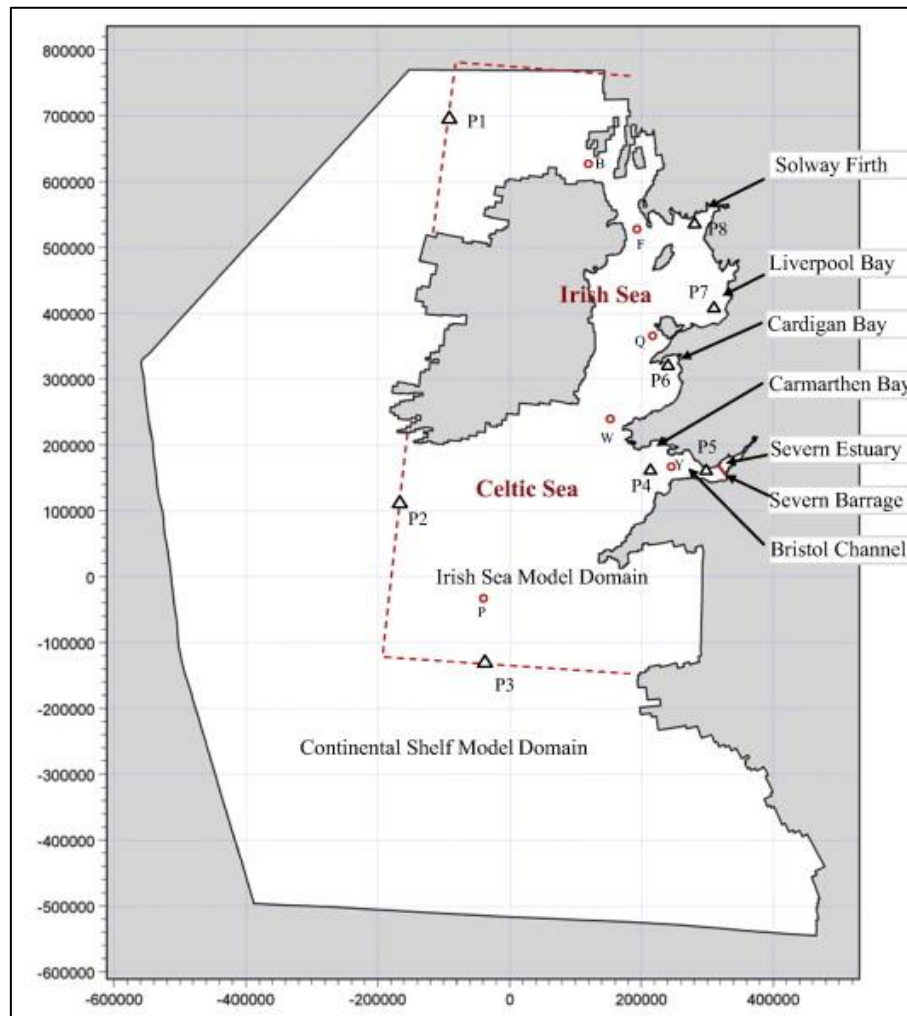


Figure 2-13 - Computational domains used to test open boundary location effect (Zhou, Pan and Falconer, 2014a)

The model showed markedly different results when using the Irish Sea Model domains and Continental Shelf Model domains, indicating that even extending the domain as far as the Irish Sea is not sufficient to ensure that the open boundary is not affected by the inclusion of a barrage, compromising the accuracy of the model predictions.

The model also showed some far-field effects of the Severn Barrage that had not been previously demonstrated, along the west coast of Scotland, as seen in Figure 2-14.

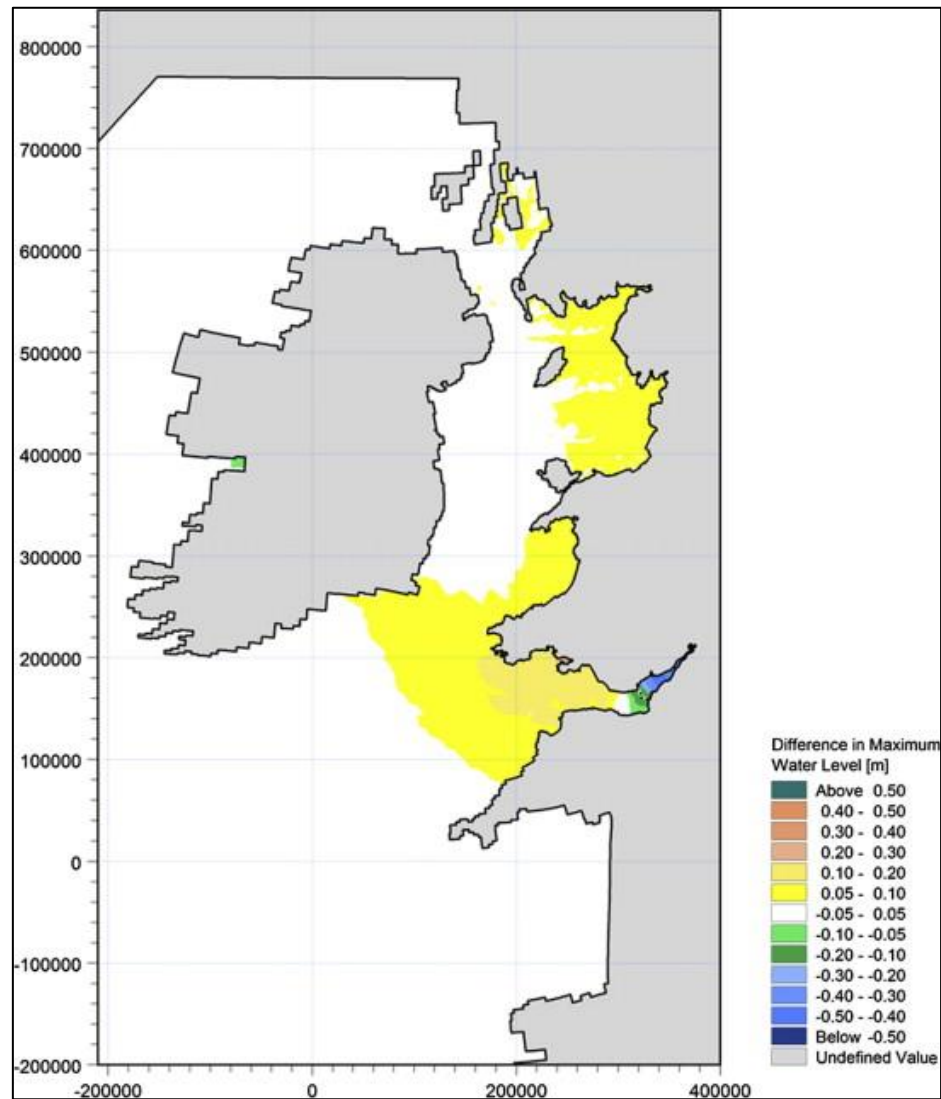


Figure 2-14 - Impact of Severn Barrage on maximum water levels (Zhou, Pan and Falconer, 2014a)

Although the EFDC CSM had shown that it might be necessary to extend the model domain when modelling a Severn Barrage, the results were not in agreement with those previously reported in the literature, e.g. Ahmadian *et al.* (2010) and Xia *et al.* (2010a), where it was predicted that the inclusion of the STPG barrage would reduce water levels upstream by up to 1m in some areas. Moreover, the EFDC CSM predicted higher water levels upstream of the barrage than downstream, again contradicting the results of previous studies.

It was thought that the main cause of the difference in the water levels predicted by the EFDC CSM was the incorrect representation of turbines and sluices in the barrage, explored further in Chapter 4. The representation of these hydraulic structures within the EFDC CSM was altered as part of this research study, as shown in Bray *et al.* (2016) and examined in detail within this thesis, with the aim of developing the first model to accurately assess the far-field effects of a Severn Barrage and demonstrate the importance of accurate hydraulic structure representation when modelling a tidal range proposal.

2.5 Hydraulic structure representation in tidal range generating proposals

This section details the ways in which hydraulic structures in tidal range generating proposals are represented in hydraulic models.

2.5.1 Internal boundary

Internal boundaries are often applied in hydraulic modelling to simulate complex physical processes, for example flow across or through hydraulic structures. The technique has been successfully employed in several hydraulic models for simulating the transfer of volume from one side of a hydraulic structure such as a barrage, dam, weir or tidal lagoon, as shown in Falconer *et al.*, (2009); Ahmadian, *et al.*, (2010); Xia *et al.*, (2010a, 2010b, 2010c); Xia *et al.*, (2012); Bray *et al.*, (2014); Fairley *et al.*, (2014); and Angeloudis *et al.*, (2016). The term “domain decomposition” can be applied to describe this internal boundary, but is usually used to describe the subdivision of a 2D domain into several domains for the purpose of

parallelising a code, including for EFDC and tidal stream generation assessment (O'Donncha *et al.*, 2014; O'donncha *et al.*, 2016); however, in this instance the term is intended to describe the division of a 2D domain in order that the flow across a turbine or sluice can be accurately represented.

In the case of using a hydrodynamic model to simulate a dam, barrage or lagoon, the domain is subdivided into two domains, one upstream and one downstream of the structure. Mass and momentum can then be transferred between the domains, according to rules and equations dependent upon the hydraulic structure the modeller wishes to represent.

2.5.2 Turbines

The discharge through a turbine is typically modelled in one of two ways. The preferred method is to use a head-discharge or “hill” chart, determined empirically by the turbine manufacturer (Goldwag and Potts, 1989; Falconer *et al.*, 2009). This will give the most accurate relationship between head and discharge, and indeed power, but clearly is not always going to be available for many proposals in early-stage development, due to their commercially sensitive nature. The alternative is to use a numerically derived estimate, evaluating flow through the turbine in a similar manner to discharge through an orifice (Baker, 1991), as given by Equation 2.4 :

$$Q = C_d * A * (2 * g * H)^{0.5} \quad 2.4$$

where Q is discharge ($\text{m}^3 \text{s}^{-1}$), C_d is a discharge coefficient, A is flow-through area (m^2), g is gravitational acceleration, and H is water level difference either side of the turbine.

In the case of the Severn Barrage, a hill-chart for the 9 m diameter, 40 MW turbines was available, as shown in Figure 2-15 below:

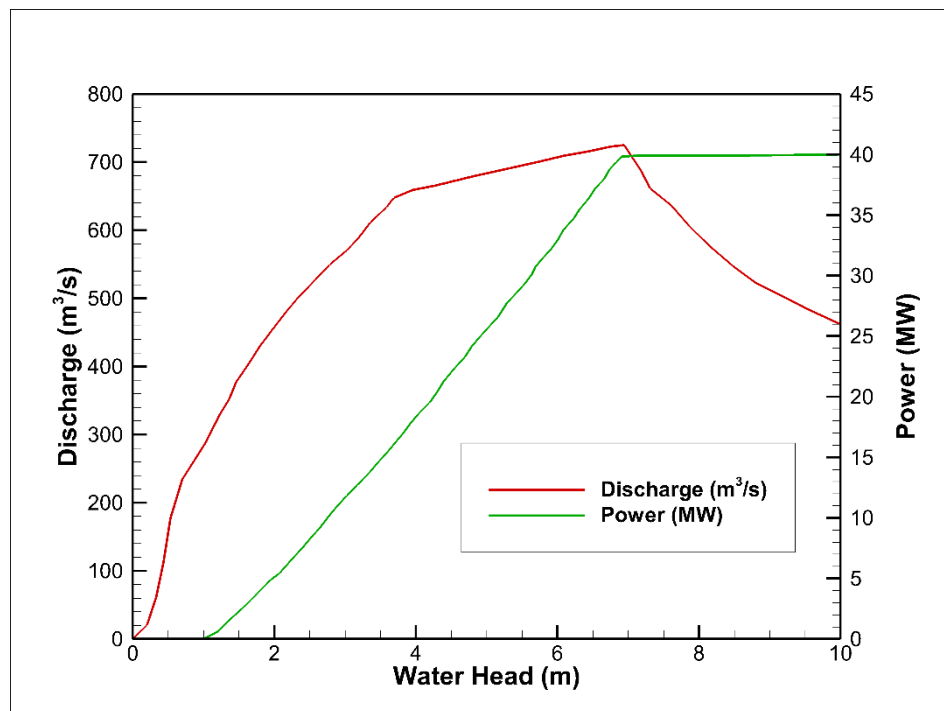


Figure 2-15- Relationship between the water head, discharge and power output (STPG, 1989)

Discharges from the hill chart differ from discharges calculated using Equation 2.4, especially at high head differences where available power through flow is higher than the turbine maximum power capacity. Therefore, the discharge through the turbine is mechanically restricted to maintain a higher head difference and increase the total power generation over the generation phase, as seen in Figure 2-16.

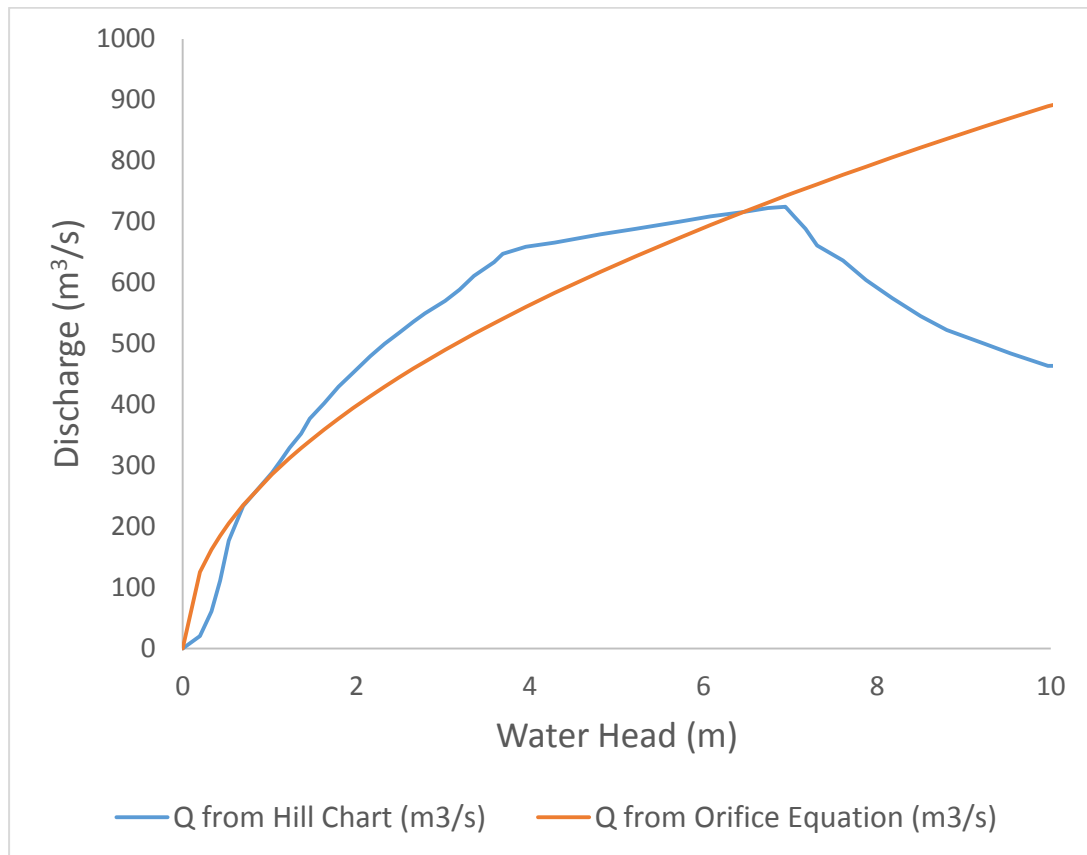


Figure 2-16 - Discharge through a turbine as calculated from the hill chart and from the orifice equation

This is explained by Equation 2.5, which expresses the formula for calculating the generation power P of each turbine:

$$P = \rho g Q h \eta \quad 2.5$$

where ρ is specific density of sea water and η is efficiency coefficient of the turbine. As the head difference becomes very large, the turbine reaches its maximum power output (e.g. 40 MW in the case of the STPG proposal) and so discharge is restricted, so as not to waste potential energy. In calculating the power using Equation 2.5, the efficiency η was assumed to be 1, as suggested by Baker (2006).

The hill chart for the suggested 9m diameter 40 MW turbines for the STPG Severn Barrage has been used in the hydrodynamic assessment of the proposal in previous studies (Ahmadian *et al.*, 2010; Xia *et al.*, 2010a; Angeloudis and Falconer, 2016), but not in a continental shelf scale model, where the orifice equation was used in determining the turbine discharge (Zhou *et al.*, 2014). Applying the hill chart to a continental shelf scale model is one of the improvements to the EFDC model detailed within this thesis, and presented in Bray *et al.* 2014; Bray *et al.* 2016.

2.5.3 Sluices

Sluice gates are important in tidal range generation, as they allow water to flow quickly to the impounded area, ensuring a maximum head for generating is achieved. Sluice gates are typically modelled in the same numerical manner described above for turbines, using Equation 2.4 (Falconer *et al.*, 2009; Ahmadian *et al.*, 2010; Xia *et al.*, 2010b; Angeloudis *et al.*, 2016), or more simply as “gaps” in a barrage wall, using cells that could be switched from open to closed, or wet to dry (Zhou *et al.*, 2014). A further improvement of applying the numerical sluice representation to the EFDC Continental Shelf Model was presented in Bray *et al.* 2014; Bray *et al.* 2016, and explored in detail in this thesis.

2.5.4 Discharge coefficient

The orifice equation (Equation 2.4) shows a directly proportional relationship between discharge and the discharge coefficient, a dimensionless factor of an orifice or valve, used to characterise the flow behaviour. While the other terms in the orifice equation are clear, there is

limited guidance and some uncertainty regarding this coefficient (Xia *et al.*, 2010a). Baker (2006) suggests a discharge coefficient value of 1, following the testing of a sluice gate prototype up to 2000 m³/s (University of Bristol, 1981). Although it is not expected that the discharge coefficient value will vary widely from the suggested value of 1, since sluice gates are designed to transfer volume as efficiently as possible and not obstruct the flow, the proportional relationship between discharge coefficient and discharge implies a potentially large impact from any uncertainty in the assumed value of 1 of C_d . As part of this research study, an investigation into the sensitivity of this parameter was undertaken, in an attempt to understand its importance and improve the confidence in hydraulic structure modelling. The results were presented in Bray *et. al* (2015), demonstrating that the continual nature of the filling of a basin is shown to render the simulation of a Severn Barrage insensitive to changes in the discharge coefficient.

2.5.5 Discharge and momentum

The numerical representation of a turbine or sluice should be conservative with respect to not only mass, as calculated above in ensuring the correct volume is transferred, but also with respect to momentum. The simple transfer of a volume from one subdomain to another may conserve mass, but does not necessarily account for the momentum that will be present as water flows through a sluice gate or turbine. The numerical model will attempt to conserve momentum using the cell width and depth to which the discharge is added. This will not, however, produce accurate results, as the surface area to which the discharge is added is in reality the flow-through

area of the turbine or sluice. Without an adjustment to the momentum calculation, the velocity of the discharge through a turbine or sluice is likely to be underestimated, and so it follows that the wake of the turbine may also be underestimated. Improvements to the momentum calculation through hydraulic structures are assessed within this thesis, to demonstrate the effect on turbine wake and current speed, in both 2D and 3D.

2.5.6 Scheme optimisation

With a basic structure in place, a hydraulic model set up to assess a tidal barrage or lagoon proposal can be modified to represent different configurations of turbine and sluice numbers, operation modes and generating parameters. This can aid the optimisation of a scheme in terms of power, energy, generating hours per day or tidal range. A scheme can then be optimised for maximum energy generation, making the project more attractive to investors, or to regulatory bodies by optimising the project to preserve as close to the natural tidal regime as possible. In reality, of course, something between the two is likely to be the best approach.

2.6 Eutrophication in estuaries and role of sediment

Eutrophication is the enrichment of a water body with nutrients. An excess of enrichment poses a risk to the environmental health of an estuary, as plants and algae are able to grow more quickly, potentially depleting the oxygen content of the water body.

The eutrophication of rivers is a problem of rising environmental concern worldwide, due to the considerable damage that can be caused to the ecosystem, and the increase in occurrences of harmful algal blooms (HABs),

as shown in Figure 2-17 below. HABs of autotrophic algae can sometimes be attributed to anthropogenic nutrient loadings (Anderson *et al.*, 2002; Sellner *et al.*, 2003) and the high oxygen demand of these blooms can result in the death of other plants and animals living in the water (Diersing, 2009), by creating anoxic conditions in deeper layers, or by limiting sunlight availability to living things under the water's surface (United Nations Environment Programme, 2010).

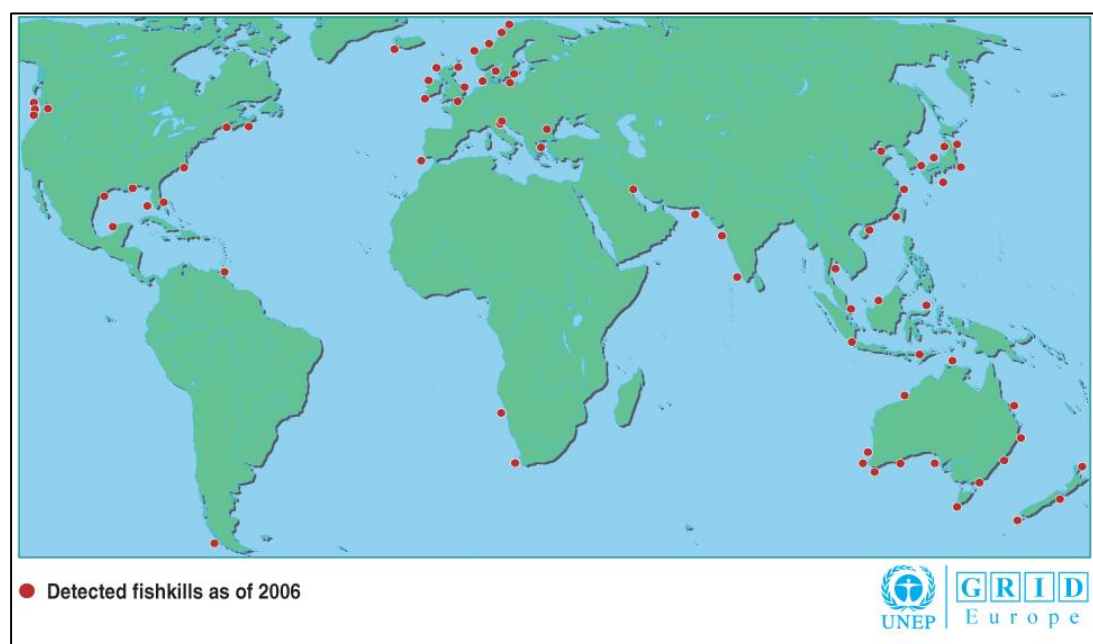


Figure 2-17 Fishkills linked to HABs, as of 2006, reproduced from Woods Hole Oceanographic Institution, 2008.

Coastal eutrophication is of particular concern because of intensive land-use of coastal areas. 28% of primary production occurs in coastal areas that cover only 8% of the world's surface (Holligan and Boois, 1993), and therefore it is here that there is greatest risk of eutrophication, due to high population densities and high levels of industry (De Jonge *et al.*, 2002). Estuarine waters are often at particular risk of heavy nutrient loading, due

to frequent inputs from both freshwater and marine sources (Hartnett and Nash, 2004).

Studies have shown that plant and algal growth in estuaries is usually phosphorus limited, and so it is this nutrient that should be closely monitored (Ryther and Dunstan, 1971; Vollenweider *et al.*, 1971; Nixon, 1995). Nutrient dynamics have a profound influence on estuarine productivity (Magnien *et al.*, 1992) and when nutrient levels are sufficient, phytoplankton uptake of nitrogen and phosphorus are calculated to be proportional to the Redfield Molar Ratio of 16:1 (Redfield, 1958).

During a spring tide in the Severn Estuary, up to 30 million tonnes of sediment can be transported in the water as suspended sediment (Knowles and Myatt-Bell, 2001), and as much as 1 million tonnes of silt per year enters the Estuary from tributary rivers (SDC, 2007).

Suspended sediment has a significant effect on the nutrient distribution throughout the water column, by adsorbing nutrients from solution onto the surface of sediment particles. The adsorption process is therefore very important when considering potential for eutrophication, as adsorbed nutrients are less readily available to algae than dissolved nutrients (Whitton, 1975), and suspended sediment with adsorbed nutrients that settle to the bed remove nutrients from the system (Kemp *et al.*, 1981). Suspended sediment can also contain species of bacteria and coliforms that consume nutrients, further reducing the availability to algae (Lin *et al.*, 2008).

Until recently the inter-reliance of suspended sediment and nutrients had not been investigated in any real detail, and the requirement for further research in this area has been outlined in recent research (Bockelmann-Evans *et al.*, 2007).

2.6.1 Phosphorus and the nutrient cycle

Phosphorus (P) is an essential element for all life forms. Its inorganic form, orthophosphate (PO_4), is the primary form of P for plant uptake, and the only form of P that can be assimilated by autotrophs (Correll, 1998).

Human activities can result in large fluxes of phosphorus in aquatic environments such as rivers and estuaries, increasing the primary production and potentially leading to eutrophication and depletion of oxygen levels.

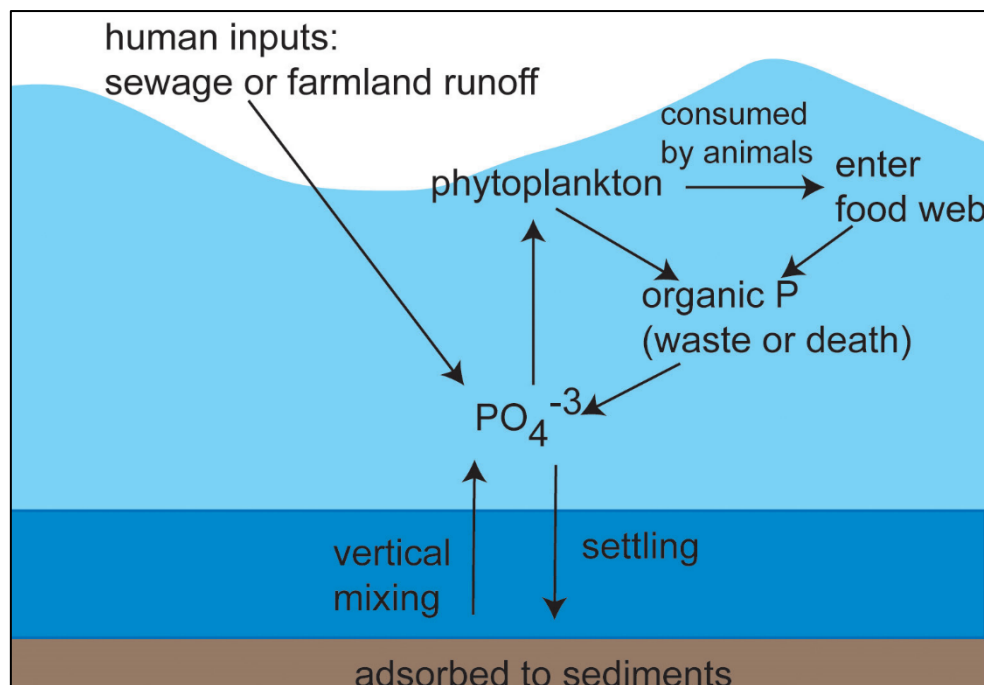


Figure 2-18 - The phosphorus cycle, reproduced from Project Waterman, Hong Kong University, 2010

As seen in Figure 2-18, inputs such as sewage or farmland runoff introduce an additional phosphorus input to the environment. This can move forms between organic and inorganic as it is consumed and used by phytoplankton and animals. Through adsorption to sediment and subsequent settling to the bed, phosphate can be removed from the water column. The phosphate can be returned to the water column through resuspension of the settled bed sediment.

There are clearly many factors that will influence the concentration of phosphate in the water column. With sediment associated phosphate being less readily available for biological uptake, and hence being a potentially important factor in eutrophication potential of an estuary, this thesis focuses on the phosphate-suspended sediment interaction. This is controlled by the phosphate partition coefficient.

2.6.2 Phosphate partition coefficient

Nutrients are present in the water column in either a dissolved phase (in solution) or in a particulate phase, where the nutrient is adsorbed to suspended sediments. The ratio of dissolved to adsorbed nutrients, in this case phosphate, is described by the partition coefficient, K_d . The formula for the partition coefficient is expressed as:

$$K_d = \frac{PO4_p}{PO4_d} \frac{1}{TSS} \quad 2.6$$

where $PO4_p$ and $PO4_d$ are the adsorbed and dissolved phosphate fractions (mg/L)/, and TSS is the total suspended sediment concentration (mg/L).

Previous laboratory and field studies (Kadiri *et al.*, 2014) have demonstrated a link between salinity and phosphate sorption to sediments due to the competition for sorption sites between seawater anions and phosphate (Zhang and Huang, 2011). This may be due to the increased ionic strength of the medium by means of ion exchange with the anions sulphate and chloride, leading to competition with phosphate for surface sorption sites (Clavero *et al.*, 1993).

The relationship between salinity and phosphorus adsorption established in Kadiri & Bockelmann-Evans (2012, 2014) could be implemented into a hydraulic model to improve the prediction for dissolved phosphate across the estuary by taking into account the salinity variation. The effect of salinity on the adsorption was described empirically as:

$$K_d = AS^{-b} \quad 2.7$$

where S is salinity (g/kg), and A and b are coefficients, the magnitude of which are dependent upon the salinity and suspended sediment concentration. This was established through a power law function by non-linear regression, using field data collected in the Seven Estuary and with strong correlation ($r^2 > 0.8$).

Although some water quality models have the capability to predict the proportion of adsorbed to dissolved phosphate, none to date have implemented a further relationship linking the partition coefficient to salinity. In estuarine modelling in particular, where there is a variation in salinity, this could have a significant impact on the accuracy of phosphate

modelling and the prediction of an estuary's eutrophic potential. This improvement is made to the EFDC code as part of this study, detailed further in Chapter 4.

2.7 Chapter summary

Tidal range power is an area of renewable energy with enormous scope for increased capacity in the UK, due to the exceptional tides generated particularly in the Severn Estuary. Several tidal range projects are in operation across the globe, including the hugely successful La Rance tidal barrage in St Malo that has generated reliable renewable electricity since 1967.

The Severn Barrage and tidal lagoons within the Severn Estuary have received substantial commercial and government attention due to their huge potential to contribute to the UK's renewable energy mix. Before any such proposal could proceed, significant investigation into the potential environmental impacts would need to be undertaken. The environmental impact assessment is underpinned by hydraulic modelling, an area of constant refinement and improvement and a very useful tool in assisting with the prediction of the consequences of the operation of tidal range generating devices.

Previous research has shown that a version of the Severn Barrage, the STPG ebb-generating barrage, could have water level impacts as far-field as the west-coast of Scotland. This was assessed using the EFDC CSM, an extended domain model created to ensure that water levels at the model open boundary were not compromised by the effects of the barrage.

All hydraulic models have scope for refinement and improvement, and in the case of the EFDC CSM, there was some uncertainty over the representation of turbines and sluices. In hydraulic structure modelling generally, there is also uncertainty over one of the key parameters, the discharge coefficient.

Phosphate concentrations in estuarine waters are an important component in assessing its eutrophic potential. Phosphate is known to be strongly sediment associated, and thus levels are difficult to predict without also modelling suspended sediment concentrations. The nutrient exists in two phases, dissolved and particulate (adsorbed to sediment), the ratio determined by a partition coefficient. There is very limited literature available regarding the value of this coefficient, however, in an experimental study at Cardiff University using samples from the estuary, an empirical relationship was developed between salinity and the partition coefficient.

The thesis will therefore attempt to advance hydro-environmental modelling of marine renewable energy devices through:

- updating the EFDC CSM representation of turbines and sluices, including their mass and momentum transferral;
- demonstrating the applicability of 2D hydraulic models in assisting with the optimisation of tidal lagoon design and environmental impact minimisation; and

- developing a tool that could be used to predict dissolved phosphate levels in the Severn Estuary, by implementing the dynamic partition coefficient detailed previously.

The EFDC model is selected to proceed with this research study as:

- it is open source;
- the CSM domain and barrage modules are available for refinement;
- the wetting and drying scheme of the model has been demonstrated to be very robust (Ji, 2017);
- it is capable of both 2D and 3D simulations; and
- it has integrated water quality and sediment transport modules, enabling the simulation and interaction of phosphate and salinity.

Chapter 3

Governing equations

3.1 Introduction

This chapter presents details of the relevant governing equations which underpin the hydraulic model. The equations of hydrodynamics, mass, solutes and sediment are considered within this chapter.

3.1 Mass and momentum

The principles of continuity of mass and conservation of momentum, the Navier-Stokes equations, are used within CFD models to simulate fluid flow. The sophistication and intended use of a model will determine the precise representation of the Navier-Stokes equations, as simplifications to the equations are required to make their solutions viable on a practical scale with current computational capability.

The Reynolds averaged Navier-Stokes (RANS) equations are widely applied in CFD models, providing a set of time-averaged equations, often coupled with turbulence models such as the k - ϵ turbulence model (Patel, Rodi and Scheuerer, 1985; Rodi, 1993) and the Mellor-Yamada turbulence closure scheme (Mellor and Yamada, 1982; Galperin *et al.*, 1988), as employed by EFDC. The turbulence closure scheme accounts for the effects of turbulent fluctuation on the mean flow of a fluid, explored further in this section.

In three-dimensional shallow water models, and particularly those designed with coastal modelling applications in mind, a sigma coordinate transformation is often applied. This allows for a coordinate system fitted to a moving water level surface and bottom topography.

Using a sigma coordinate system, (x,y,z) space is transformed to (x,y,σ) space using the following relationship:

$$\sigma = \frac{z + h}{H} \quad 3.1$$

where z is the sigma coordinate, $H = \zeta + h$ and represents the total water depth, ζ is the surface elevation above or below the still-water level, and h is the initial water level. This maps the bottom at $z = -H(x,y)$ to $\sigma = -1$, and so the domain is made square.

The three-dimensional RANS equations, for unsteady, incompressible turbulent flows, in sigma coordinate system are as follows (Hamrick and Wu, 1997):

Continuity of mass:

$$\frac{\partial H}{\partial t} + \frac{\partial Hu}{\partial x} + \frac{\partial Hv}{\partial y} + \frac{\partial w}{\partial \sigma} = Q_H \quad 3.2$$

Conservation of momentum equations:

$$\begin{aligned} \frac{\partial(Hu)}{\partial t} + \frac{\partial(Huu)}{\partial x} + \frac{\partial(Huv)}{\partial y} + \frac{\partial uw}{\partial \sigma} - fHv \\ = -H \frac{\partial(p + p_{atm} + \Phi)}{\partial x} + \frac{\partial p}{\partial \sigma} \left(\frac{\partial z_b}{\partial x} + \sigma \frac{\partial H}{\partial x} \right) + \frac{\partial}{\partial \sigma} \left(\frac{A_v}{H} \frac{\partial u}{\partial \sigma} \right) \end{aligned} \quad 3.3$$

$$\begin{aligned} \frac{\partial(Hv)}{\partial t} + \frac{\partial(Huv)}{\partial x} + \frac{\partial(Hvv)}{\partial y} + \frac{\partial vw}{\partial \sigma} + fHu & \quad 3.4 \\ = -H \frac{\partial(p + p_{atm} + \Phi)}{\partial y} + \frac{\partial p}{\partial \sigma} \left(\frac{\partial z_b}{\partial y} + \sigma \frac{\partial H}{\partial y} \right) + \frac{\partial}{\partial \sigma} \left(\frac{A_v}{H} \frac{\partial v}{\partial \sigma} \right) \end{aligned}$$

$$\frac{\partial p}{\partial \sigma} = -gH \frac{(\rho_w - \rho_0)}{\rho_0} = -gHb \quad 3.5$$

$$\tau_{xz}, \tau_{yz} = \frac{A_v}{H} \frac{\partial}{\partial \sigma} (u, v) \quad 3.6$$

where t is time (seconds), u and v are the velocities in x and y directions (m/s), Q_H is the volumetric source/sink term (including rainfall, evaporation, infiltration, lateral inflows and outflows with negligible momentum) (m^3/s), f is the Coriolis parameter ($1/\text{s}$), p is water column hydrostatic pressure (m^2/s^2), p_{atm} is atmospheric pressure (Pa), Φ is the free surface potential, z_b is the physical vertical coordinate of the bottom bed, A_v is the turbulent momentum diffusion coefficient (eddy viscosity) (m^2/s), g = acceleration due to gravity (m/s^2), ρ_w is actual water density (kg/m^3), ρ_0 is the reference water density (kg/m^3), b is buoyancy and τ_{xz} and τ_{yz} are the vertical shear stresses in the x and y directions (Pa).

3.1.1 Solute transport

Solute transport modelling is a feature of some CFD models, providing the opportunity to investigate how temperature, salinity, nutrients and other solutes may behave in a given scenario. Since it is proposed in this thesis to

amend the calculation for dissolved phosphate levels based on salinity, the theoretical background associated with the solute transport equations is discussed below.

The generic transport equation in EFDC for a dissolved or suspended constituent C (e.g. salinity or temperature) may be expressed as:

$$\begin{aligned} \frac{\partial HC}{\partial t} + \frac{\partial HuC}{\partial x} + \frac{\partial HvC}{\partial y} + \frac{\partial wC}{\partial \sigma} & \quad 3.7 \\ & = \frac{\partial}{\partial x} \left(HA_x \frac{\partial C}{\partial x} \right) + \frac{\partial}{\partial y} \left(HA_y \frac{\partial C}{\partial y} \right) + \frac{\partial}{\partial \sigma} \left(\frac{A_b}{H} \frac{\partial C}{\partial \sigma} \right) + Q_c \end{aligned}$$

where C is the concentration of the variable (mg/L) (e.g. salt, heat), A_x and A_y are the turbulent diffusivities in the x and y directions respectively (m^2/s), A_b is the vertical turbulent eddy diffusivity (m^2/s) and Q_c represents internal and external sources and sinks, including subgrid scale horizontal diffusion.

The last three terms on the left-hand side of Equation 3.7 represent the advective transport, and the first three terms on the right-hand side (RHS) represent the diffusive transport.

3.2 Turbulence closure

The RANS equations can be closed to the effects of turbulence using either an eddy viscosity model, or via transport equations for Reynolds stresses, i.e. a Reynolds-Stress Model (RSM). RSM is extremely computationally intensive, and therefore in many cases does not provide a practical solution to a modelling application.

As such, the RANS equations are often coupled with eddy viscosity turbulence models, the most common of which is the k- ϵ model, to simulate mean flow characteristics for turbulent flow conditions (Launder and Spalding, 1974). This is a two-equation model which gives a general description of turbulence, providing an approximation of the turbulent kinetic energy and its rate of dissipation, at a far less computationally intensive scale than RSM.

Equations 3.1 - 3.7 provide a closed system for the variables u , v , w , p , ζ , ρ , and C , provided that the vertical turbulent or eddy viscosity and diffusivity, A_v and A_b , are specified. In EFDC the terms are provided by the second moment turbulence closure model initially developed by Mellor & Yamada (1982) and modified by (Galperin *et al.*, 1988). In this model, the vertical turbulent viscosity and diffusivity are related to the turbulent intensity, q^2 (m^2/s^2), a turbulent length scale, l (m), and the Richardson number, R_q , by the following equations:

$$A_v = \phi_v q l = 0.4(1 + 36R_q)^{-1}(1 + 6R_q)^{-1}(1 + 8R_q)ql \quad 3.8$$

$$A_b = \phi_b q l = 0.5(1 + 36R_q)^{-1}ql \quad 3.9$$

$$R_q = \frac{gH\partial_z b}{q^2} \frac{l^2}{H^2} \quad 3.10$$

where ϕ_v and ϕ_b are used as stability functions to account for changes to vertical mixing or transport in vertically density stratified environments.

Two transport equations determine the turbulence intensity and turbulence length scale:

$$\begin{aligned} \frac{\partial Hq^2}{\partial t} + \frac{\partial Huq^2}{\partial x} + \frac{\partial Hvq^2}{\partial y} + \frac{\partial Hwq^2}{\partial z} & \quad 3.11 \\ & = \frac{\partial \left(\frac{A_q \partial_z q^2}{H} \right)}{\partial z} + Q_q + 2 \frac{A_v}{H} ((\partial_z u)^2) + (\partial_z v)^2 \\ & + 2gA_b \partial_z b - 2H(B_1 l)^{-1} q^3 \end{aligned}$$

$$\begin{aligned} \frac{\partial Hq^2 l}{\partial t} + \frac{\partial Huq^2 l}{\partial x} + \frac{\partial Hvq^2 l}{\partial y} + \frac{\partial Hwq^2 l}{\partial z} & \quad 3.12 \\ & = \frac{\partial \left(\frac{A_q \partial_z q^2 l}{H} \right)}{\partial z} + Q_l + \frac{E_1 l A_v}{H} ((\partial_z u)^2) + (\partial_z v)^2 \\ & + gE_1 E_3 l A_b \partial_z b - HB_1^{-1} q^3 (1 + E_2 (\kappa L)^{-2} l^2) \end{aligned}$$

$$l^{-1} = H^{-1} (z^{-1} + (1 - z)^{-1}) \quad 3.13$$

where B_1 , E_1 , E_2 , and E_3 are empirical constants, and Q_q and Q_l are additional source-sink terms such as subgrid scale horizontal diffusion. The vertical diffusivity, A_q , is generally taken as equal to the vertical turbulent viscosity, A_v .

3.3 Suspended sediment

Transport formulations for sediment and sorptive contaminants are a feature of some CFD models, ranging in sophistication and complexity.

Cohesive sediment is of particular relevance to this study, as it is to this cohesiveness that phosphate can adsorb, affecting the dissolved proportion. EFDC, in particular, has a very sophisticated and comprehensive sediment module, capable of simulating multiple classes of cohesive and non-cohesive sediments simultaneously, along with their settling, deposition, resuspension, consolidation and sorptive processes. The extensive theoretical background regarding the sediment module can be found in the EFDC Sediment Transport User Manual (Tetra Tech, 2007). The processes of special relevance to this study, the transport equation for suspended sediment and the sorptive process for cohesive sediment are outlined below.

3.3.1 Cohesive sediment

The transport equation for suspended sediment is shown in Equation 3.14:

$$\begin{aligned} \frac{\partial HS}{\partial t} + \frac{\partial HuS}{\partial x} + \frac{\partial HvS}{\partial y} + \frac{\partial wS}{\partial z} - \frac{\partial w_{sj}S}{\partial z} & \quad 3.14 \\ & = \frac{\partial HK_H \partial_x S}{\partial x} + \frac{\partial HK_H \partial_y S}{\partial y} + \frac{\partial \frac{K_V}{H} \partial_z S}{\partial z} + Q_S \end{aligned}$$

where S is the suspended sediment concentration (mg/L), K_v and K_H are the vertical and horizontal turbulent diffusion coefficients (m^2/s), w_{sj} is a positive settling velocity, and Q_S represents external sources and sinks.

3.3.2 Adsorption and phosphate partition coefficient

Nutrients are present in the water column in either a dissolved phase (in solution) or in a particulate phase, where the nutrient is adsorbed to suspended sediments. The distribution between the two phases is controlled

by a number of factors, with the suspended sediment concentration being the most important (Sibley and Myttenaere, 1986; Van Der Kooij *et al.*, 1991).

The transport equation can be solved using a fractional step procedure which decouples the biogeochemical processes terms (kinetic terms) from the physical transport terms. This allows for the addition of new state variables and refinement of kinetic formulations (Park and Kuo, 1996): this is explored later in this thesis through the manipulation of the partition coefficient. The kinetic step is expressed as:

$$\frac{\partial C}{\partial t} = K \cdot C + R \quad 3.15$$

Where C is the concentration of the nutrient (mg/L), K is the kinetic rate (s^{-1}), and R is the source/sink term ($mgL^{-1}s^{-1}$). For phosphate, the kinetic portion of the equation is:

$$\begin{aligned} & \frac{\partial}{\partial t} (PO_4d + PO_4p) && 3.16 \\ & = \sum_{x=c,d,g,m} (FPI_x \cdot BM_x \cdot FPIP \cdot PR_x - P_x) APC_x \cdot B_x \\ & + K_{DOP} \cdot DOP + \frac{\partial}{\partial z} (WS_{TSS} \cdot PO_4p) + \frac{BFPO_4p}{\Delta z} \\ & + \frac{WPO_4t}{V} \end{aligned}$$

where c , d , g and m refer to the four algal groups, cyanobacteria, diatoms, green algae and macroalgae respectively. PO_4d is dissolved phosphate (g/m^3), PO_4p is adsorbed phosphate (g/m^3), FPI_x is the fraction of

metabolised phosphorus by algal group produced as inorganic phosphorus, $FPIP$ is the fraction of predated phosphorus produced as inorganic phosphorus, WS_{TSS} is the settling velocity of suspended solid (m/day), $BFPO_4d$ is the sediment water exchange flux of phosphate (g/m²/day), and WPO_4t is the external loads of total phosphate (g/day).

The complex interaction between the algal groups and phosphate are not considered as part of the research within this thesis, which focuses on the sediment interaction. The dissolved and adsorbed phosphate fractions in the water column are determined by the equilibrium partitioning of their sum as a function of total suspended sediment concentration and are expressed as:

$$PO_{4d} = \frac{1}{1 + K_d TSS} PO_{4t} \quad 3.17$$

$$PO_{4p} = \frac{K_d TSS}{1 + K_d TSS} PO_{4t} \quad 3.18$$

Where PO_{4t} is the total phosphate (g/m³), TSS is the total suspended sediment concentration (g/m³), and K_d is the partition coefficient described in Section 2.6.1. Given that K_d is the ratio of the adsorbed to the dissolved phosphate it is expressed as:

$$K_d = \frac{PO_{4p}}{PO_{4d}} \frac{1}{TSS} \quad 3.19$$

There is very limited data available in current literature regarding the value of the phosphate partition coefficient K_d , thus implementing the empirical link from Kadiri *et al.* (2012) in the hydraulic model is a useful improvement. The value that will be used for K_d in this study is 0.5 L/g, as used by Wang (2011), and is of the same order as the partition coefficient used by Abdulgawad (2010).

3.4 Chapter summary

The governing equations of hydrodynamics, mass, solutes and sediment are described within this chapter to provide the theoretical background for the development of a hydraulic model. Chapter 4 describes the numerical implementation of these governing equations in EFDC.

Chapter 4

Numerical model details

4.1 Introduction

This chapter describes the EFDC model in detail: the implementation of the governing equations; the models developed as part of this research study; and the refinements to the EFDC source code to improve hydro-environmental modelling.

4.2 Implementation of governing equations

To make the governing equations suitable for numerical implementation, the governing equations described in Chapter 3 must be replaced by a set of algebraic equations which calculate the variables at a finite set of points in the space-time domain (Casulli, 1990; Anderson and Wendt, 1995). The process of obtaining algebraic equations from the partial differential governing equations is called discretization, and can largely be split into three categories (Mattiussi, 1997): finite difference methods; finite element methods; and finite volume methods.

The finite element method divides a domain into a finite number of small sub-domains (finite elements), yielding approximate values of the unknowns at the discrete points determined by the mesh (Logan *et al.*, 2007). The sets of element equations for the finite elements are recombined into a global system to model the entire problem and return the solution (Zienkiewicz, Taylor and Zhu, 2013). A large advantage of the method is the largely unconstrained sub-division of the domain into the smaller elements, generally allowing for a fully unstructured mesh and providing the capability to represent very complex geometries (Bathe and Wilson, 1976; Zienkiewicz *et al.*, 1977; Reddy, 1993). This does, however, result in a computationally

expensive algorithm, with a large number of calculations being required at each model time-step (Ferziger and Peric, 2002).

Finite volume method is a discretized method based on the integral form of the conservation laws rather than pure continuum mathematics concepts (Roache, 1998). The domain is divided into a number of non-overlapping finite control volumes, encompassing the entire domain of the study area. The differential equation is then integrated over each control volume (Versteeg and Malalasekera, 2007) before assembling the equations into a discrete algebraic system to solve. The finite volume is considered to be more conceptually intuitive than other discretisation methods (Alcrudo, 2004), and is widely used in industry CFD modelling (Neelz *et al.*, 2010) due to the flexibility offered by the mesh that control volumes allow, and the relative algebraic simplicity enabling highly parallelised codes and faster model run times.

Finite difference method is based upon a Taylor expansion to approximate the differential equations (Anderson and Wendt, 1995). The Taylor series describes the derivatives of a variable as the differences between the values of the variable at neighbouring points. The order to which the Taylor series is developed dictates the accuracy of the approximation of the solution. The finite difference method had traditionally been the discretisation method of choice for industry standard software, due to its simplicity of numerical implementation and hence less intensive computational power requirements, and innate compatibility with gridded ground models (Alcrudo, 2002; Néelz, Pender and Britain, 2009). A significant limitation of

the finite difference method is that due to geometric inflexibility it is largely applied to structured grids. This has led to a significant decline in the popularity of finite difference based models in flood modelling consultancy in recent years, due to an increased requirement for highly detailed meshes capable of representing very complex geometries.

The numerical methods for discretisation are further divided into three main categories: explicit schemes; implicit schemes and; semi-implicit schemes (Bui, 2010).

In an explicit or forward-looking scheme, the solution at the next time level, i.e. $n+1$ is calculated from the known solution at the previous time step. As a result, the scheme is relatively simple to program in comparison with an implicit scheme and is therefore popular amongst researchers and software developers. A key advantage of the programming simplicity is the opportunity to parallelise the code, potentially significantly reducing model run-time. It is this advantage that has led to a rise in the usage of explicit scheme models in flood modelling consultancy, such as with the software package Infoworks ICM. Explicit schemes are conditionally stable and do not necessarily guarantee numerical stability. To provide stability for explicit schemes and prevent the appearance of numerical oscillations in the solution, the Courant-Friedrichs-Lewy (CFL) condition must be satisfied (Lax and Wendroff, 1960; Courant *et al.*, 1967). This states that:

$$C = \frac{u_x \Delta t}{\Delta x} + \frac{u_y \Delta t}{\Delta y} \leq C_{max} \quad 4.1$$

where u and v are velocity in the x and y directions (m/s), Δt is the time step (s), Δx is the length interval (m) and C is the dimensionless Courant number. The Courant number is typically set to 1 for explicit schemes, to try to ensure convergence is still achieved. Conceptually this can be imagined as a fluid particle not being permitted to travel through more than one cell at each time step. In complex geometries with very high mesh resolution this can result in a miniscule time step, in the order of hundredths of a second. The time step becomes unrelated to the physics behind the problem and can lead to an enormous number of time steps required, potentially rendering any gains from parallelisation of the explicit scheme computationally pointless.

Implicit or backward-looking schemes use an iterative technique to obtain a solution to the differential equations using the variables calculated at the previous time step as well as the variables calculated at the present time step, coupling together all cells across domain within the computational procedure. Hydraulic effects can therefore be transmitted across the entire computational mesh in an implicit scheme, but at a significantly increased computational cost and coding complexity. Implicit schemes are unconditionally stable and generally allow longer time steps, more in keeping with the reality of the modelled event. Despite unconditional stability, a CFL limit of 8 is generally used in practice to ensure a numerically accurate solution. The additional computational cost per time step of an implicit scheme can often render an implicit solver faster than an explicit method that requires a far greater number of time steps. However, the coding complexity makes implicit schemes difficult to fully

parallelise, and a parallelised explicit code will generally outperform a serial implicit code.

A semi-implicit scheme, such as that used by EFDC, treats some derivatives explicitly and others implicitly. This brings together the advantage of the absolute solution consistency of implicit schemes, while gaining some of the performance advantages in using the explicit method where deemed appropriate. Larger timesteps are permitted than with explicit methods, and the computational cost per time step is less than that of a fully-implicit scheme.

4.3 EFDC

The Environmental Fluid Dynamics Code (EFDC) is an open-source modelling package for simulating 3D flow, transport and biogeochemical processes in surface water systems (DSI, 2013). It was developed at the Virginia Institute of Marine Science (Hamrick, 1992), originally for coastal and estuarine modelling, but has since been used for a wide variety of hydrodynamic and water quality studies and applications worldwide, and in particular in partnership with the US Environmental Protection Agency (US-EPA, 2006a, 2006b). EFDC is a complex, sophisticated model capable of simulating a range of hydrodynamic, water quality and sediment effects, including cohesive and non-cohesive sediment transport, the transport and fate of toxic contaminants, dissolved oxygen and nutrient interaction (eutrophication), vegetative resistance, wetting and drying, hydraulic structures, and near-shore wave induced currents.

Four major modules comprise the EFDC model: the hydrodynamic model, the water quality model, the sediment transport model, and the toxics model, as shown in Figure 4-1 below:

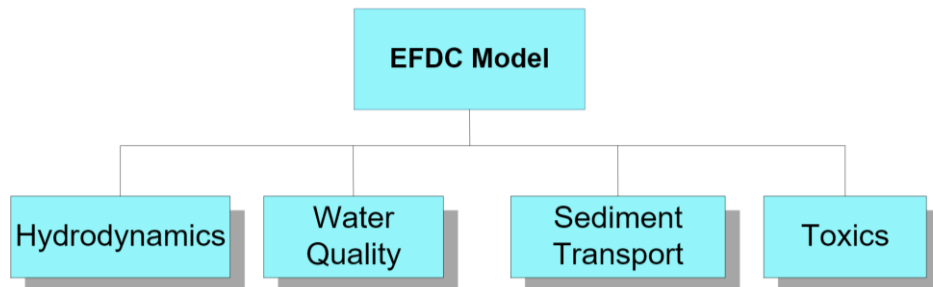


Figure 4-1 - EFDC modules (DSI, 2013)

The hydrodynamic model is further divided into the six transport models shown on Figure 4-2:

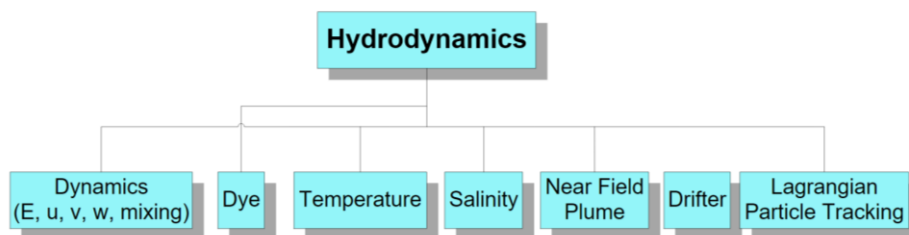


Figure 4-2 - Hydrodynamic modules (DSI, 2013)

EFDC solves the 3D vertically hydrostatic, free surface, turbulent averaged equations of motion for a variable density fluid (Hamrick, 1992). The Mellor-Yamada level 2.5 turbulence closure scheme (Mellor and Yamada, 1982; Galperin *et al.*, 1988) described in Chapter 3 is implemented in the transport equations. A semi-implicit finite difference scheme solves the equations of motion to second order accuracy, on a staggered or C grid.

The model uses a stretched or sigma coordinate in the vertical (Figure 4-3), and a curvilinear, orthogonal horizontal grid. The curvilinear grid allows for a higher-resolution grid around particular areas of interest, for example hydraulic structures, and larger grid size in areas where fine resolution isn't required, for example in the open sea. This particularly suits estuarine and coastal modelling where greater detail is likely to be required around the coast than in the ocean.

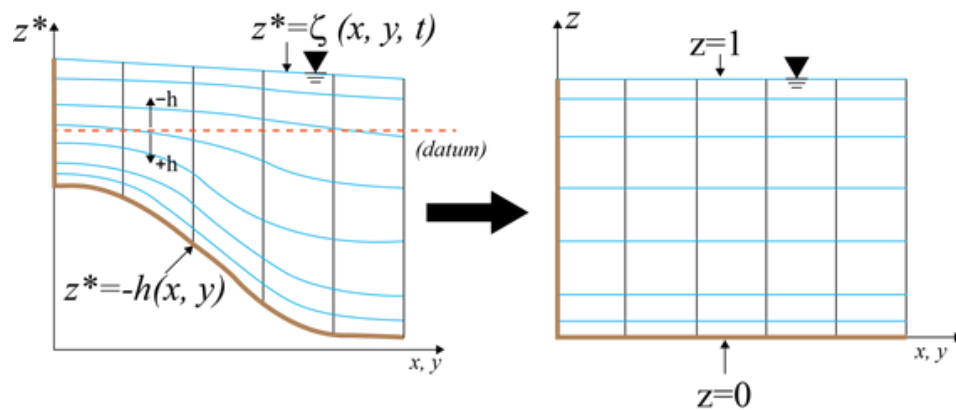


Figure 4-3 - Vertical sigma coordinate system in EFDC (Craig, 2017)

The curvilinear grid is created in either DELFT's RGFGGrid (Delft, 2006), or with DSI's tool CVLGrid (DSI, 2016). Both require an outline of the intended model boundary, onto which the user creates splines to dictate areas of fine and coarse resolution when the grid is formed, as shown in Figure 4-4:

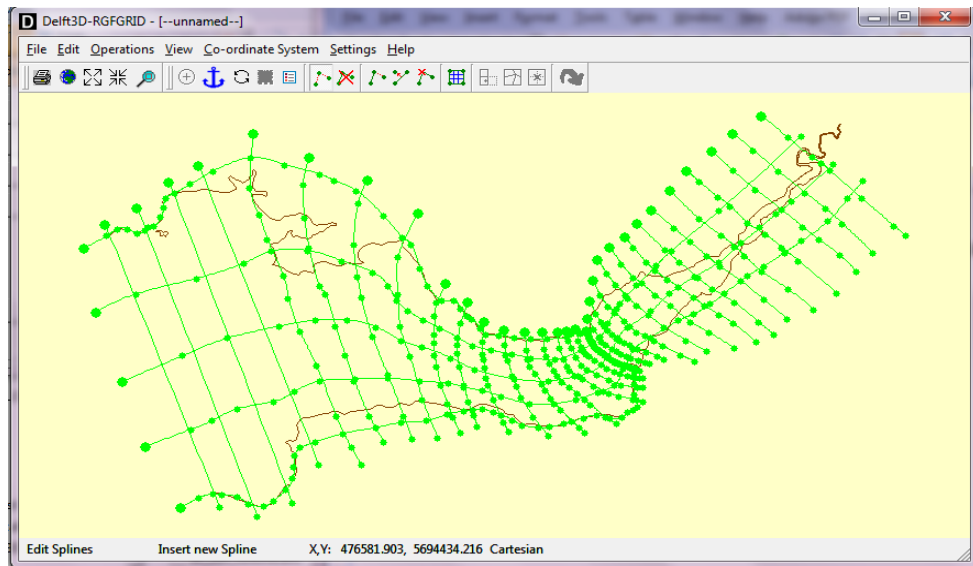


Figure 4-4 - RGFGrid screenshot - Severn Estuary grid creation

The original EFDC model was written in Fortran 77 but subsequent additions and refinements have been written in FORTRAN-90. Although the model is open-source, an executable is provided by DSI for users who do not need to make changes to the programming. A large number of input files are required, specifying the grid arrangement, bathymetry and boundary conditions. These can be produced through either the Graphical User Interface (GUI), EFDC Explorer, or accessed via a text editor.

EFDC was chosen for this research for the following key reasons:

- It is open-source;
 - A barrage module had been added by Zhou (2014), which could be further developed to improve barrage and lagoon modelling;
 - It uses a curvilinear grid - ideally suited to coastal and estuarine modelling, particularly where high resolution would be required around the hydraulic structures associated with barrages and lagoons;
- and

- It is capable of water quality and sediment transport simulation, enabling the modelling of suspended sediment, salinity and phosphate, facilitating the implementation of the improved phosphate adsorption calculation.

4.3.1 EFDC models

Two models were set up to implement the refinements made as part of this research study and to demonstrate their impact. To further the understanding of the potential hydro-environmental impacts of tidal range generating proposals, the Continental Shelf Model (CSM) was used. This huge model domain was demonstrated to be required to fully capture the potential impacts of a Severn Barrage on water levels (Zhou *et al.*, 2014a), as discussed in Chapter 2. A second model domain, The Severn Estuary Model (SEM) was used in 2D and 3D to show the phosphate modelling improvements and impact of the momentum equation updates respectively.

The CSM domain is shown in Figure 4-5, extending to beyond the Continental Shelf, to avoid impacts on the open boundary from the alteration to the tidal regime caused by the inclusion of a barrage. The grey area represents inactive or land cells, leaving a very large active area of simulation, approximately 846,000 km², with cell sizes ranging from 50×50 m² in the areas of specific interest, e.g. around the barrage, to 5000×5000 m² in the open ocean. The large active area is spread over a wide range of bottom elevations, from 5000 m below Ordnance Datum in deep water, to 5 m above Ordnance Datum in the Severn Estuary, along its narrower reaches.

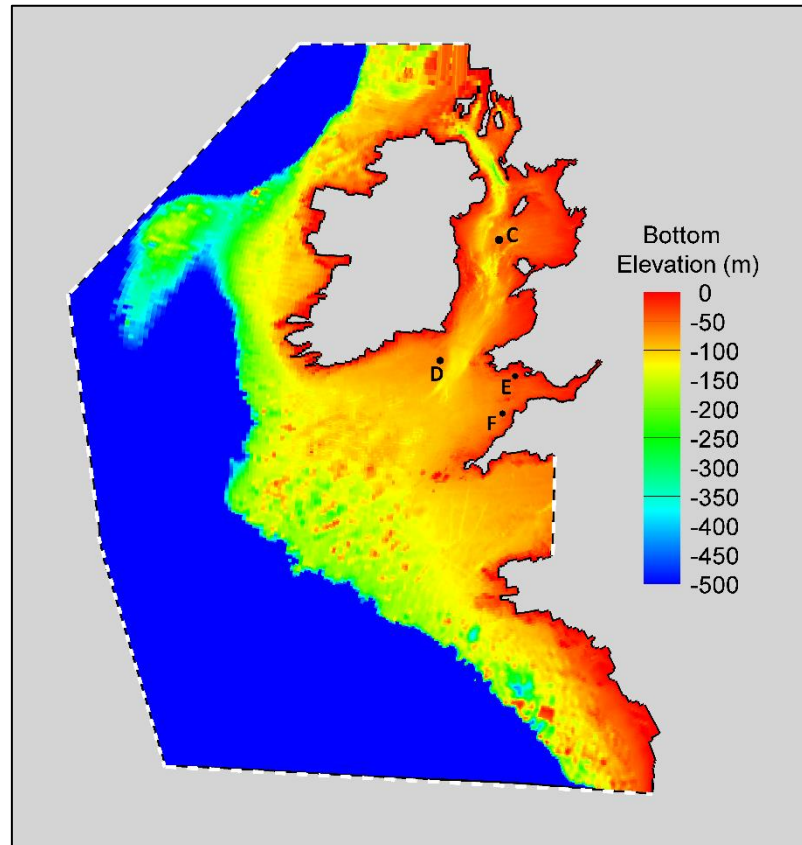


Figure 4-5 - Computational domain of the CSM, with black dots showing example validation sites and dotted lines to indicate open boundaries

A typical neap-spring tidal cycle for a period of 14 days, from 1 to 14 March 2005, was used for this study. The dotted lines in Figure 4-5, demonstrate the open boundaries of the model domain, at which tidal elevations were specified. These open boundaries were split into a total of 1331 distinct sections, and elevations series for each section are specified along the model boundary. The tidal elevation used as the model boundaries were obtained from the MIKE21 global model (Warren and Bach, 1992; DHI, 2014).

The unaltered CSM, without the inclusion of a barrage structure, had been validated in previous studies (Zhou *et al.*, 2014; Zhou *et al.*, 2014a). To add further granularity to the validation of the model, the water levels, depth averaged current velocities and current directions were compared with

measured field data from Admiralty Charts at locations in the Irish Sea, Celtic Sea and Bristol Channel. Figure 4-6 shows the typical validation results for 4 sites, as displayed in Figure 4-5, with similar comparisons observed at other validation sites. To measure the predictive capability of the EFDC CSM, the Nash-Sutcliffe model efficiency coefficient (NSE) was used. The NSE, presented by (Nash and Sutcliffe, 1970), is based on the following equation:

$$NSE = 1 - \frac{\sum_{i=1}^n (O_i - S_i)^2}{\sum_{i=1}^n (O_i - \bar{O})^2} \quad 4.2$$

where O_i is the observed data, S_i is the simulated data, and \bar{O} is the mean of the observed data. The NSE result can range from $-\infty$ to 1, where an efficiency of 1 corresponds to an exact match between predicted and observed data, and 0 indicates that the mean of the observed data is as good a predictor as the model.

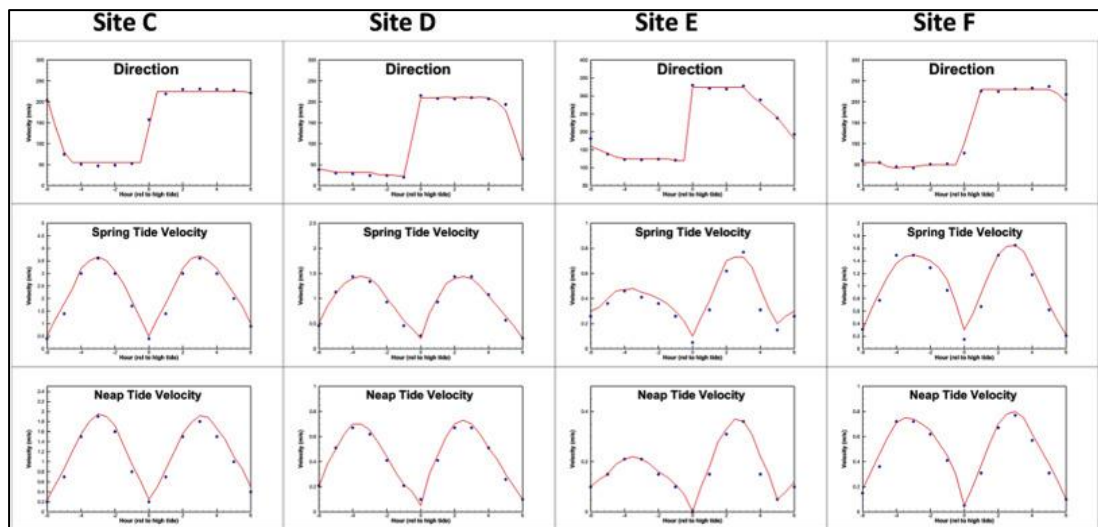


Figure 4-6 - Comparisons between observed (blue dots) and calculated (red lines) tidal stream current speeds and directions

The NSE for the model predictions for current direction were excellent, with an efficiency of 0.86. The efficiencies for the spring and neap tide velocities were 0.82 and 0.86 respectively. These very high NSE results indicated that the model was a strong predictor for tidal directions and velocities in the Continental Shelf Domain, allowing for the inclusion of the barrage module so that the impacts of tidal range renewable proposals, any changes brought about by modifications to the hydraulic structure representation, and the sensitivity of the modelling to changes in the discharge coefficient parameter could be assessed.

For both the CSM and the SEM, the EFDC barrage module requires inputs for the starting and minimum head for generation, to determine when to move between the four phases of operation of the ebb-generating barrage seen in Figure 2-2. As per the STPG proposal, a starting head of 4 m and a minimum head for generation of 2 m were used.

The SEM was developed as part of this research study to model the following:

- The impact of a correction to the momentum calculation through turbines in the Severn Barrage, in both 2D and 3D;
- The impact of different configurations of turbines in the Bridgwater Bay Lagoon, and how 2D modelling can be used to optimise a lagoon design; and
- The impact of the implementation of the salinity linked partition coefficient on phosphate levels in the Severn Estuary.

The adjustment to the momentum calculation was expected to have near-field effects, in the vicinity of the turbines only. Similarly, the Bridgwater

Bay Lagoon was not expected to have impacts outside of the Bristol Channel, and phosphate levels are not of concern in the open sea. As such, a domain as large as the CSM's was not required for these aspects of research, and a smaller domain as shown in Figure 4-7, was used in order to reduce computational requirements:

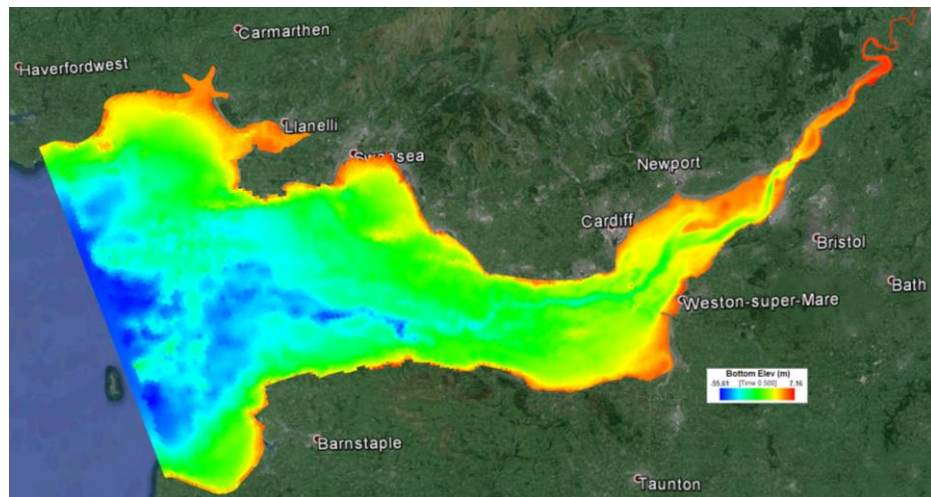


Figure 4-7 - SEM domain, showing bathymetry of the Severn Estuary and Bristol Channel

The 2D model used to show the impact of the refinement to the momentum representation, and the improvement to phosphate predictions had around 55,000 cells, ranging in size from 50x50 m around the barrage site, to 500x500 m at the open boundary at the Bristol Channel. When running the simulation in 3D, 5 vertical layers were used, giving around 250,000 cells.

A more refined SEM was used to model the Bridgwater Bay Lagoon and demonstrate the applicability of 2D models in assisting with scheme optimisation. The refined SEM had over 500,000 cells, providing much greater detail around the lagoon hydraulic structures.

4.4 Refinement to hydraulic structure representation

The following refinements to turbines, sluices and momentum calculations were made as part of this research study, and assessed via the two EFDC models described above.

4.4.1 Turbines and sluice operation

Turbines are typically represented in 2D hydraulic models in one of two ways. The first method uses the orifice equation (Equation 2.4) described in Chapter 2, and the second method uses a Head-Discharge curve, or hill chart, typically obtained experimentally (Goldwag and Potts, 1989; Falconer *et al.*, 2009). Prior to this research study, only the former representation had been implemented into the EFDC barrage modelling module, and so the functionality was added to improve the module and provide the first accurate assessment of the far-field impacts of the barrage, and also to assess the importance of realistic hydraulic structure representation.

Sluice gates were initially represented in the EFDC barrage module as cells which could be switched from open to closed, or wet to dry. This does not reflect the physical reality of the scenario, and so a further improvement was made to the module to amend the discharge through the sluice gates to that calculated by the orifice equation.

The updated representation to turbines and sluices was tested using the EFDC CSM, for a Severn Barrage generating on the ebb tide only, as originally proposed by the Severn Tidal Power Group (STPG, 1989). In this scheme, 166 large sluices and 216 x 40 MW bulb-turbines would allow the basin upstream of a 16 km barrage to fill with the incoming tide. Once high water is

reached, the sluices and turbines are closed and a head difference either side of the barrage structure is caused by ebbing tide on the seaward side of the barrage. Once a sufficient head differential is achieved, the 216×40 MW bulb-turbines are opened for electricity generation, until the minimum head at which they can operate effectively is reached. The water is held at a constant level until the next flood tide causes the sea level outside of the barrage to rise above the basin water level, at which point the sluices and turbines are re-opened and the basin refilled.

A ramp function is employed to represent the gradual opening and closing of the sluice gates and turbines. This representation is more realistic than turning the sluice gates and turbines on or off and removes the numerical oscillations caused by instant opening of the hydraulic structures, as suggested by Ahmadian *et al.* (2010). This ramp function is expressed in the form of a half-sinusoidal function, where an opening or closing time is set according to the expected operation times, i.e. typically in the region of 10-20 minutes.

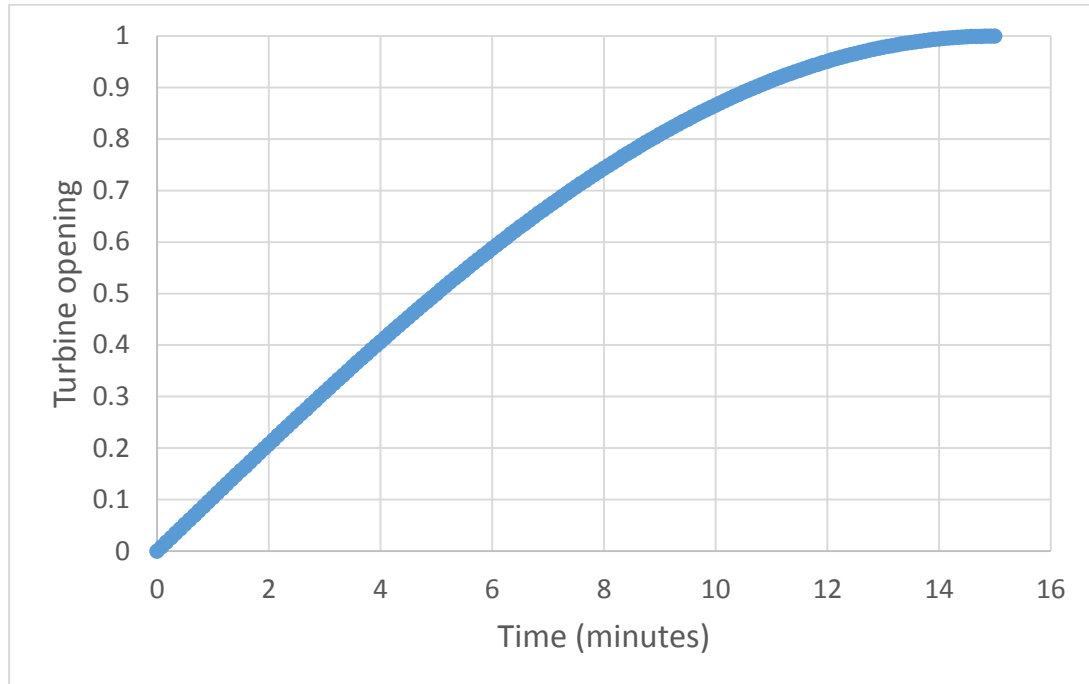


Figure 4-8 - Turbine half-sinusoidal ramp function

Figure 4-8 shows the gradual opening of the turbine using the half-sinusoidal function and an opening time of 15 minutes.

4.4.2 Momentum correction

A further adjustment was made to the calculation of momentum through hydraulic structures to improve their representation. The technique of applying an internal boundary, described in Section 2.5.1, was used to transfer mass and momentum across or through hydraulic structures. Although the EFDC barrage module takes into account the sluice or turbine flow-through area when calculating the discharge, or rate of volume transferred across the boundary, the momentum calculation was performed by the EFDC internal solution. The momentum was therefore calculated as if the volume was added to the entire cell depth and width, when in reality it is added to the cell via the turbine or sluice flow-through area.

The correction was therefore applied such that at turbine or sluice downstream cells, the cell side area (water depth x cell width) was overwritten by the flow-through area of the hydraulic structure.

This was tested and compared using a 2D and a 3D scenario with the SEM. For the 3D scenario, all of the discharge and hence momentum was added to the second of five vertical layers, where the first layer is in contact with the bed.

Impacts of the refinements to hydraulic structure representation are presented and assessed in Chapter 5. With the improvements in place, the refined SEM was used to demonstrate the applicability of 2D models to assist with the optimisation of tidal lagoon design, presented in Chapter 6.

4.5 Refinement to phosphate modelling

In order that the new phosphate partition coefficient could be implemented, salinity, total phosphate and suspended sediment had to be simulated and validated.

4.5.1 Salinity and phosphate

Salinity was applied via the open boundary at the Bristol Channel, setting the salinity along this line to that of the open sea, 35 parts per thousand. With very limited field data gathered for salinity in the Severn Estuary it is difficult to validate the SEM's capability for predicting salinity levels. The SEM was used in Zhou *et al.* (2014) to assess the impact a barrage may have on salinity, and it was observed that although EFDC's predicted salinity level patterns are similar to those observed patterns reported by Stephens (1986)

and Uncles (1984), the results could not be considered conclusive without additional field data.

Phosphate in rivers and estuaries are chiefly influenced by sewage treatment work outflows, and as such, phosphate levels are heavily affected by population density. The figures below give the locations for the main industrial discharge points and sewage works along the estuary:

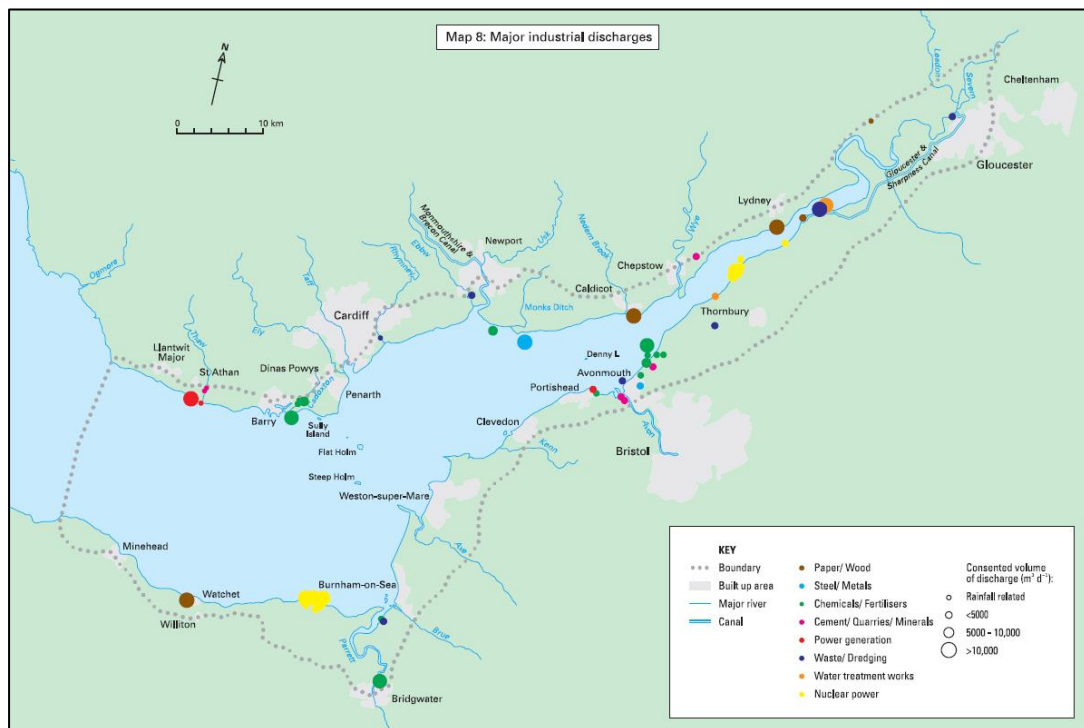


Figure 4-9 - Major industrial discharges (Severn Estuary Partnership, 2001)

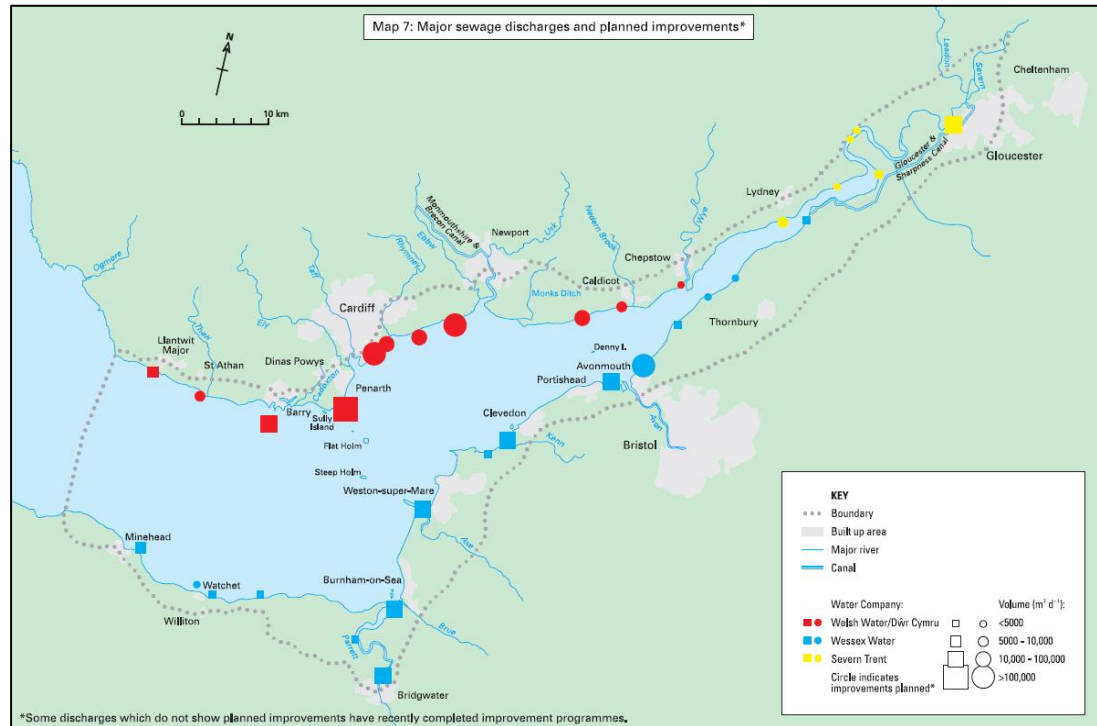


Figure 4-10 - Major sewage discharges (Severn Estuary Partnership, 2001)

The Environment Agency and Natural Resources Wales were contacted by the Cardiff Hydro-environmental Research Centre to obtain phosphate loads from the Severn Estuary tributaries and wastewater treatment plant mean outflows. Sufficient information was provided so that a total of 42 phosphate input series could be applied to the SEM. There was, however, no comprehensive source of field data against which the model could be validated, other than very limited sampling undertaken in an undergraduate adsorption study (Bray, 2009), and other limited data collected as part of the study that established the new phosphate partition coefficient (Kadiri and Bockelmann-Evans, 2012). The available field data was not sufficient for phosphate modelling validation, and although the computed phosphate levels were similar to the limited field data, the results can only be considered preliminary without additional verification.

4.5.2 Sediment parameters

Sediment in the Severn Estuary is suspended largely due to tidally induced currents (Kirby and Parker, 1983). An Environment Agency report (Stapleton *et al.*, 2007) provided suspended sediment concentrations for two sites, Minehead and Southerndown, against which the predicted suspended sediment concentrations could be validated.

A cohesive sediment class was set up in EFDC, with the default parameters for specific volume, specific gravity and settling velocity. An initial water column suspended sediment concentration of 20 mg/L was set. A series of calibration simulations were then processed, varying the initial concentration of bed mass until the results were in reasonable agreement with the field data collected at Minehead, using a tidal time series to coincide with the sampling date and times.

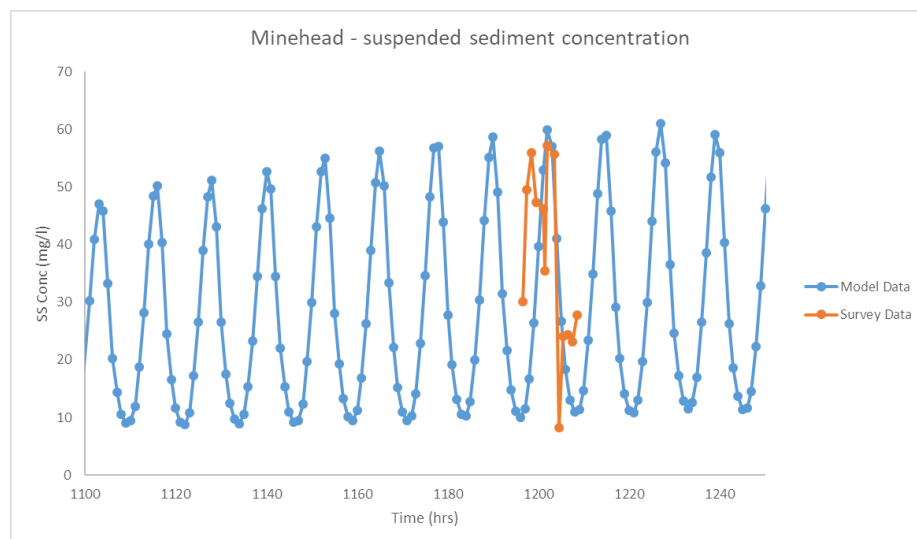


Figure 4-11 - Predicted suspended sediment concentration at Minehead, plotted against survey data

Figure 4-11 demonstrates that the model was simulating the suspended sediment concentration at Minehead to sufficient accuracy. The agreement was best when an initial concentration of bed mass of 20000 g/m² was set. The model was validated against the second set of collected field data, at Southerndown, to produce a comparison of comparable accuracy, as seen in Figure 4-12:

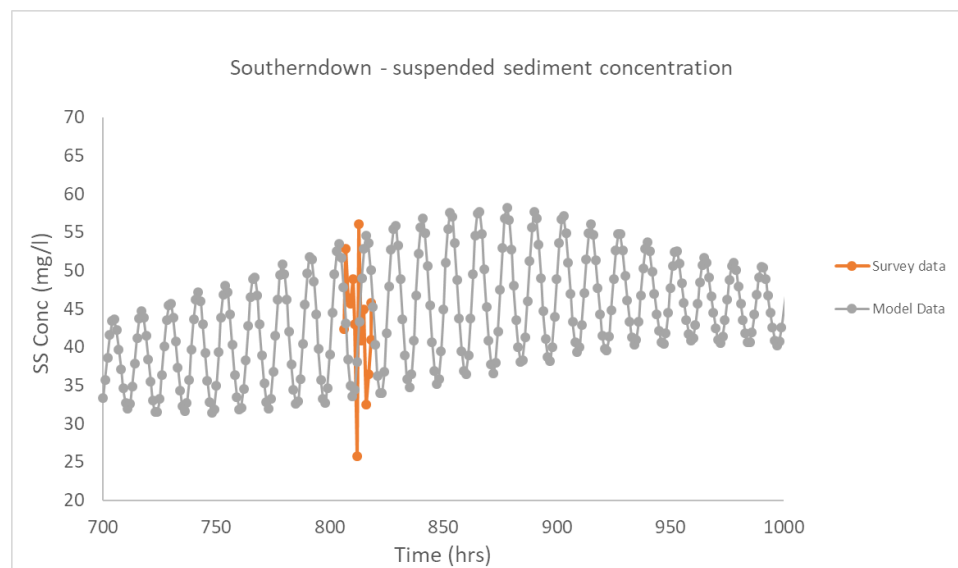


Figure 4-12 - Predicted suspended sediment concentration at Southerndown, plotted against survey data

In the absence of further field data against which to validate the model, the suspended sediment predictions from the SEM were deemed sufficiently accurate to pursue with the implementation of the partition coefficient.

4.5.3 Implementation of updated partition coefficient

Experimental data (Kadiri and Bockelmann-Evans, 2012) showing a strongly correlated link between salinity and the phosphate partition adsorption coefficient produced a range of partition coefficients dependent upon the sediment concentration, as seen in Table 4-1:

Table 4-1 - Coefficients of $K_d = AS^{-b}$ for the suspended sediment concentrations used in the study, reproduced from (Kadiri and Bockelmann-Evans, 2012)

Suspended sediment concentration (g/L)	$K_d = AS^{-b}$		
	A	b	r^2
1	664.8	0.10	0.82
2	439.6	0.12	0.94
3	352.3	0.17	0.97

The relationship was incorporated into EFDC as a piecewise function, applying a partition coefficient to the corresponding suspended sediment concentration.

To assess the influence of the implementation of the salinity linked partition coefficient, the SEM was run initially without suspended sediment, providing total phosphate levels in the estuary. The model was then run with the sediment module active, and using a range of constant partition coefficients. Finally, the model was run with the variable, salinity-linked partition coefficient and the results compared in Chapter 7.

4.6 Use of High Performance Computing

High-performance computing (HPC) is a rapidly evolving area of research and is becoming increasingly important in CFD modelling applications. Ever-more computationally intensive and detailed models would become impractical to run without the advances to programming and computer hardware.

There are various modes of parallelisation that can be explored to improve the efficiency of a CFD code. The first is Graphics Processing Unit (GPU) parallelisation, whereby a code is adapted to run on a graphics card as

opposed to the traditional CPU. This has the advantage of being able to run on potentially thousands of virtual cores, but is a difficult programming task and generally only applicable to explicit codes due to their relative simplicity of structure in comparison with implicit schemes. The second method of parallelisation is using OpenMP, enabling the code to be divided across the multiple cores of a desktop computer. This is relatively simple to implement from a programming perspective, and generally gives a good return of increased efficiency per core added - typically a 500% speed up can be seen in moving from 1 core to 8 in CFD applications (TUFLOW, 2016). The speed increase is, however, limited by the current hardware; commercially available CPUs typically have a maximum of 10-12 cores. With the introduction of each core, a diminished return on speed is achieved through OpenMP parallelisation. The third method is parallelisation using OpenMPI, enabling the code to run on a cluster of networked computers, passing information between CPUs. This is difficult to implement efficiently, as significant information must be passed between CPUs, potentially causing a lot of overhead in data transfer rather than actual model solution. If an efficient code is programmed, however, this method can be used to run a simulation on potentially thousands of cores.

Although EFDC was a serial code, an OpenMP version became available towards the end of this research study. Unfortunately, it was not open-source, and hence not compatible with the barrage module, amendments to hydraulic structures and water quality improvements.

Even with a serial code, however, it is possible to make excellent use of HPC infrastructure in CFD applications. This was particularly relevant to the suspended sediment modelling undertaken in this study, where dozens of calibration runs were required, each taking up to 6 days to complete. On a single desktop PC, this might require weeks to run a range of incrementally adjusted scenarios, but with the HPC facilities available at HPC-Wales, the dozens of simulations were able to be run simultaneously, rapidly increasing the speed with which the model could be calibrated.

4.7 Chapter summary

Chapter 4 described the numerical implementation of the governing equations to the EFDC model. The EFDC model uses a semi-implicit finite difference scheme to solve the equations of motion on a staggered or C grid. The curvilinear grid used by EFDC is ideally suited to tidal renewable modelling, allowing for very high resolution around the hydraulic structures, and larger cell sizes in the open sea to reduce computational demands.

Refinements to the representation of turbines and sluices were implemented to improve the CSM's predictive capability of the impacts of tidal renewable devices. Adjustments to the calculation of volume for hydraulic structures were described, as well as a correction to the calculation of momentum.

The dynamic, salinity-linked partition coefficient was incorporated into the EFDC model as a piecewise function, giving a spatially and temporally variable K_d in place of the literature suggested value.

High-performance computing was identified as a useful tool in hydraulic modelling, even in a case such as this where the code is serial. It provides the opportunity for multiple simultaneous runs, aiding model calibration where potentially hundreds of runs are required.

Chapter 5

Model application 1 - Severn Barrage

5.1 Introduction

To demonstrate the impact of the refinement to the representation of turbines and sluices, described in Section 4.4.1, the ebb-only Severn Barrage was simulated and the results compared with those prior to amendments.

Application of the refinements to hydraulic structure representation demonstrates the following:

- The impact of correct hydraulic structure representation in modelling the Severn Barrage;
- The far-field impacts of the Severn Barrage;
- The sensitivity to the discharge coefficient;
- The importance of correct momentum representation in hydraulic structures; and
- Correct momentum representation in 3D modelling, and the difference between 2D and 3D results.

5.2 Impact of representation of turbines and sluices and far-field impacts of the Severn Barrage

The impact of representation of hydraulic structures in modelling a Severn Barrage was demonstrated with the CSM, as the extended domain model was shown to be necessary to capture all the effects of the barrage and negate the effect on the open boundary.

Two scenarios were modelled to investigate the improved representation of turbines and sluices:

Table 5-1 - Scenarios for hydraulic structure representation

Scenario	Sluice representation	Turbine representation
1	Wet/dry cells	Orifice
2	Orifice	Hill chart on generating, orifice on filling

Scenario 1 represents the original EFDC barrage module, prior to the refinements made in this research study. Scenario 2 included improvements that represented the barrage structure more appropriately, by modelling the sluices and turbines as orifices of different areas during the filling phase, and calculating the turbine flow during power generation from the bulb-turbine hill chart. The flow through sluice gates during the holding and generating phases was set to zero.

Having validated the CSM against Admiralty Chart Data (Bray *et al.*, 2016), the effects of the modifications were investigated by comparing Scenarios 1 and 2. Figure 5-1 below shows points A and B, each of which is 6 km either side of the barrage structure. Points A and B are of particular importance as they are used to determine the operational phase of the barrage in the CSM.

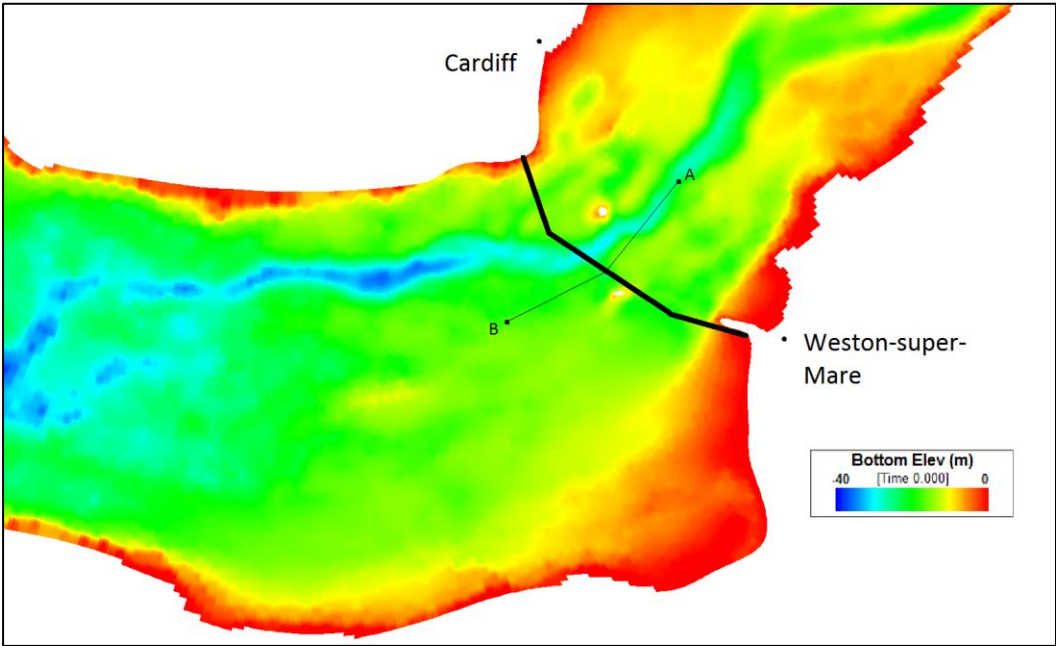


Figure 5-1 - Barrage location and Points A and B, used to demonstrate effects of refinements

Figure 5-2 and Figure 5-3 shown the water level comparisons at Points A and B for Scenarios 1 and 2 respectively.

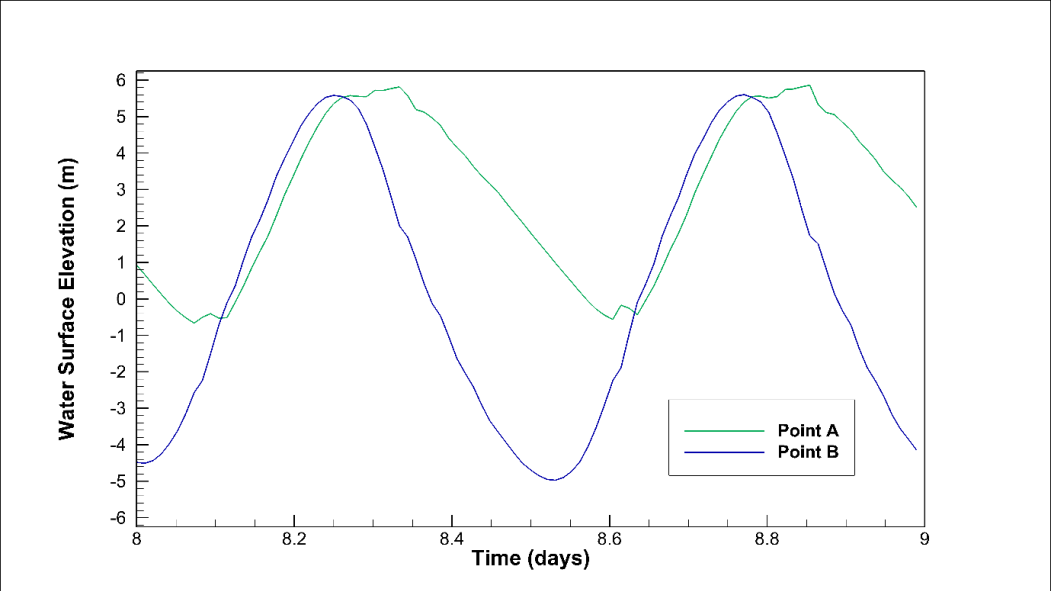


Figure 5-2 - Upstream (green) and downstream (blue) water levels for Scenario 1

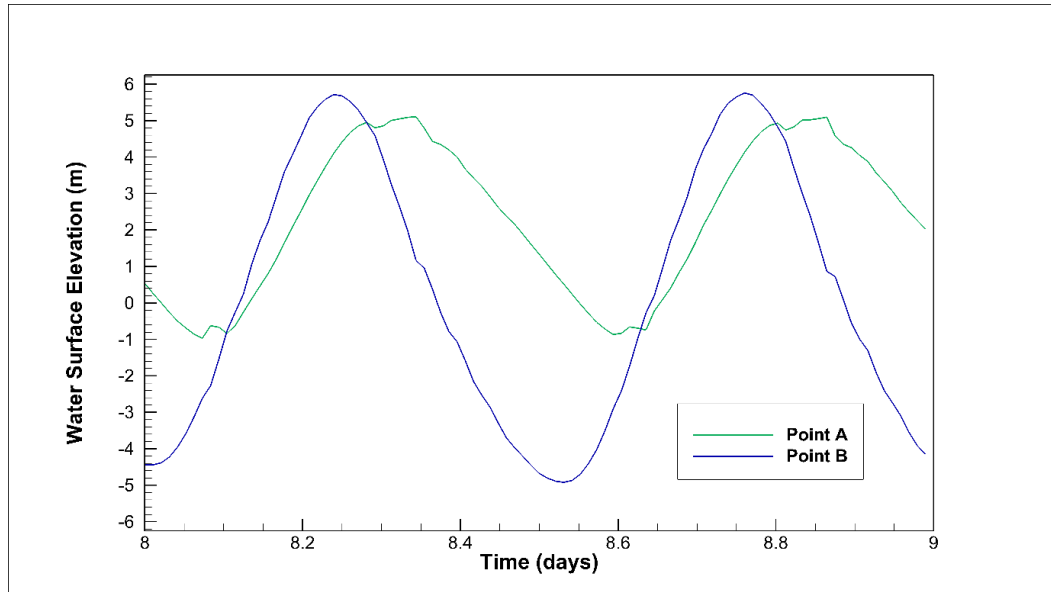


Figure 5-3 - Upstream (green) and downstream (blue) water levels for Scenario 2

It is clear that for Scenario 1 the barrage has had a large impact on the tidal regime upstream of the barrage, substantially raising the minimum water levels. The upstream maximum water levels were not significantly affected, and are higher than the maximum water levels found downstream.

In Scenario 2, the maximum water levels upstream are up to 1 m lower than the prediction levels from Scenario 1; the levels are also lower than the predicted maximum water levels downstream. The minimum water levels upstream are almost unaffected by the changes to turbine and sluice representation. The maximum and minimum upstream water levels predicted for Scenario 2 were similar to those values reported in the literature such as in Ahmadian *et al.*, (2010), where a reduction in upstream maximum water levels of 1 m was produced. Figure 5-4 shows the impact of the refinements on water levels upstream of the barrage, Point A, over a 7-day period. The model has been run for 30 days, to ensure a steady-state

had been achieved. The maximum water levels are reduced at each peak, and correspondingly the minimum water levels are lowered.

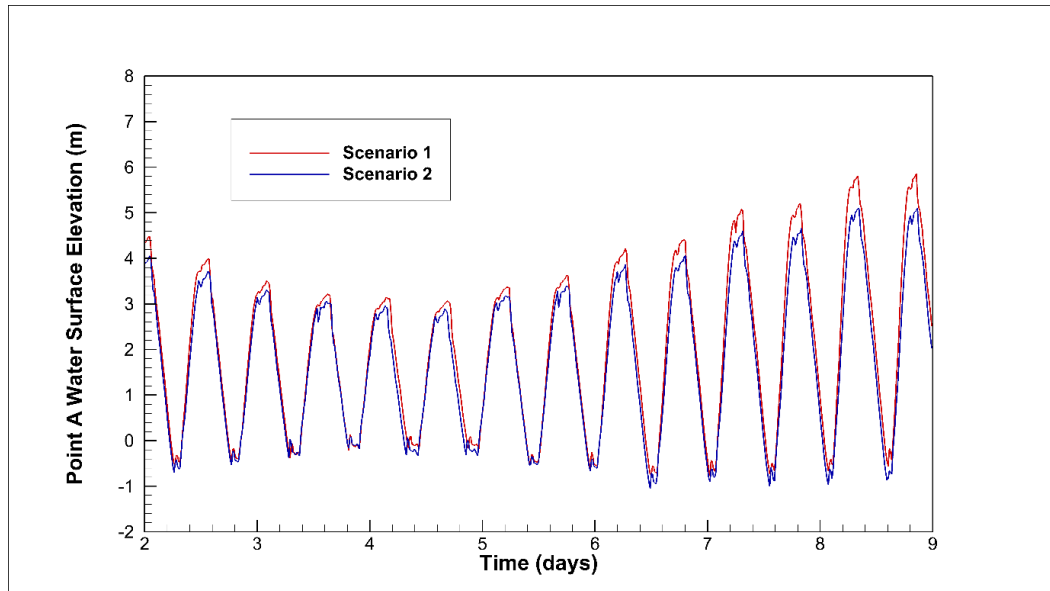


Figure 5-4 - Impact of hydraulic structure refinements on water levels at Point A

Figure 5-5 shows the changes to maximum water levels caused by the inclusion of the Severn Barrage as represented in Scenario 1. Changes to maximum water levels can be seen as far-field as the West-Coast of Scotland. Immediately downstream of the barrage, maximum water levels are reduced, contrary to the impacts shown in Falconer *et al.* (2009), Xia *et al.* (2010), and Ahmadian *et al.* (2014). In Figure 5-6, the changes to maximum water levels caused by the inclusion of the Severn Barrage as represented by Scenario 2 are displayed. The refinements to hydraulic structure representation have reduced the far-field effects, with far less impact seen on the Scottish and Welsh West coasts. The figures imply different effects from the inclusion of a barrage in the Severn Estuary and Bristol Channel, investigated further in Figure 5-7 through subtracting the maximum water levels in Scenario 1 from Scenario 2.

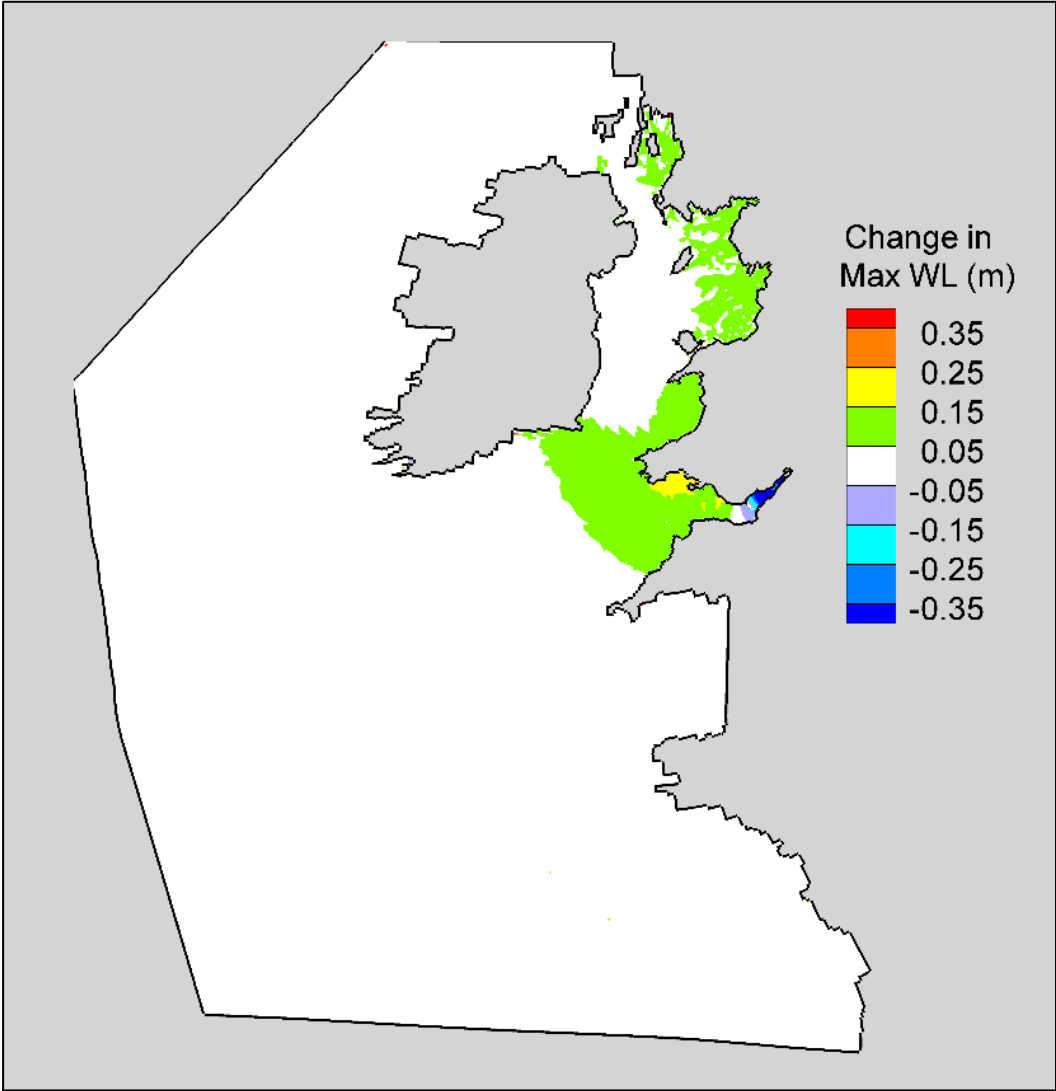


Figure 5-5 - Domain-wide maximum water level changes caused by barrage Scenario 1

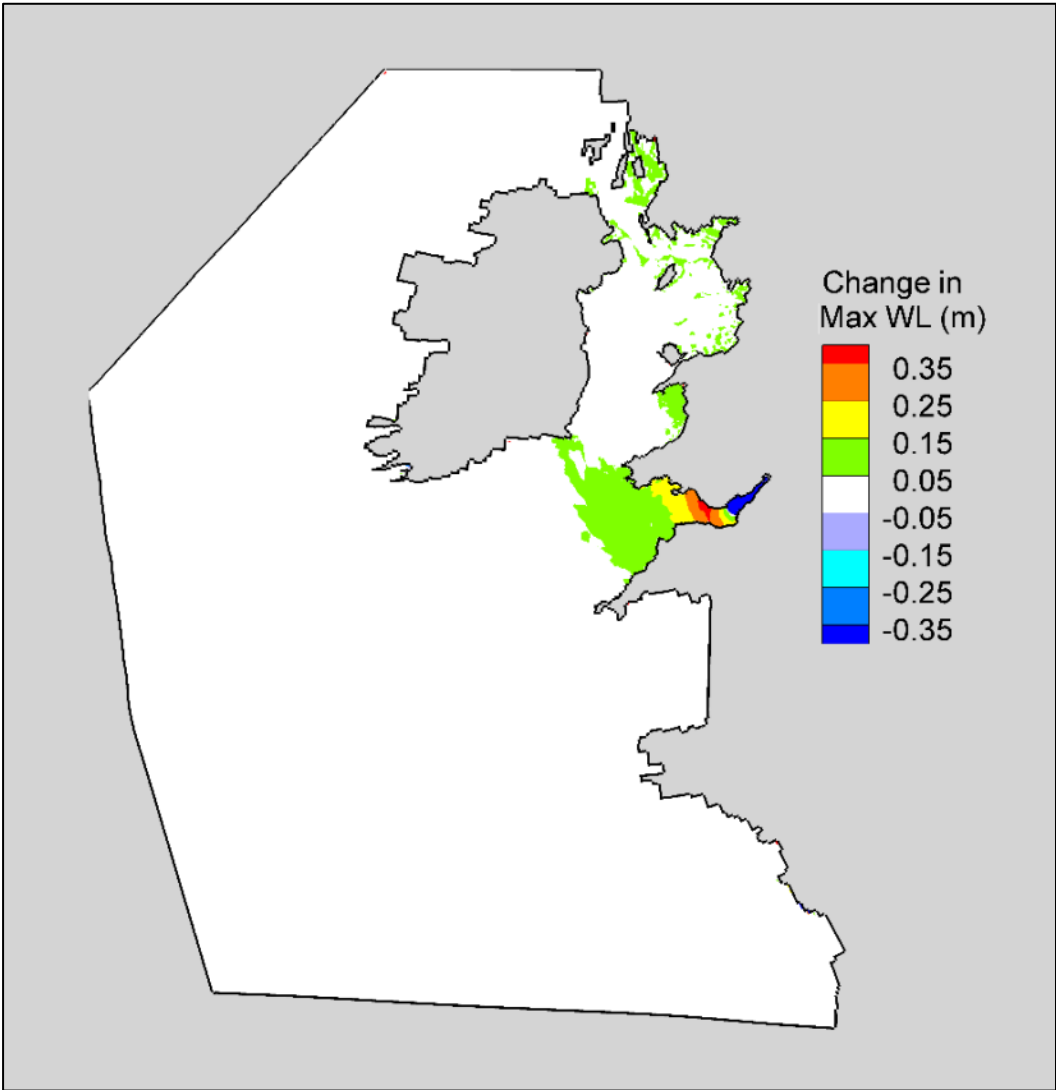


Figure 5-6 - Domain-wide maximum water level changes caused by barrage Scenario 2

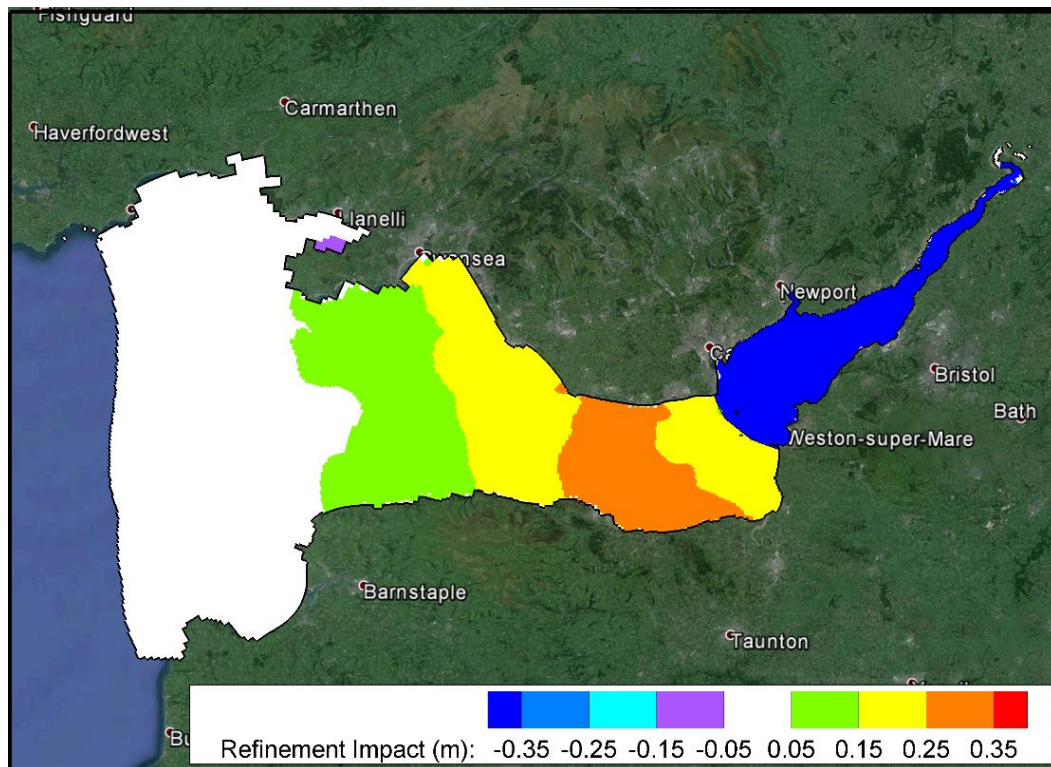


Figure 5-7 - Impact of hydraulic structure refinements on maximum water levels in the Severn Estuary and Bristol Channel

The refinements have had a significant impact; they have raised the maximum water levels downstream of the Barrage by up to 0.25 m in some areas, and reduced the maximum water levels upstream by up to 0.75 m in much of the region. This is caused mainly by the change in the discharge through the structures as a result of the refinements; flow through the sluices during filling was significantly reduced in Scenario 2 compared to Scenario 1, resulting in the basin water level not getting so high.

5.2.1 Analysis

Changes in the representation of sluices and turbines within the numerical model of the Severn Barrage can be seen to have a dramatic impact on water levels within the estuary. When the sluices gates were only modelled as wet cells, i.e. in Scenario 1, the upstream water levels were only slightly lower

than if the barrage was not included in the simulation. This is not consistent with the operation schemes suggested by Baker (2006) for the Severn Barrage and for the La Rance barrage, where higher upstream than downstream water levels are achieved only through pumping (Hammons, 1993; Retiere, 1994). For Scenario 2, where the representation of hydraulic structures was improved, the water levels upstream of the barrage were reduced by nearly 1 m in comparison. For the latter case the water levels matched closely with the predictions reported in previous studies (Ahmadian *et al.*, 2010; Xia *et al.*, 2010b), with upstream water levels significantly reduced by the inclusion of a barrage, lowering the peak levels to below those found immediately downstream of the structure. The agreement or otherwise between models cannot be statistically compared due to different boundary conditions being used, however, the comparison of peak water levels upstream and downstream demonstrate the concurrence of the prediction from Scenario 2 with the predictions from several other models. Scenario 1's predictions are in contrast to this, with upstream peak water levels remaining higher than those downstream, likely due to the insufficient resistance to flow offered by unrealistic physical representation of the hydraulic structures, as seen in Brammer *et al.* (2014). The refinements included in Scenario 2 are a more physical representation of the process of discharge through a sluice gate, and as such, coupled with the close agreement in water levels with predictions from other models, the updated prediction from Scenario 2 supersedes the prior results.

The reduced maximum water levels upstream are caused by more realistic filling of the basin. In Scenario 2, there is an added resistance to flow caused

by modelling the sluices as orifices rather than wet cells, thereby effectively reducing the flow-through area. The rate of volume transfer is reduced, as can be seen in Figure 5-3, where the gradient in the increase in the upstream water level is less steep than in Figure 5-2.

This slower rate of volume transfer during filling results in the upstream basin not reaching the water level that it would without the barrage, and in this sense would offer significant flood protection to floodplain areas.

In Scenario 2, the resistance to flow, and consequently the reduction in discharge through the sluices, causes an increase in the discharge through the turbine cells during filling, despite their numerical representation for filling being identical in Scenarios 1 and 2. Where previously, in Scenario 1, the sluice cells offered a route of significantly less resistance to flow, this disparity in resistance to flow was reduced by modelling both as orifices in Scenario 2, albeit with different flow-through areas.

The lower water levels upstream also have the effect of reducing the head difference across the structure for power generation. During the spring-tide cycle, the head difference in Scenario 1 was often higher than 7 m, at which point, according to the Head-Discharge curve used for the 40 MW turbines used in this study, the discharge would be limited as the turbines would have reached their maximum power output. In Scenario 2, the reduction in head difference was sufficient that the discharge would not have needed to be restricted, allowing the 40 MW turbines proposed for this scheme to operate as intended.

5.3 Sensitivity to discharge coefficient

The sensitivity to the discharge coefficient, C_d (described in Equation 2.4), was tested using the refined hydraulic structure representations from Scenario 2 and a further 10 scenarios varying the C_d and sluice area.

A C_d value of 1 is recommended by Baker (2006), used as the base line in this study. Sensitivity tests of 5 and 10% changes to this base value created the first 5 scenarios, as shown in Table 5-2:

Table 5-2 - Scenarios 3-7 detailing the discharge coefficient sensitivity scenario setups

Scenario	Sluice Area (m ²)	Discharge Coefficient
3	35,000	0.9
4	35,000	0.95
5	35,000	1
6	35,000	1.05
7	35,000	1.1

In anticipation that a reduction in the C_d would negatively impact the performance of the barrage, the following scenarios were set up to investigate whether changes in the sluice area could compensate for any uncertainties in the C_d value. This is of particular importance as it demonstrates whether changes in the design of the sluices, which may result in a lower C_d value, could be compensated for by adding more sluices. In these scenarios, the power generated by the Severn Barrage was assessed when the sluice area is increased/reduced by the same proportion that the

C_d is reduced/increased, e.g. a 10% increase in sluice area is applied when the C_d value is reduced to 0.9. Table 5-3 shows the sluice area mitigation scenarios.

Table 5-3 - Scenarios 8-12 detailing difference sluice areas to mitigate for discharge coefficient changes

Scenario	Sluice Area (m ²)	Discharge Coefficient
8	38,500	0.9
9	36,750	0.95
10	35,000	1
11	33,250	1.05
12	31,500	1.1

The maximum water levels for Scenarios 3, 4 and 5 were compared to assess the impact of a reduction in the discharge coefficient. Although the full CSM domain was used for the purpose of the sensitivity test, no change was observed outside the Severn Estuary and Bristol Channel and so a reduced view of the full CSM domain is shown.

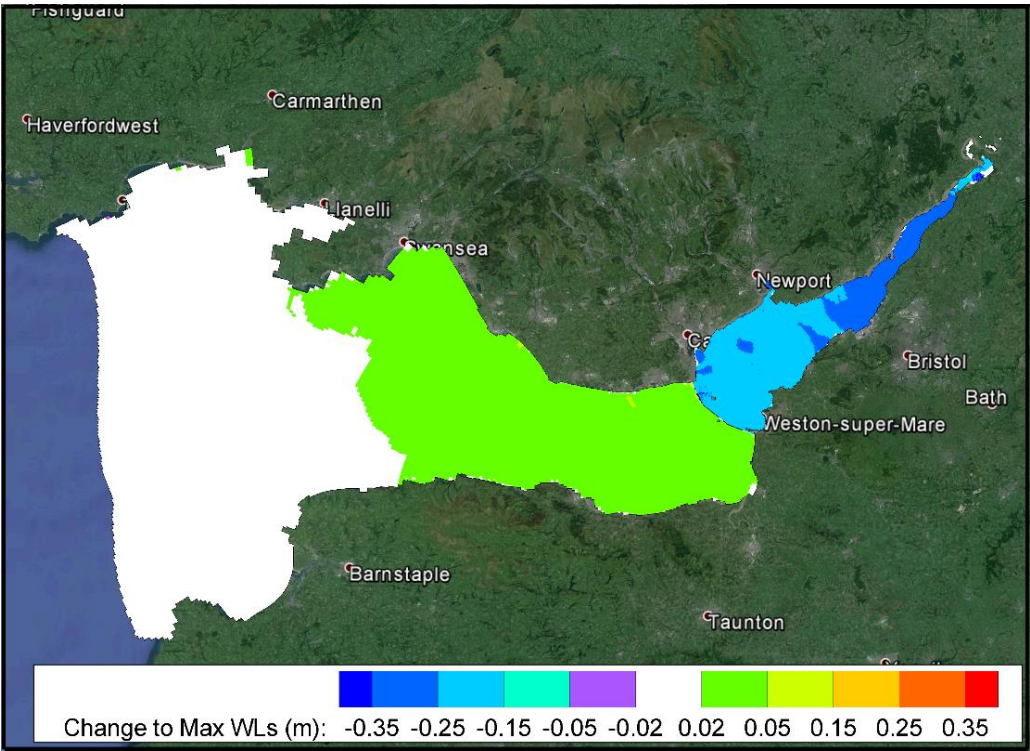


Figure 5-8 - Maximum water level changes caused by a 10% reduction in the C_d

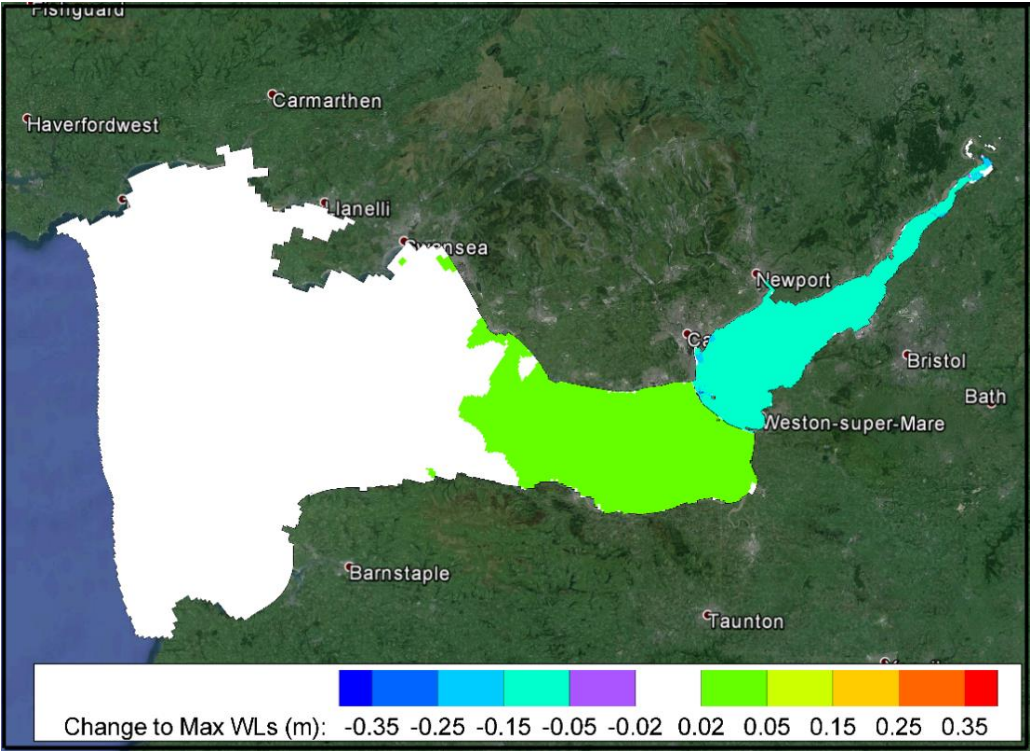


Figure 5-9 - Maximum water level changes caused by a 5% reduction in the C_d value

Figures Figure 5-8 and Figure 5-9 show the effects of a 5% and 10% reduction to the C_d , respectively. When the C_d value is reduced, the maximum water levels upstream are lowered, due to the reduction in discharge through the sluice gates during the filling stage. An effect is also seen downstream of the barrage, where the reduced capacity of the sluices to convey water to the basin results in slightly elevated maximum water levels just downstream of the barrage.

Figure 5-10 compares the power generated by the barrage for Scenarios 3-7. A reduction in the C_d value causes a reduction in the power output due to lower head differences across the structure.

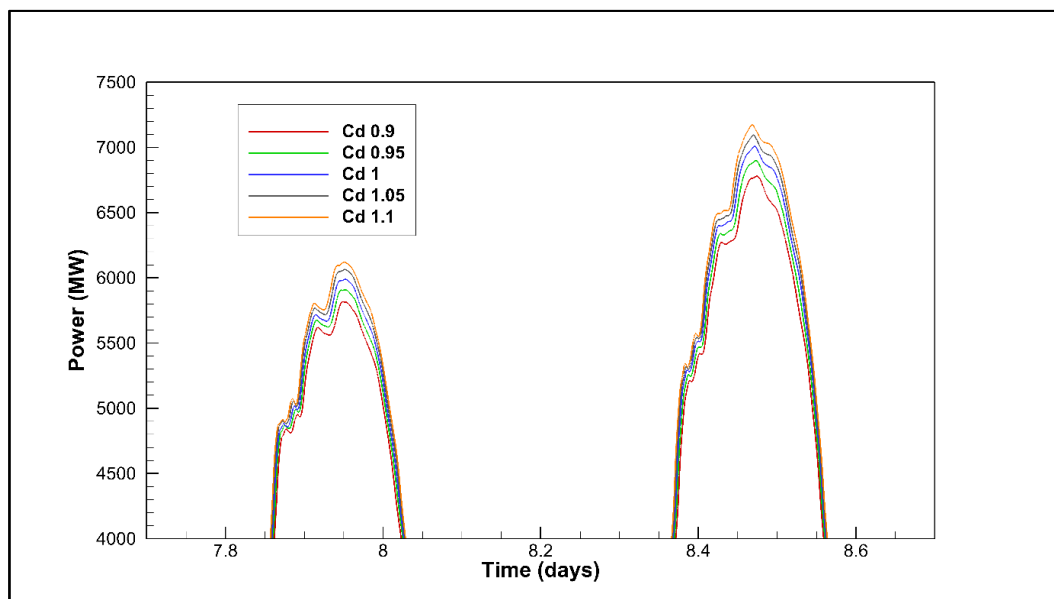


Figure 5-10 - Power generated by the barrage when varying C_d over one day

5.3.1 Mitigation through increased sluice capacity

Scenarios 8-12 were compared to assess whether the reduced performance of the Severn Barrage caused by a lower C_d could be mitigated by adding sluice capacity.

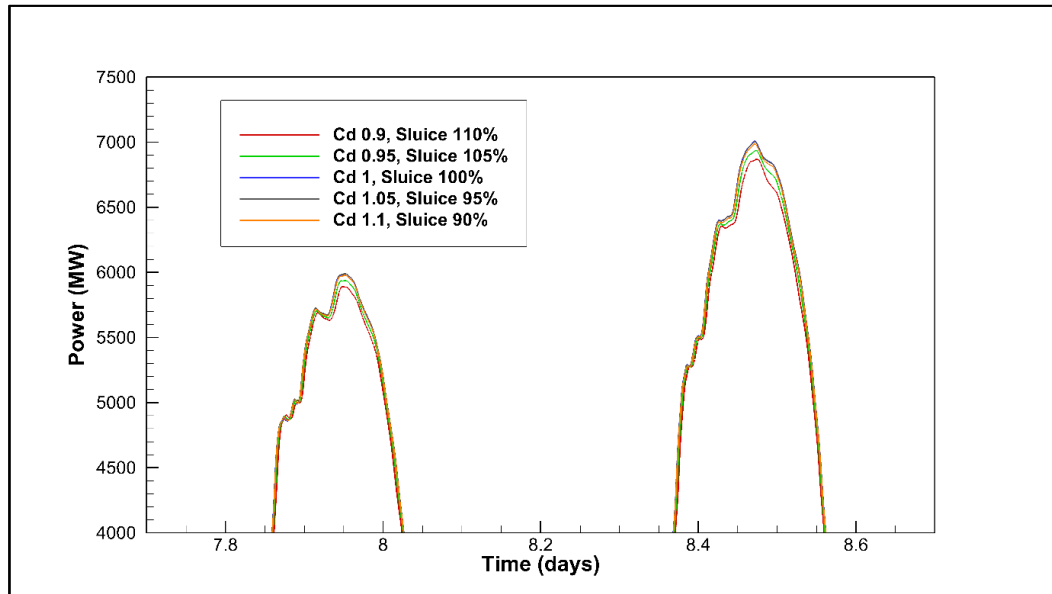


Figure 5-11 - Power generated by the barrage when varying C_d and sluice capacity

The differences in power generated due to a reduction in C_d were reduced significantly when matched with a corresponding increase in the sluice area, as can be seen by the lower spread of results from Figure 5-11 than in Figure 5-10.

5.3.2 Analysis

In assessing the sensitivity of the maximum water levels to changes in C_d , it can be seen that the impacts are contained entirely within the Severn Estuary, with no effects seen outside of this basin. A reduction in C_d lowered discharge through the sluice gates and turbines during the filling phase of the barrage operation, causing the basin to fill more slowly and not reach the same water level as for the case with a higher discharge coefficient. Reducing the C_d value by 10%, i.e. from 1 to 0.9, caused an average reduction in the maximum water levels upstream of 3.8%. A 5% reduction in the C_d value caused an average 2.3% reduction in the maximum water levels

upstream. Despite the instantaneous discharge being directly proportional to the C_d value, the continual nature of the filling the basin, and the increased head difference at each succeeding time step caused by the reduced discharge, has mitigated the effect of lowering the C_d value. This has, therefore, caused smaller changes to the water levels, discharge and power generation. This is further evidenced by the power generation statistics given in Table 5-4.

Table 5-4 - Power generation comparison for Scenarios 3-7

Scenario	Discharge Coefficient	Energy (14 days, MWh)	Energy per annum (TWh)	% of STPG C_d 1
3	0.9	629617	16.4	95.77
4	0.95	644270	16.8	97.99
5	1	657431	17.1	100
6	1.05	666885	17.4	101.43
7	1.1	676627	17.6	102.91

Table 5-4 demonstrates that a 10% reduction in the discharge coefficient causes a 4% decrease in predicted annual energy generation. Likewise, an increase in the discharge coefficient causes a proportionally smaller increase in energy generation.

Despite being mitigated by the continual nature of filling the basin, there are some power losses caused by a reduction in the discharge coefficient. Figure 5-11 shows that this power loss can be reduced by adding further sluicing capacity to the barrage and that, in fact, the power loss is negligible

when an assumed discharge coefficient is matched by a proportional increase in the sluicing capacity, with the power outputs for Scenarios 8-12 displayed below in Table 5-5:

Table 5-5 - Power generation comparison for Scenarios 8-12

Scenario	Discharge Coefficient	Sluice Capacity	Energy per annum (TWh)	% of STPG C_d 1
8	0.9	110% (38,500m ²)	16.61	97.14
9	0.95	105% (36,750m ²)	16.93	99.00
10	1	100% (35,000m ²)	17.1	100
11	1.05	95% (33,250m ²)	17.1	99.9
12	1.1	90% (31,500m ²)	17.1	99.6

5.4 Momentum representation in hydraulic structures

As discussed in Section Error! Reference source not found., the representation of momentum through the turbines was also amended. To assess the impact of the refinement, the velocities and turbine wakes were compared with and without the momentum correction.

Initially the momentum transferred between domains (through e.g. a turbine) was calculated from the EFDC internal solution. This approach does not take into account the flow-through area of the hydraulic structure, since this is included only in the barrage module and is dynamically linked only to the transfer of mass between the two discretised domains. In the updated approach, the momentum is calculated from the flow-through area of the turbine or sluice, as opposed to using the cell width and water depth. As a result, the momentum transferred between the domains is conserved, and an improved prediction for velocity in the turbine wake is observed.

Figure 5-12 and Figure 5-13 compare snapshots of the velocities in the Severn Estuary at the same point in time, midway through the ebb-generating phase, pre- and post- momentum refinement.

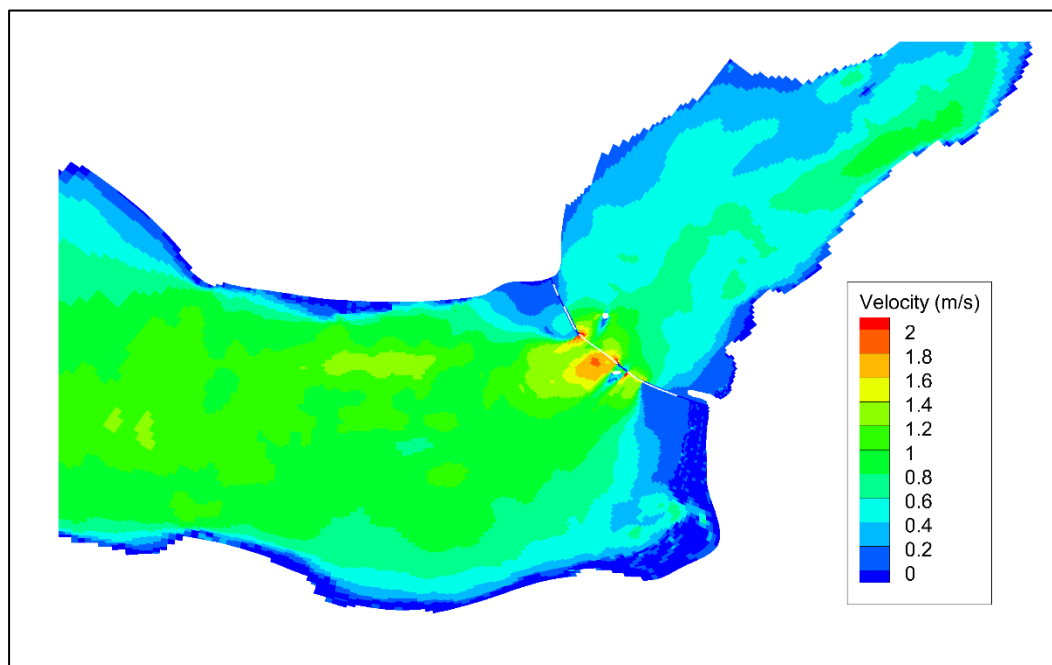


Figure 5-12 - Velocity magnitudes at mid-generating phase, pre-momentum adjustment

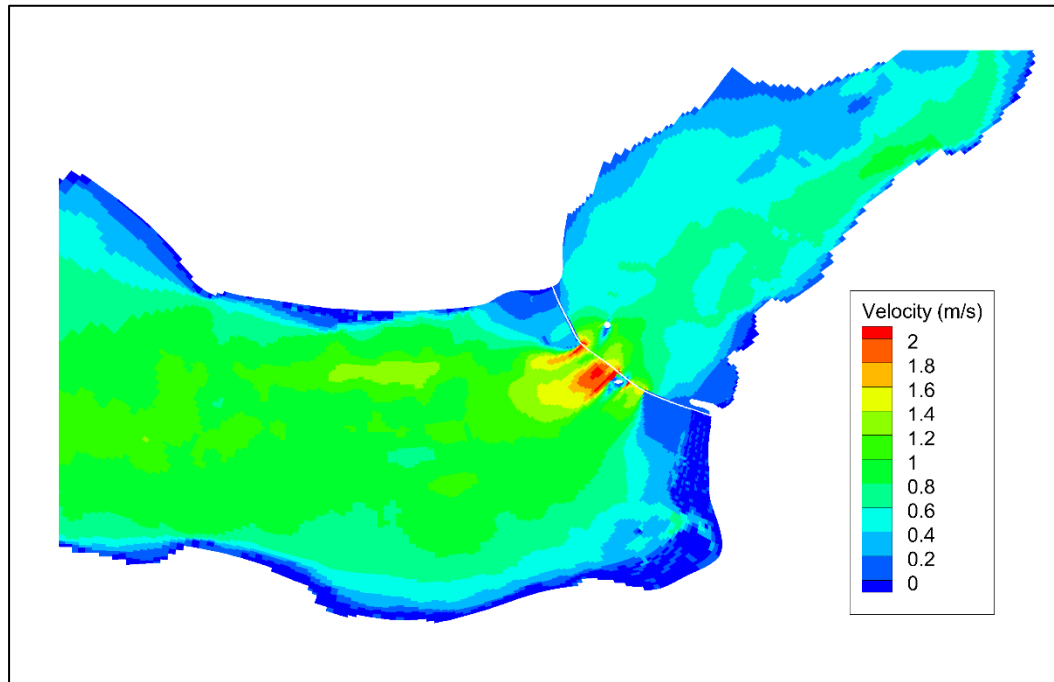


Figure 5-13 - Velocity magnitudes at mid-generating phase, post-momentum adjustment

An increase in the velocity downstream of the turbines can be seen when the momentum adjustment is included. The turbine wake also persists further downstream, potentially worsening recirculation effects, as can be seen in Figure 5-14 and Figure 5-15 below:

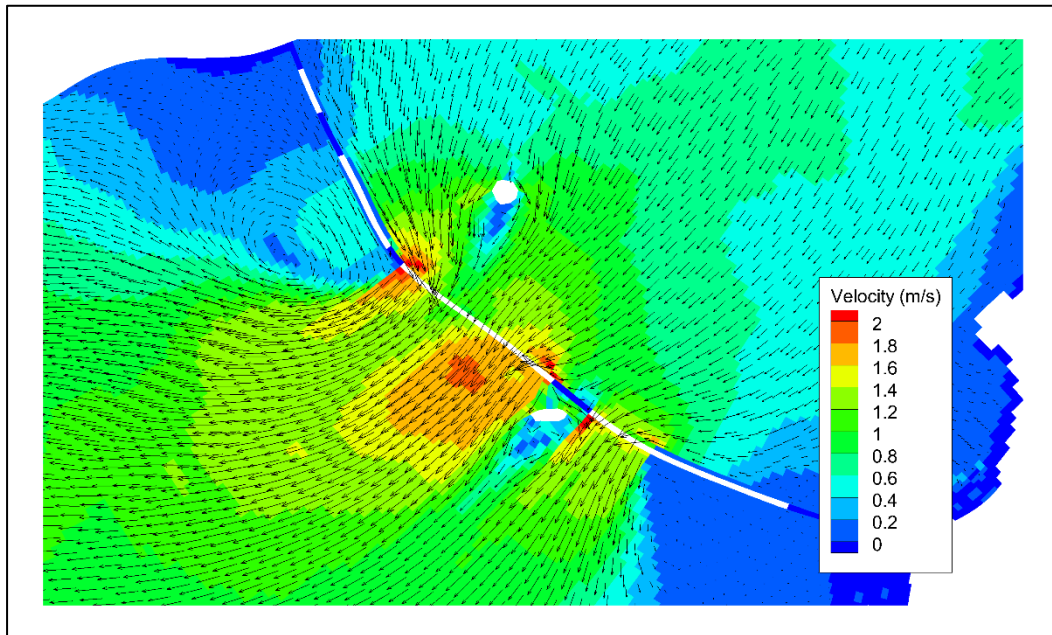


Figure 5-14 - Velocity magnitudes and vectors at mid-generating phase, pre-momentum adjustment

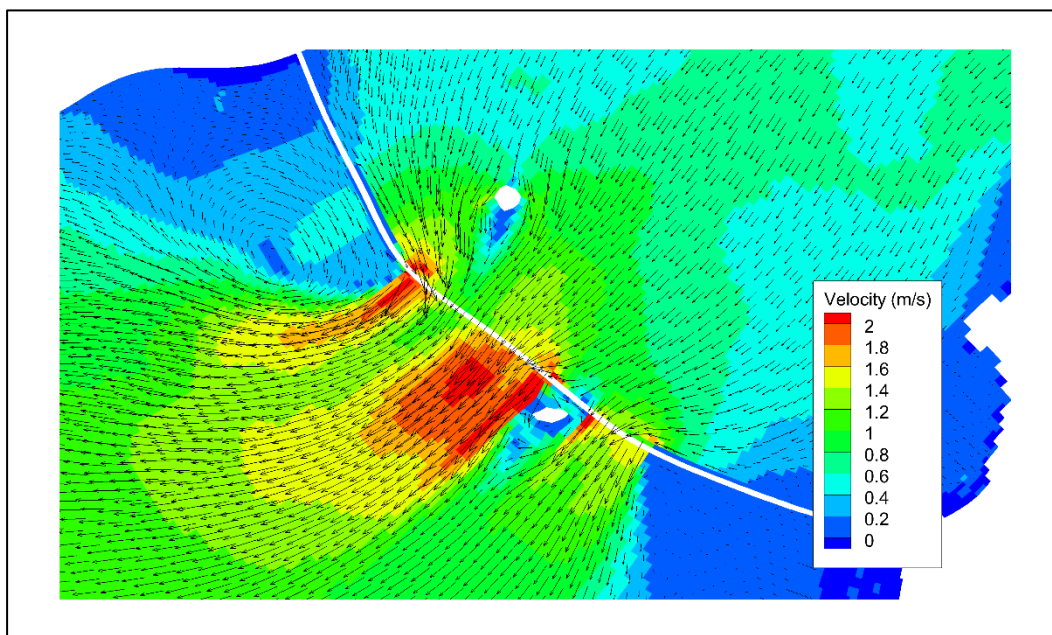


Figure 5-15 - Velocity magnitudes and vectors at mid-generating phase, post-momentum adjustment

The increased velocities and longer wake create more hazardous, turbulent conditions in the estuary. Problems associated with recirculation effects, such as sediment deposition may also be encountered. The effect is likely

to be magnified and have more severe consequences in tidal lagoons where the surface area is more limited (Angeloudis, Falconer, *et al.*, 2016).

Increasing the number of vertical layers to 5 in the EFDC SEM allows the vertical velocity profile to be assessed, as seen in Figure 5-16.

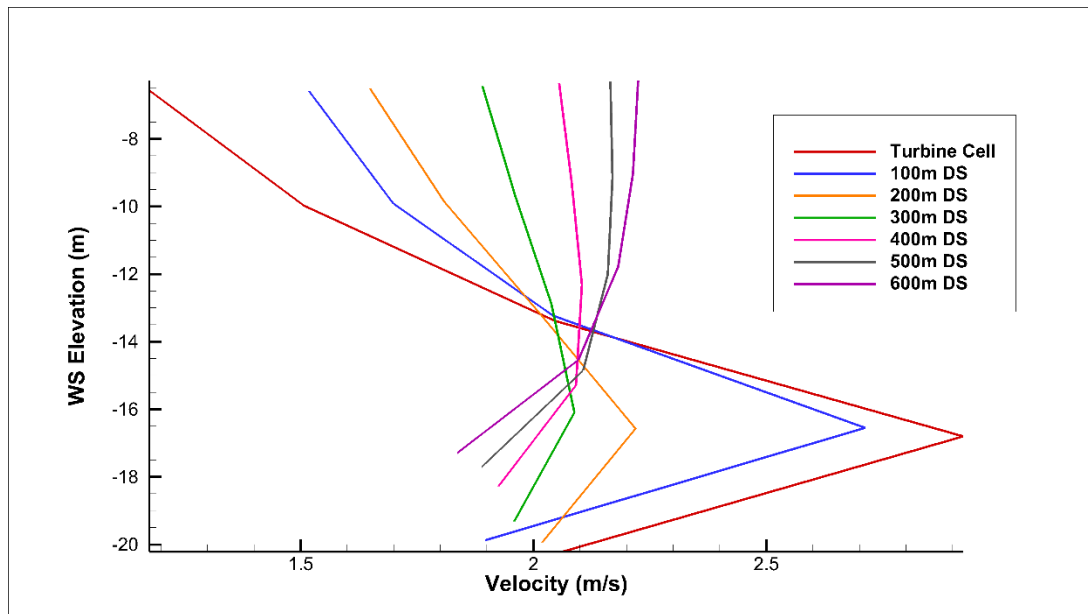


Figure 5-16 - Velocity profile through the water column 100m increments downstream of a turbine cell

Figure 5-16 shows the velocity profile through the water column at every 100 m downstream of a turbine cell, using 5 vertical layers and the updated momentum representation. In this instance, the volume and momentum is added to the 2nd layer of 5, where the first is in contact with the bed. At the turbine cell itself, the effect is very prominent - with very high velocity in the 2nd layer compared to the bed and surface. The vertical velocity profile returns to a more typical profile between 300 and 400 m downstream.

5.5 2D vs 3D barrage modelling

Extending the EFDC SEM to 5 vertical layers gave the opportunity to compare 2D and 3D model outputs. Figure 5-17 compares water levels either side of the barrage in 2D and 3D:

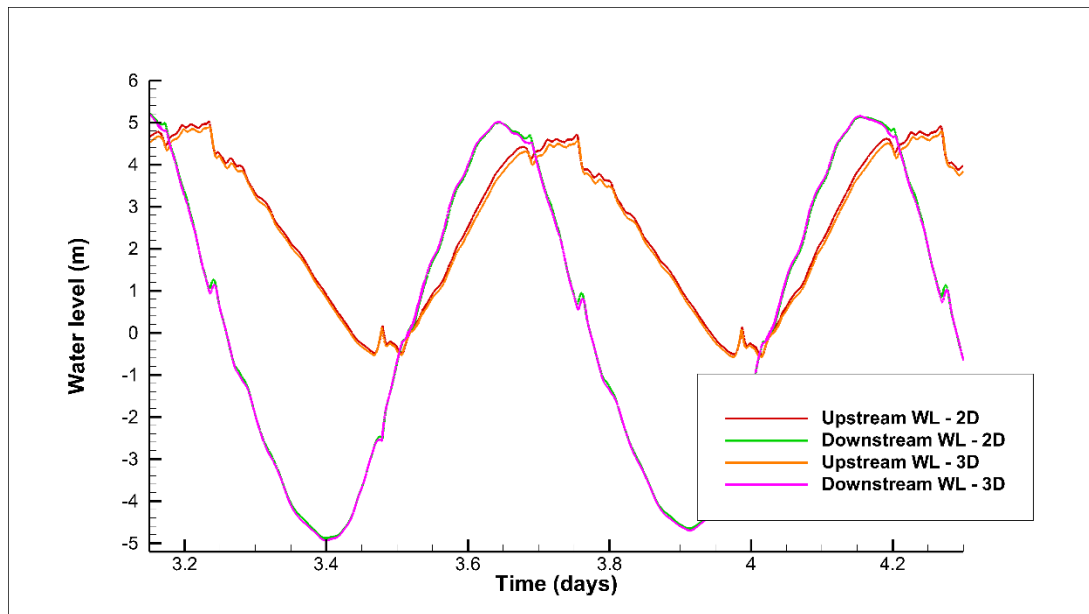


Figure 5-17 - Water levels upstream and downstream of the barrage, in 2D and 3D

Very little difference in the water levels can be seen from the model output. Correspondingly, the prediction of Severn Barrage power outputs from the 2D and 3D models are near identical:

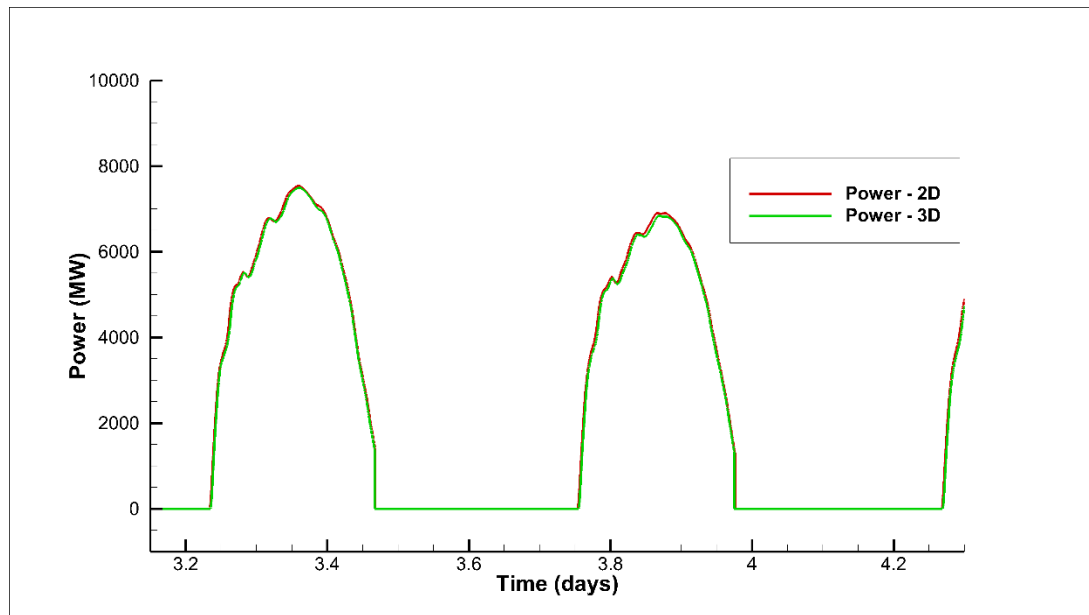


Figure 5-18 - Power output comparison for 2D and 3D STPG ebb-generating barrage simulations

The water level and power output results for the 2D and 3D simulations of the ebb-generating STPG barrage show no differences. This indicates that the processes are adequately simulated in 2D and in the case of the Severn Barrage, in an estuary known to be well-mixed vertically due to the tidal range (Uncles, 1984), it is not necessary to simulate in 3D unless looking at the vertical velocity profile of the turbine induced wake.

5.6 Chapter summary

Chapter 5 assessed the impact of the refinements to the representation of turbines and sluices within the EFDC model.

Amendments to the calculation of discharge through turbines and sluices has significantly changed the EFDC CSM's prediction of the Severn Barrage impact on peak water levels. The importance of correct hydraulic structure representation is thus highlighted.

An analysis on the sensitivity of barrage modelling to the discharge coefficient, a parameter of importance in the orifice equation, demonstrated (relative) insensitivity despite the proportional relationship to discharge. A 10% reduction in the discharge coefficient caused only a 4% reduction in barrage energy output performance.

A correction to the calculation of momentum through hydraulic structures was applied, ensuring the continuity and altering the velocity and wake of the turbines represented in the Severn Barrage. Increased velocity and wake length as a result of the refinements may be of hydro-environmental concern, particularly in the case of smaller tidal lagoons.

3D modelling of the Severn Barrage with corrected mass and momentum calculations produced an assessment of the vertical velocity profile of the turbine wake. Very high velocities are produced in the turbine cell, with the vertical velocity profile returning to a typical profile approximately 300-400 m downstream.

Chapter 6

Model application 2 - Bridgwater Bay Lagoon

6.1 Introduction

Bridgwater Bay is located 5 kilometres north of Bridgwater in Somerset. The Rivers Parrett, Brue and Washford, as well as several man-made ditches drain the Somerset Levels into the bay.

Bridgwater Bay was a site shortlisted in the DECC study (DECC, 2010b) as a potential site for tidal power generation. Bridgwater Bay has a large tidal range of 8.5 m, and a shape that lends itself readily to impoundment. The severe flooding of winter 2013-2014 in the Somerset Levels prompted further interest in the Bridgwater Bay Lagoon, as a tidal lagoon would potentially have been able to protect against the tidal storm surge that exacerbated the flood depths and extent. Much of the Somerset Levels are below sea level, making them particularly vulnerable to fluvial and coastal flooding, as seen in the Environment Agency Flood Map for Planning below:

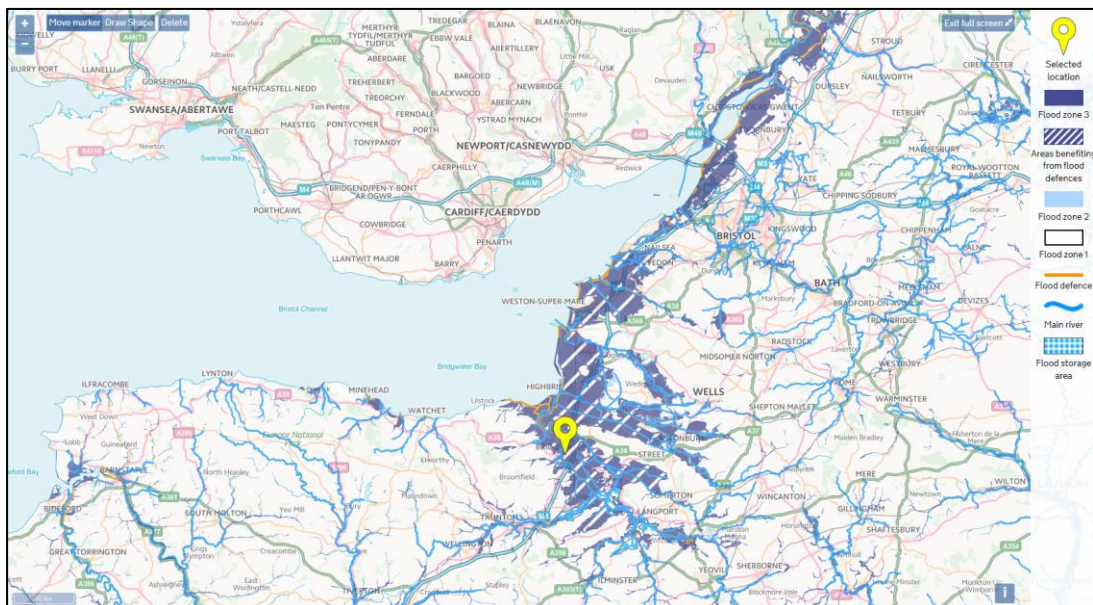


Figure 6-1 - EA Flood Map for Planning - Bridgwater (Environment Agency, 2017)

With a lagoon in place, closing the turbines and sluices in the event of a tidal storm surge would keep water levels within the Bridgwater Bay lower, potentially improving the conveyance of the rivers draining the Levels and reducing flood depths and extents.

In the DECC report, the Bridgwater Bay Lagoon was reported to have a cost of £12 billion, producing 6.2 TWh/yr of energy through 144 25 MW turbines for a total 3600 MW capacity.

To demonstrate the applicability of 2D hydraulic models to aid design and optimisation of such proposals, the Bridgwater Bay Lagoon was modelled within the SEM using a range of turbine numbers from 60 to 360. 2D modelling of the lagoon with the different turbine configurations will assist planning and design through providing data on:

- The peak power that can be generated
- The energy that can be extracted
- The tidal range that can be preserved within the lagoon
- The number of hours per day that electricity can be generated

6.2 Refined mesh and model setup

The lagoon was not expected to have hydrodynamic effects beyond the Severn Estuary and Bristol Channel, so the SEM was used rather than the CSM. To provide a more detailed representation of the lagoon and the associated hydrodynamic processes, the SEM grid was refined to give a cell size around the lagoon of 15 x 15 m. The refined SEM contained 500,000

cells, taking approximately 60 hours to simulate a 7-day run. Figure 6-2 shows the location of the Bridgwater Bay Lagoon within the SEM.

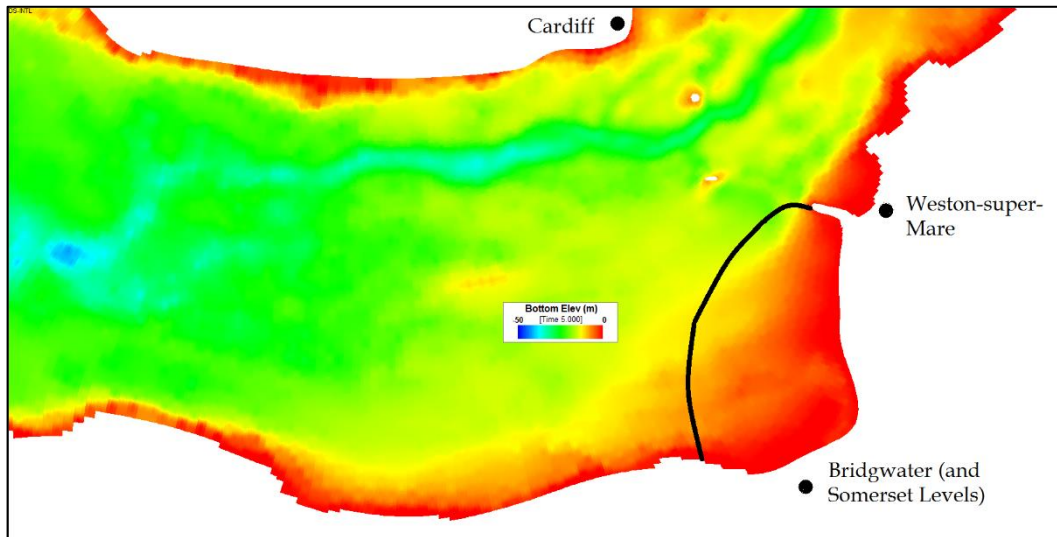


Figure 6-2 - Bridgwater Bay Lagoon within the refined SEM

The DECC report suggested two locations for turbine housings within the lagoon wall:

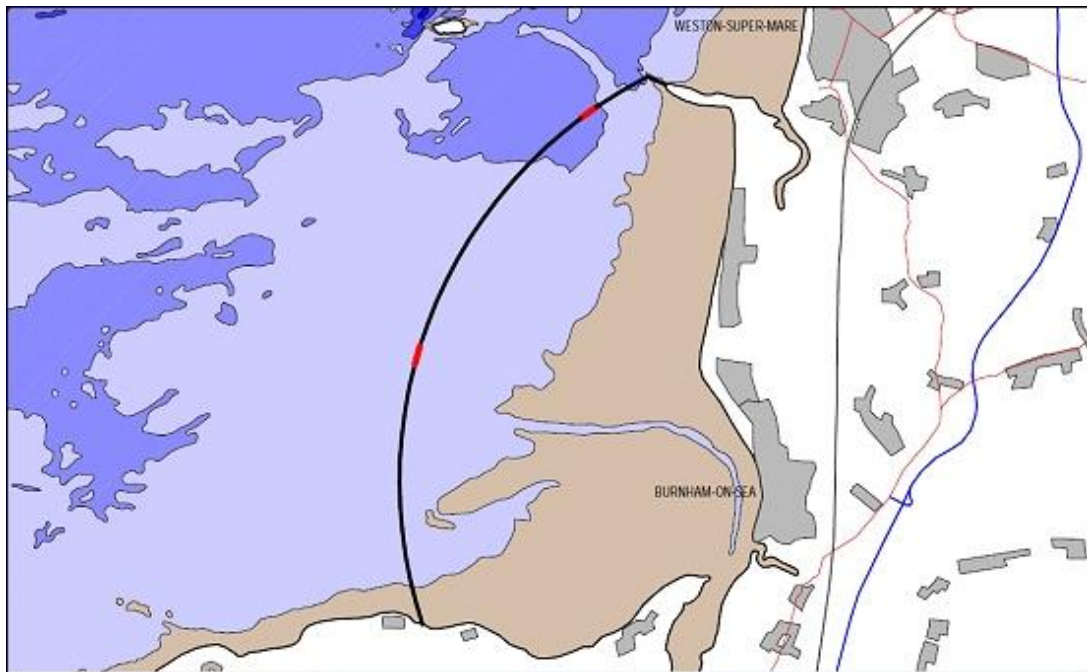


Figure 6-3 - Locations of turbines (in red) along the Bridgwater Bay Lagoon wall

The turbines proposed for the Swansea Bay Tidal Lagoon are 20 MW and 7.5 m in diameter. The turbines would need to be submerged at all times, to reduce potential damage. Figure 6-4 below investigates the potential turbine housing sites along the proposed lagoon line, by plotting the bed elevation profile (green), against the minimum water level experienced in a full tidal cycle (blue). Assuming the 7.5 m turbines must always be submerged, and adding a freeboard to account for exceptionally low tides, waves and high-pressure systems, a minimum depth of 10 m was chosen. The yellow line shows the areas along the lagoon wall with a minimum depth always above 10 m, corresponding only to the northern turbine housing site, and ruling out the southern site.

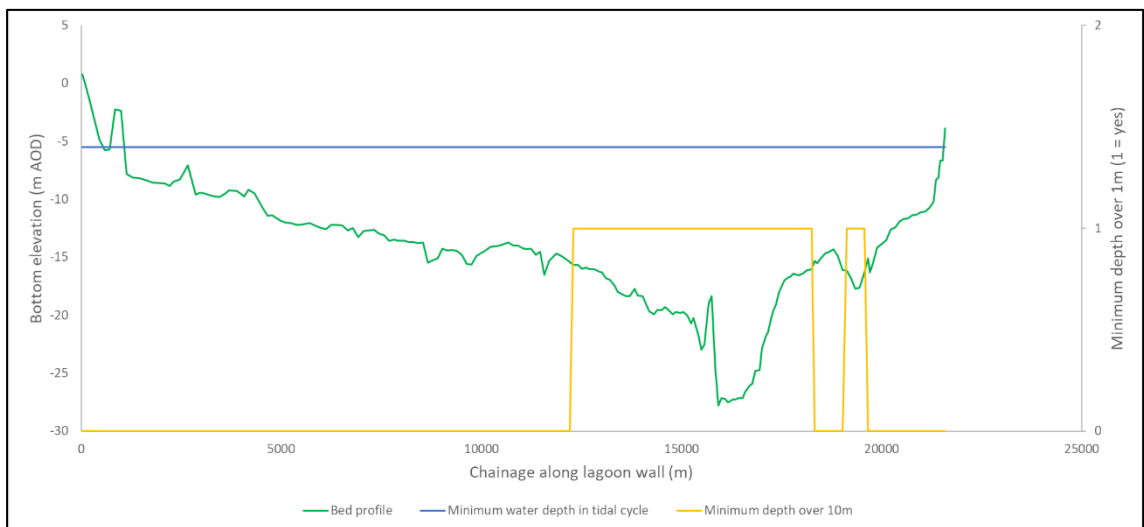


Figure 6-4 - Bed elevation profile (green), minimum water depth (blue) and potential turbine housing locations (yellow) along the Bridgwater Bay Lagoon line

The northern turbine housing site gives a length of approximately 5.5 km with sufficient depth for 7.5, diameter turbines. A range of turbine configurations were set up and tested in the model to optimise lagoon

performance. The turbine numbers ranged from 60 to 360 turbines, giving a turbine spacing of 13 turbine diameters to 2 turbine diameters.

In each case, a starting head for generation of 4.5 m was used, with a minimum generating head of 2 m. In a full optimisation suite a range of starting and minimum heads would be required, but to limit the number of test cases and demonstrate the 2D model capability of optimisation modelling, the generating head elevations were fixed for this study.

6.3 Outputs and analysis

Figure 6-5 below shows the operation of the lagoon over the course of 24 hours, where the red line represents water level within the lagoon, green the water level outside of the lagoon, and blue the phase of the lagoon corresponding to the description above. In this case 100 turbines were used, as an initial run to ensure the model was functioning correctly.

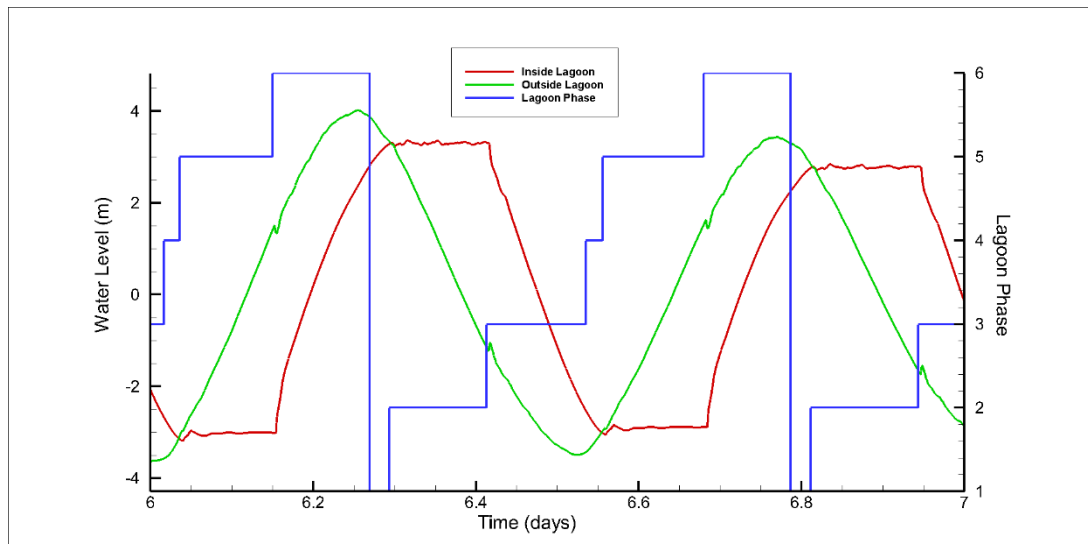


Figure 6-5 - Bridgwater Bay Lagoon operational phases

The 13 turbine configurations were then simulated, allowing for the comparison of peak power output, energy generated, the tidal range within the lagoon and average generating hours per tidal cycle.

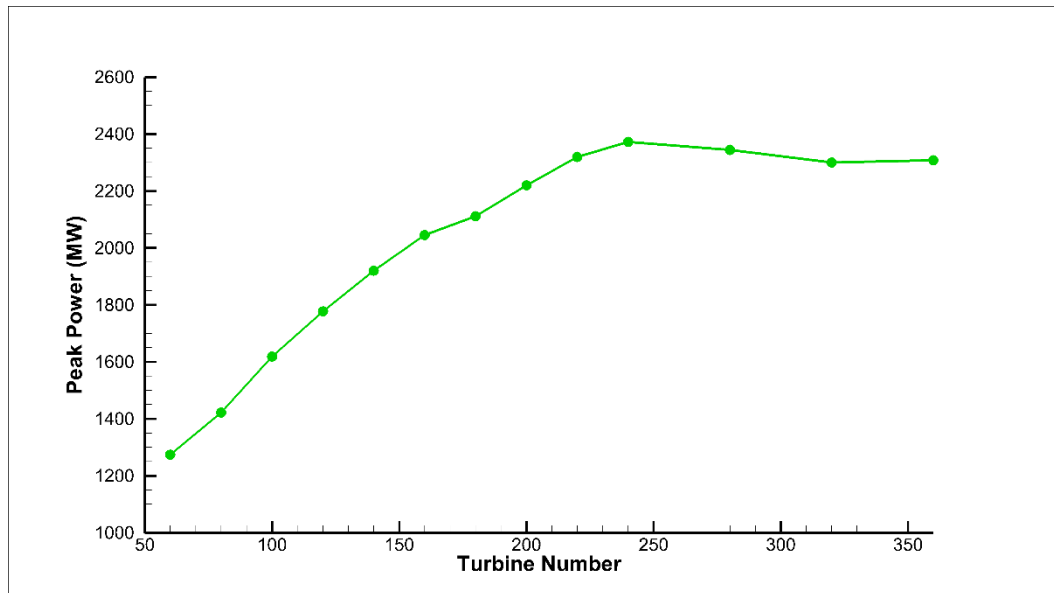


Figure 6-6 - Peak power output of the Bridgwaer Bay Lagoon when varying the turbine number

Figure 6-6 - Peak power output of the Bridgwaer Bay Lagoon when varying the turbine number
 Figure 6-6 displays the peak power output achieved during the simulation, for each of the 13 different turbine configurations. The peak power is 2372 MW, occurring when 240 turbines are used. Additional turbines after 240 in fact cause a slight reduction in the peak power achieved, due to a lower head difference either side of the lagoon wall being achieved.

Table 6-1 - Peak power achieved as a percentage of installed capacity

Number of turbines	Installed capacity (MW)	Peak power (MW)	Peak as % of capacity
60	1500	1273.95	84.93
80	2000	1421.61	71.08
100	2500	1618.52	64.74
120	3000	1777.54	59.25
140	3500	1920.09	54.86
160	4000	2045.58	51.14
180	4500	2111.34	46.92
200	5000	2220.23	44.40
220	5500	2319.48	42.17
240	6000	2372.23	39.54
280	7000	2344.25	33.49
320	8000	2300.45	28.76
360	9000	2307.73	25.64

Table 6-1 gives the installed capacity of each simulation, along with the peak power achieved and hence the peak power achieved as a percentage of the installed capacity. For upwards of 180 turbines, less than half the installed capacity is achieved.

Annual energy output for the range of turbine configurations is displayed in Figure 6-7.

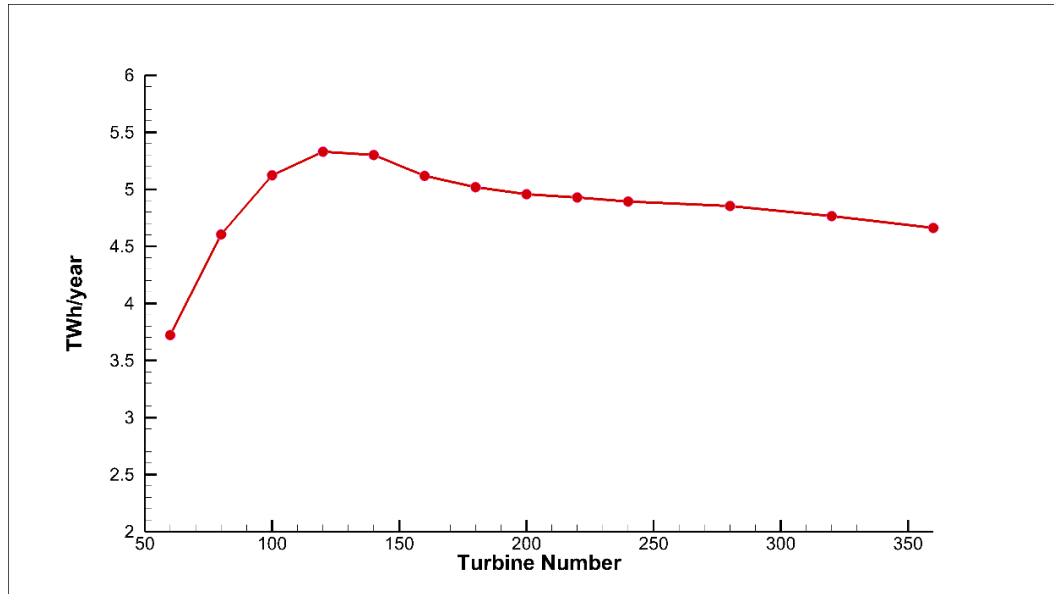


Figure 6-7- Annual energy output of Bridgwater Bay Lagoon when varying the turbine number

The figure shows that the peak energy is generated when only 120 turbines are used. This is partially explained by Figure 6-8, which shows that as the turbine numbers are increased, the length of time the lagoon is in a generating phase is reduced. This is due to the faster emptying or filling of the lagoon, causing the minimum head for generation to be reached sooner. With fewer turbines, the generating cycle is also operated at a higher head difference, which in the case of the Bridgwater Bay has more than made up for the lower installed capacity, which appears largely wasted for the higher turbine numbers.

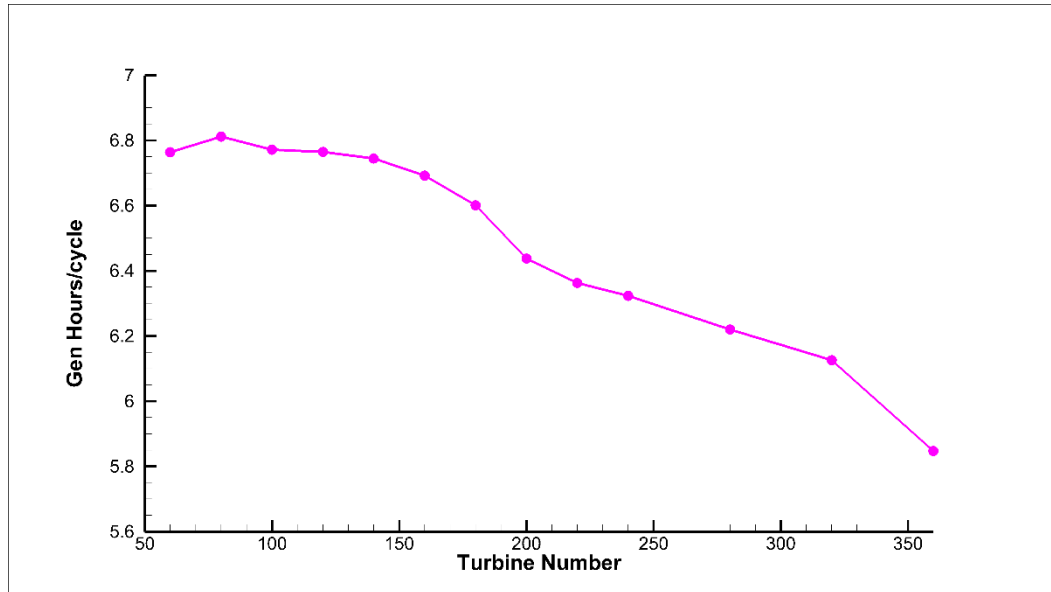


Figure 6-8 - Hours of generation per tidal cycle when varying the turbine number

Generating hours per cycle is also likely to be of importance from an electricity demand and national grid perspective. A criticism often levelled at the ebb-only generating STPG barrage is the two large spikes of energy generated over the day. A lower, more regular energy output is preferable in terms of transmission to the grid and onwards, reducing losses and reducing dependency on other sources of electricity.

From an environmental perspective, the aim should be to preserve the baseline tidal regime as far as is possible. Intertidal mudflats are of critical importance as habitats to the wildlife of the estuary.

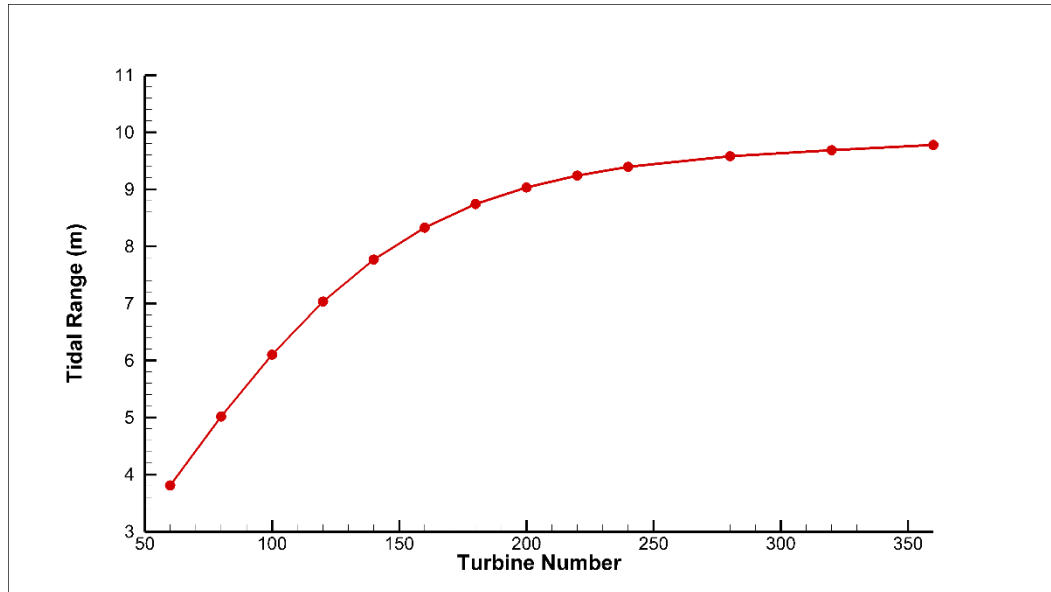


Figure 6-9 - Tidal range within the Bridgwater Bay Lagoon when varying the turbine number

Figure 6-9 demonstrates one of the problems faced with the design of a tidal lagoon. Despite performing strongly in terms of annual energy output and generating hours per cycle, the lagoon configuration with 120 turbines does not preserve the tidal range of the bay, losing approximately 3 m. This would have to be addressed to ensure the operation of the barrage had the most minimal of environmental impacts as possible. There are various options that could help to preserve the tidal range, such as sluice gates or pumping, both of which would have to be explored in detail in a full suite of appraised options for the formal design process.

6.4 Chapter summary

Chapter 6 demonstrates how a 2D hydraulic model can be used to assist the optimisation and design of tidal lagoon proposals, through the testing of a range of configurations of the Bridgwater Bay Lagoon.

The refined SEM model allows the comparison of the hydro-environmental impacts of a scheme, as well as giving the opportunity to optimise a proposal for energy output.

The results showed that a surplus of turbines in a tidal lagoon scheme may reduce the energy output, by cutting down the generating time of the lagoon and generating over a lower head difference.

2D modelling can feed into a design process that aims to minimise hydro-environmental impacts while maximising energy and efficiency.

Chapter 7

Model application 3 - water quality modelling

7.1 Introduction

As discussed in Section 4.5, previous laboratory and field studies have demonstrated a link between salinity and phosphate sorption to sediments due to the competition for sorption sites between seawater anions and phosphate. Since sediment-associated nutrients are not readily available for biological uptake, the dissolved proportion of phosphate is of particular importance when trying to predict the growth of phytoplankton and the potential for eutrophication.

Implementing the salinity-linked phosphate partition coefficient into the EFDC model and testing its effect required first that salinity, suspended sediment and total phosphate must be simulated to within acceptable tolerances of accuracy.

7.2 Salinity

Figure 7-1 below shows a model snapshot of salinity, modelled by setting the salinity at the open boundary to 35 parts per thousand (ppt), and all riverine inflows at 0 ppt. The initial salinity concentration was set to 10 ppt, and the simulation run for 250 days. This ensured the salinity gradient in the estuary reached a steady state, as can be seen from the salinity timeseries, Figure 7-2, at a point in the centre of the estuary between Minehead and Cardiff Airport, shown as Point A on Figure 7-1.

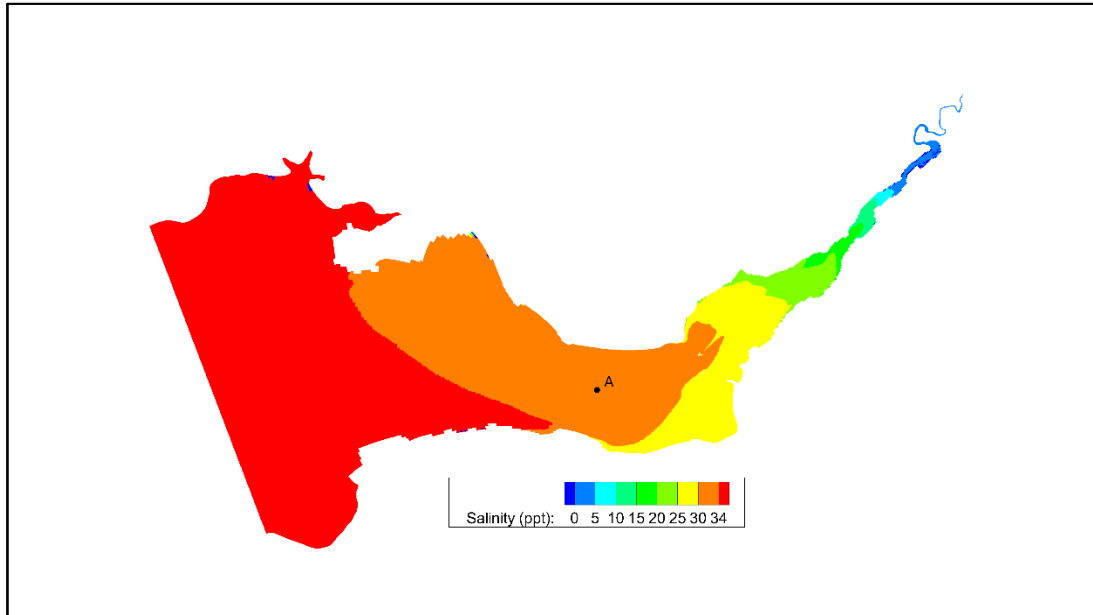


Figure 7-1 - Snapshot of predicted salinity in the Severn Estuary and Bristol Channel

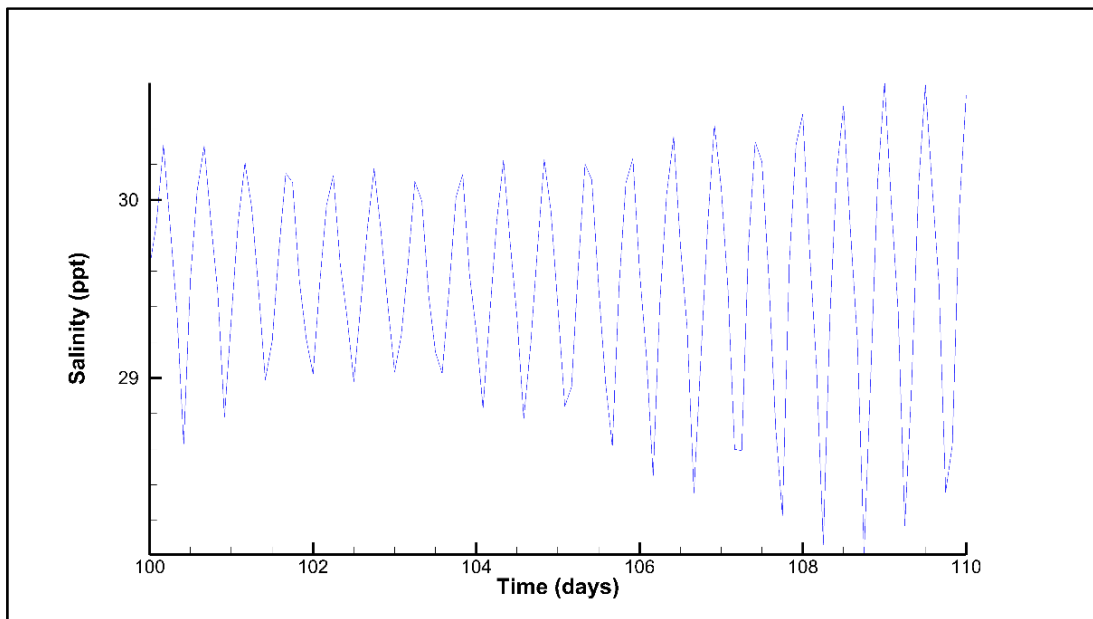


Figure 7-2 - Timeseries of salinity in the estuary between Minehead and Cardiff Airport

As discussed in Section 4.5, there is insufficient field data for the salinity outputs to be considered final, but the results appear to concur with the data available in Uncles (1984) and Stephens (1986).

7.3 Suspended sediment

Suspended sediment modelling was calibrated using Environment Agency field data collected at Minehead and Southerndown. The cohesive sediment model parameters used are shown in Figure 7-3 below.

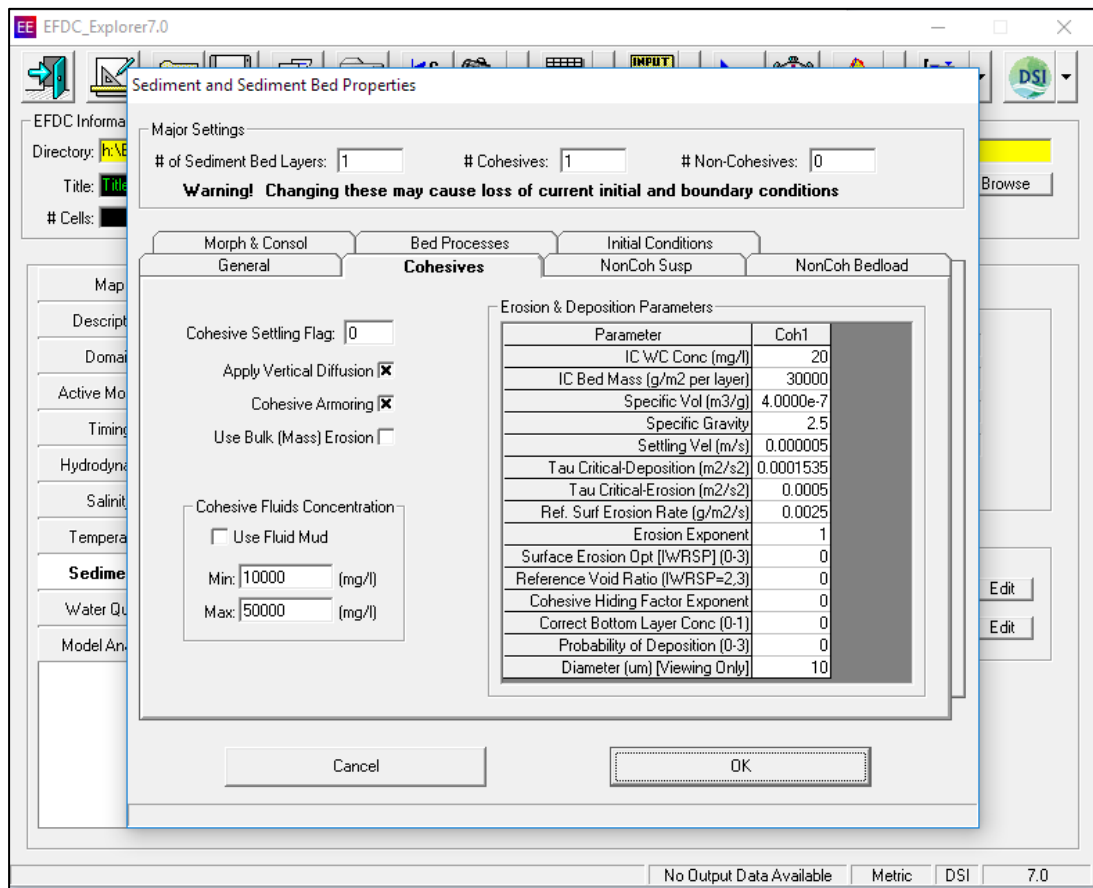


Figure 7-3 - Cohesive sediment parameters

The initial bed mass concentration was adjusted until the results were in agreement with the field data at Minehead, and then validated against the data at Southerndown. With no further data against which to test the model, the SEM was considered to be simulating suspended sediment levels to a sufficient degree of accuracy to proceed with the partition coefficient

study. Figure 7-4 shows a snapshot of suspended sediment concentrations in the estuary midway through the ebb tide.

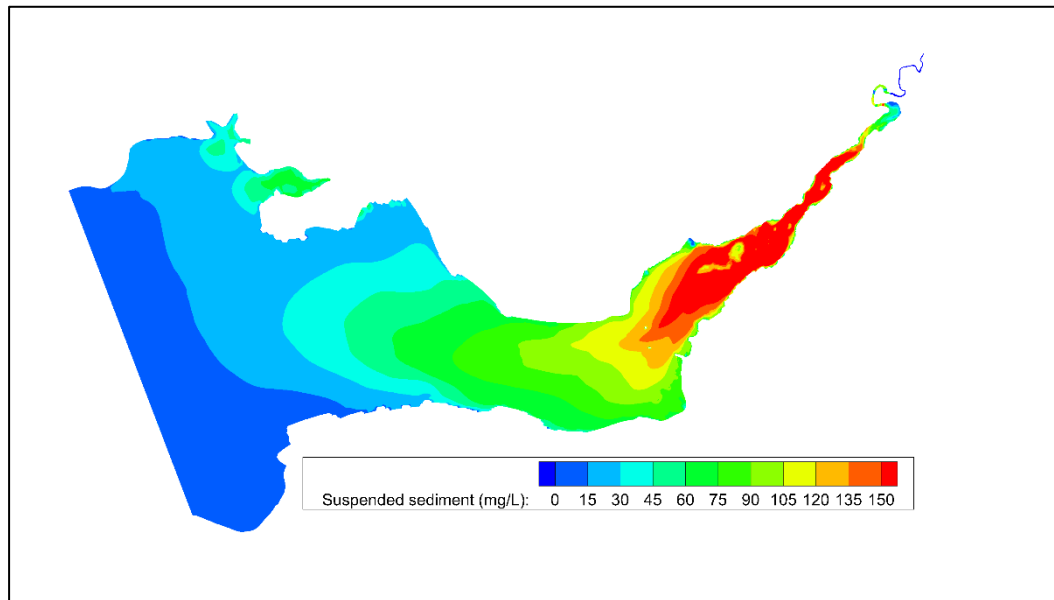


Figure 7-4 - Snapshot of suspended sediment concentrations in the Severn Estuary midway through the ebb tide

7.4 Total phosphate

Field data relating to dissolved and total phosphate levels in the Severn Estuary is held by Cardiff University but only in restrictive quantities; 9 sites in the estuary were sampled at 6 times in the summer of 2011. Clearly this is insufficient to validate the model against, and can therefore only provide confirmation that the model is predicting phosphate levels in the correct range. The locations of the 9 sample points are shown on Figure 7-5 below.

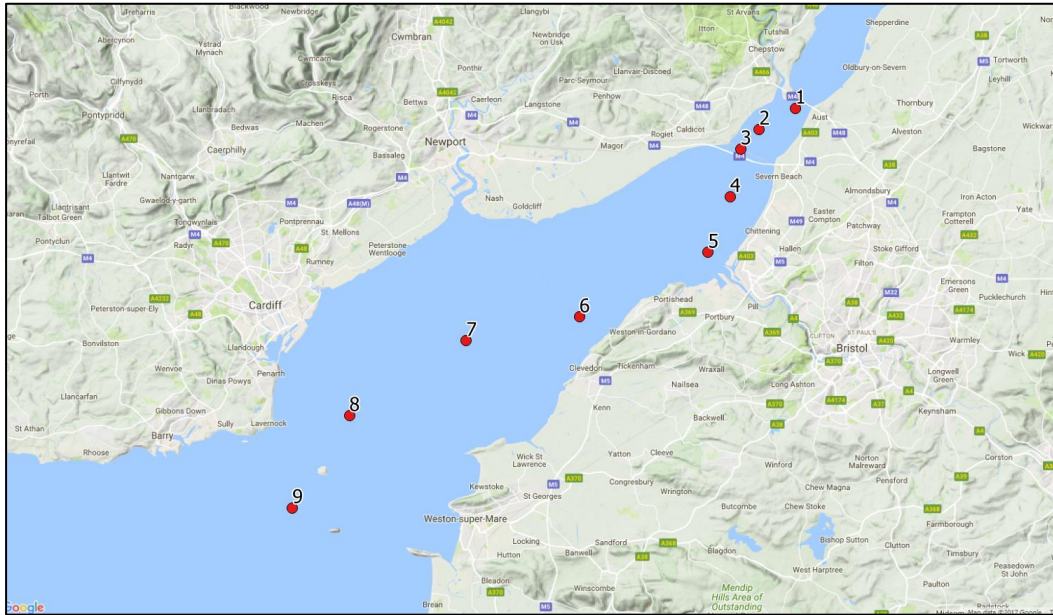


Figure 7-5 - Locations of sample sites with phosphate concentration data

The range of concentrations encountered at each sample site is shown on Table 4-1.

Table 7-1 - Phosphate field data for the Severn Estuary

Sample Point	Dissolved PO ₄ (mg/L)		Total PO ₄ (mg/L)	
	Minimum	Maximum	Minimum	Maximum
1	0.09	0.91	0.70	4.92
2	0.08	0.95	0.50	5.28
3	0.06	0.66	0.66	6.43
4	0.15	0.93	0.53	5.24
5	0.11	0.99	0.38	4.25
6	0.09	0.57	0.43	5.21
7	0.05	0.72	0.45	2.98
8	0.16	0.81	0.44	1.83
9	0.13	1.15	0.36	1.86

To ensure that the model was predicting phosphate levels in a similar range to the field data, the maximum and minimum total phosphate concentrations were extracted at the 9 locations. A snapshot of the model

total phosphate showing distribution across the estuary is shown in Figure 7-6.

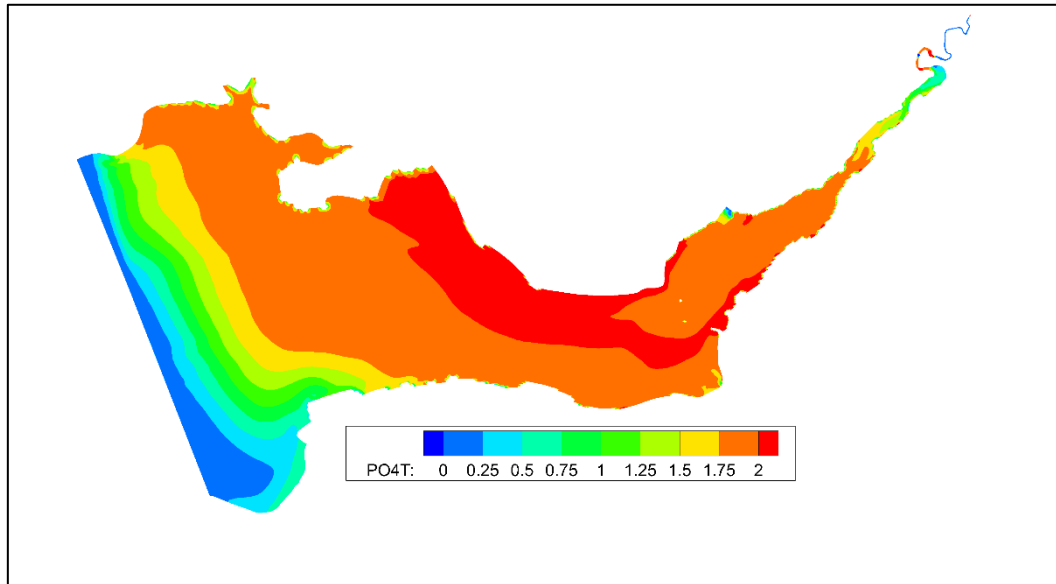


Figure 7-6 - Snapshot of the SEM's total phosphate predictions during the simulation

Table 7-2 compares the model total phosphate range with the field data phosphate range. The range of model predictions are in the same order as the field data, but insufficient to consider final. Whilst the absence of adequate field data will prevent the confirmation that the EFDC SEM is accurately predicting phosphate levels, the model can be used to demonstrate the impact of incorporating sediment interaction to phosphate predictions.

Table 7-2 - Maximum and minimum total phosphate levels encountered at the 9 sample points, compared with field data

Sample Point	Field total PO4 (mg/L)		Model total PO4 (mg/L)	
	Minimum	Maximum	Minimum	Maximum
1	0.70	4.92	2.10	3.56
2	0.50	5.28	1.13	2.22
3	0.66	6.43	2.13	4.60
4	0.53	5.24	2.08	4.38
5	0.38	4.25	1.82	4.13
6	0.43	5.21	1.13	2.66
7	0.45	2.98	0.61	1.99
8	0.44	1.83	0.55	1.92
9	0.36	1.86	0.53	1.97

7.5 Dissolved and adsorbed phosphate

If no sediment interaction is simulated only the total phosphate can be modelled, with no prediction of the division between dissolved and particulate states. If the total phosphate levels above were assumed all to be dissolved and hence readily bioavailable, the eutrophication potential of the estuary could be falsely exaggerated.

An improvement to the SEM's prediction of dissolved phosphate levels could therefore be made through linking the phosphate to suspended sediment via the partition coefficient - initially a constant K_d , and then using the salinity-linked coefficient. A constant partition coefficient of 0.5 L/g was used, as used by Wang (2011). This value is within the range of the empirically salinity-linked partition coefficient, which varies between 0.5 - 0.7 L/g for suspended sediment concentrations under 1 g/L. A snapshot from the model of the salinity-linked K_d is shown in Figure 7-7.

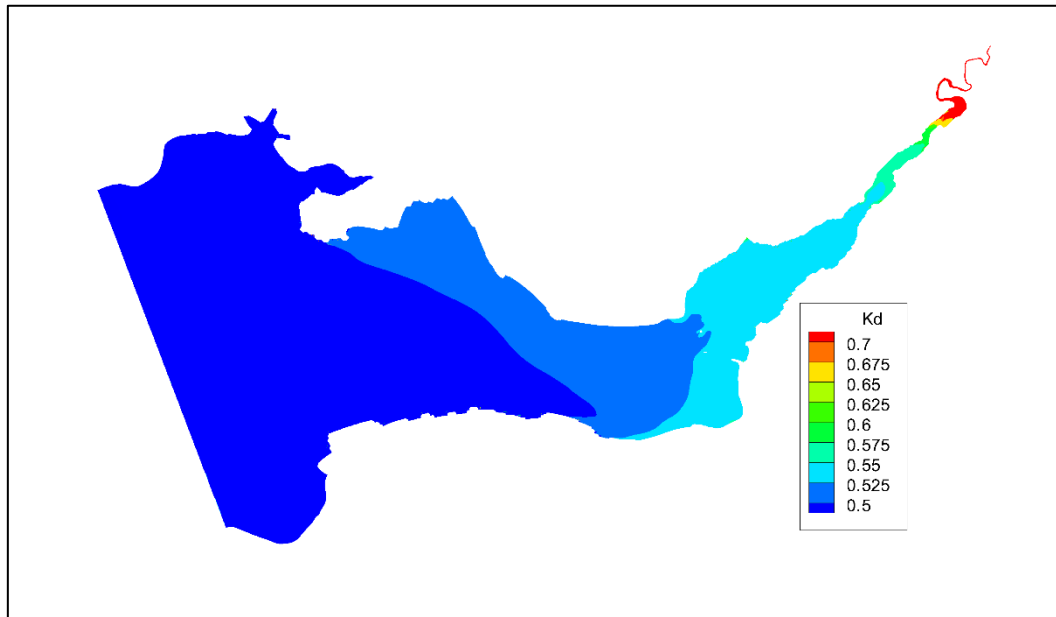


Figure 7-7 - Salinity-linked partition coefficient through the SEM

Since the dynamic salinity-linked partition coefficient largely only varies significantly from the assumed constant K_d at low salinity, we would not expect to see a difference in the model results in the Bristol Channel. In the upper regions of the Severn Estuary, the salinity-linked partition coefficient is up to 50% higher than the assumed constant coefficient, potentially significantly increasing adsorption and removing phosphate from the dissolved phase.

Table 7-3 shows the improvement to the prediction of dissolved phosphate through the introduction of sediment interaction, using a constant K_d , compared to simulating only total phosphate.

Table 7-3 - Comparison of field and model predicted dissolved phosphate levels

Sample Point	Field - dissolved PO4 (mg/L)		Model total PO4 - no sediment interaction (mg/L)		Model dissolved PO4 – constant K_d (mg/L)	
	Minimum	Maximum	Minimum	Maximum	Minimum	Maximum
1	0.09	0.91	2.1	3.56	1.13	1.83
2	0.08	0.95	1.13	2.22	0.62	1.15
3	0.06	0.66	2.13	4.6	1.25	2.30
4	0.15	0.93	2.08	4.38	1.18	2.33
5	0.11	0.99	1.82	4.13	1.05	2.25
6	0.09	0.57	1.13	2.66	0.65	1.36
7	0.05	0.72	0.61	1.99	0.35	1.00
8	0.16	0.81	0.55	1.92	0.28	0.97
9	0.13	1.15	0.53	1.97	0.27	1.06

The introduction of sediment with a partition coefficient has produced dissolved PO4 levels of approximately half the initially predicted total levels. The range of predicted phosphate levels are much closer to the field data, but still generally overpredicting the dissolved concentrations.

Since the salinity-linked partition coefficient is higher at all of the sample sites, the expected result is that the dissolved concentrations will be lower still than when the constant K_d was used. Figure 7-8 and Figure 7-9 compare domain-wide dissolved PO4 levels at the same point in the tidal cycle.

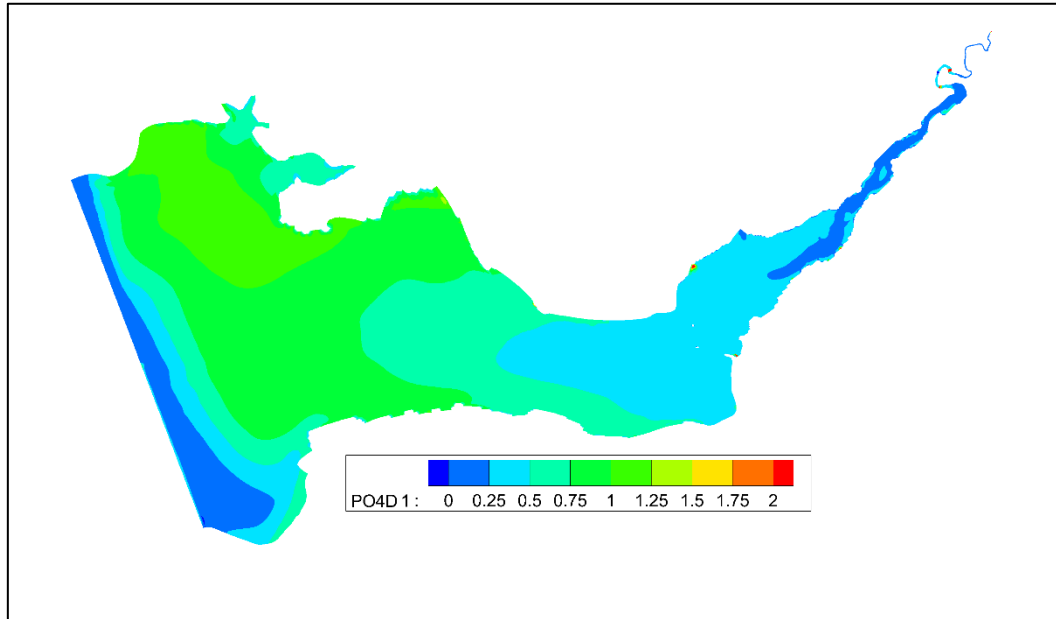


Figure 7-8 - Domain-wide dissolved PO4 levels when using a constant K_d

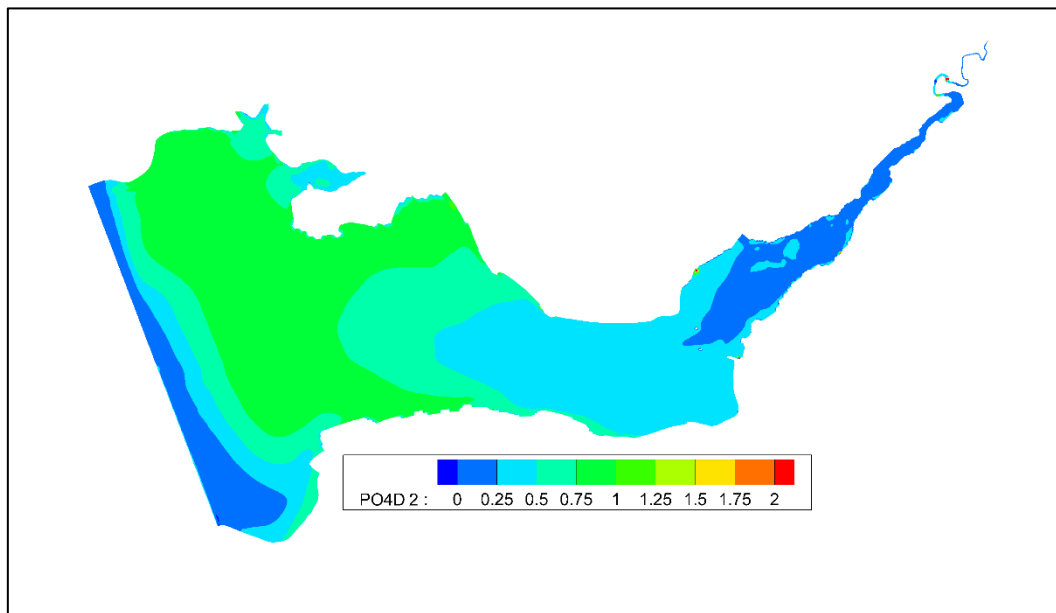


Figure 7-9 - Domain-wide dissolved PO4 levels when using a variable K_d

The figures demonstrate that the inclusion of the salinity-linked partition coefficient has had a measurable impact on dissolved phosphate levels in the Severn Estuary. The effect does not persist into the Bristol Channel, where the variable and constant partition coefficients are very similar.

Model application 3 - water quality modelling

Table 7-4 - Comparison of field and model predicted dissolved levels, moving from constant to dynamic K_d

Sample Point	Field - dissolved PO4 (mg/L)		Model dissolved PO4 - constant K_d (mg/L)		Model dissolved PO4 - dynamic K_d (mg/L)	
	Minimum	Maximum	Minimum	Maximum	Minimum	Maximum
1	0.09	0.91	1.13	1.83	0.71	1.38
2	0.08	0.95	0.62	1.15	0.36	0.87
3	0.06	0.66	1.25	2.30	0.72	1.73
4	0.15	0.93	1.18	2.33	0.85	1.69
5	0.11	0.99	1.05	2.25	0.66	1.77
6	0.09	0.57	0.65	1.36	0.46	1.14
7	0.05	0.72	0.35	1.00	0.28	0.82
8	0.16	0.81	0.28	0.97	0.25	0.84
9	0.13	1.15	0.27	1.06	0.24	0.81

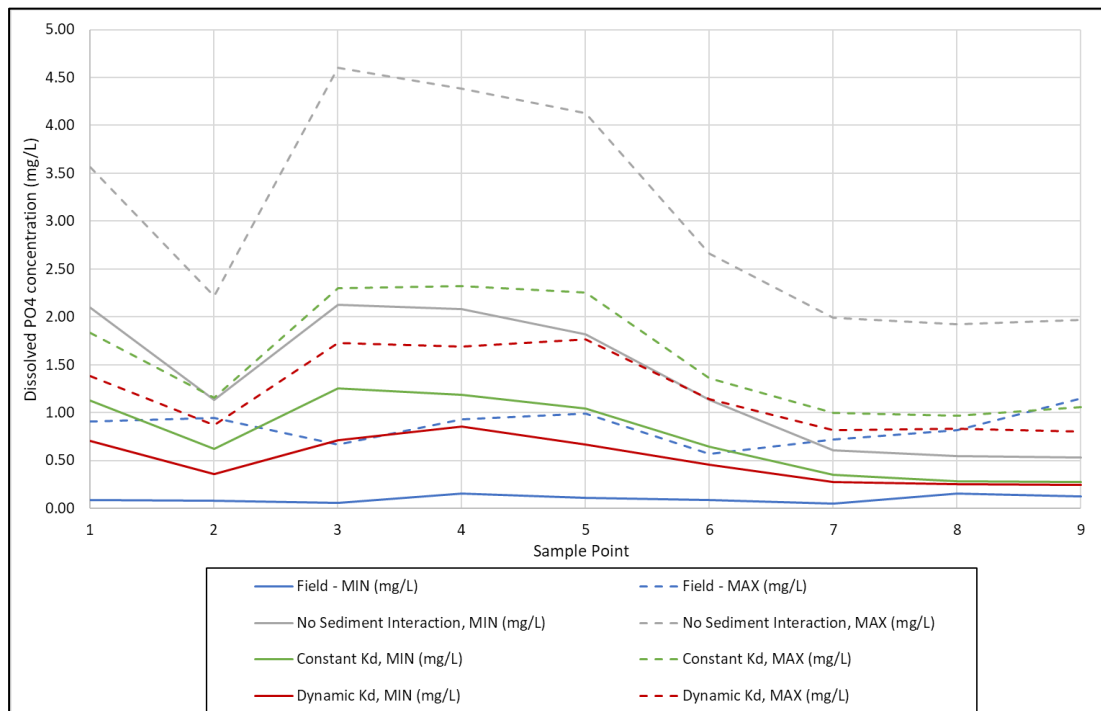


Figure 7-10 - Comparison of dissolved PO_4 ranges at each sample point when varying the prediction method

Table 7-4 and Figure 7-10 show the reduced concentrations predicted by the model when using the salinity-linked partition coefficient. The decrease to predicted dissolved levels is larger as the sample points move up the

estuary, due to the lower salinity and thus higher partition coefficient. As the complexity of the model increases, from no sediment interaction, to a constant K_d , and finally to a dynamic K_d , the predicted range of dissolved PO_4 levels move closer in line with the field data.

7.6 Chapter summary

The SEM was taken from a model without a water quality set up, to one that was capable of simulating salinity, suspended sediment, phosphate, and the interaction between the three.

When simulating phosphate only, the SEM was shown to be a poor predictor of dissolved phosphate levels. Without sediment interaction only total phosphate levels can be calculated, with no divide between the states of dissolved and adsorbed. This leads to an overprediction of the biologically available phosphate compared to dissolved levels measured in the estuary.

The addition of the simulation of suspended sediment, validated against Environment Agency data, enabled the distinction between the phases of phosphate. By assuming a constant partition coefficient, taken from the limited literature available, the prediction of dissolved phosphate levels was roughly halved, the other half being sorbed to the suspended sediment. This brought the dissolved prediction much closer in line with the range of the field data.

A further refinement to the prediction was made by modelling salinity, and incorporating a relationship found in experimental work between salinity and the partition coefficient for phosphate. A piecewise function described

the equation in EFDC, allowing a K_d that varied spatially and temporally with changes in suspended sediment and salinity. In general, this raised the partition coefficient, particularly in the upper reaches of the estuary where the salinity is lower. This had the effect of increasing the proportion of the phosphate adsorbed to suspended sediment, lowering the dissolved concentration and bringing the model results further in agreement with the field data.

The implication of the findings is that without modelling sediment and associating phosphate, the eutrophication potential of an estuary or river may be overestimated as the bioavailable proportion of phosphate cannot be ascertained.

Whilst the improvement from the inclusion of the dynamic K_d may have been subtle, the significance goes beyond the difference of the predicted dissolved levels, as the values were based on experimental data using samples from the Severn Estuary. This helps to remove some of the uncertainty in phosphate modelling, since the suggested K_d value from previous literature was within the range of the dynamic partition coefficient. Although the partition coefficient forms only one of the many variables in the complex process of the phosphorus cycle and the ratio of dissolved to sorbed phosphate, the results demonstrate that

Phosphate levels and sediment association is of particular relevance to the Severn Estuary, and to the subject of tidal power. The tidal renewable proposals discussed in previous chapters would undoubtedly have an effect on suspended sediment levels within the estuary. If the effect was a

reduction in suspended sediment levels, it could have the consequence of increasing dissolved phosphate levels due to fewer sorption sites, increasing the eutrophication potential of the estuary.

Chapter 8

Conclusions and future work

8.1 Conclusions and limitations

The research presented in this thesis focused on improvements to hydro-environmental modelling, by applying updates to the EFDC model to tidal renewable case studies and water quality simulation in the Severn Estuary.

The literature review identified several gaps in tidal renewable modelling work to date, including:

- an accurate assessment of the far-field impacts of a Severn Barrage;
- an assessment of the impact of hydraulic structure representation on model predictions in tidal renewable modelling;
- uncertainty around the discharge coefficient in modelling sluice gates and turbines;
- correct momentum conservation in modelling turbines using domain decomposition/an internal boundary;
- 3D modelling of the Severn Barrage;
- the role of 2D hydraulic models in design optimisation for tidal lagoons;
- uncertainty around the partition coefficient for phosphate adsorption; and
- the effect of the inclusion of an experimentally derived salinity-linked partition coefficient on dissolved phosphate predictions.

8.1.1 Hydraulic structure representation and barrage impact assessment

It was shown that in modelling the ebb-generating STPG barrage, the domain must be extended to that of the CSM to ensure the operation of the structure has no impact on the open boundary. Refinements to the representation of turbines and sluices within the EFDC CSM, namely representing the discharge through turbines from an industry provided hill-chart and through sluice gates using the orifice equation, provided the first accurate assessment of the far-field effects of the Severn Barrage. The refinements altered the model's predictions of the impacts on maximum water levels upstream of the barrage by almost 1 m, and raised maximum levels downstream. The far-field impacts were reduced, with a significantly diminished effect on the west coasts of Wales and Scotland. In providing the updated assessment of the potential effects of the barrage, the importance of accurate hydraulic structure was highlighted by the considerable changes in model prediction of maximum water levels.

Using the updated EFDC CSM, a suite of simulations was created to assess the sensitivity of the model to the discharge coefficient. The discharge coefficient is directly proportional to the flow through an orifice, and hence a critical parameter in the representation of sluice gates and turbines. With limited literature available on the value to use for C_d , model scenarios were created varying the value by 5 and 10% in either direction from the suggested value of 1 by Baker (Baker, 2006) and the impact on water levels and energy output of the barrage compared. Despite the instantaneous

discharge being directly proportional to the C_d value, the continual nature of the filling the basin, and the increased head difference at each succeeding time step caused by the reduced discharge, mitigated the effect of lowering the C_d value, such that a 10% reduction in the C_d value caused a 4% reduction to annual energy output. The results reduce the uncertainty associated with the discharge coefficient by demonstrating the (relative) insensitivity to its value considering its directly proportional role. An additional 5 scenarios were created to demonstrate that any performance loss in the barrage caused by potential overestimation of the C_d value could be mitigated through a proportional increase in sluice capacity.

The EFDC model represents the discharge through hydraulic structures in a tidal renewable device through a technique of applying an internal boundary. The volume is calculated based on the head difference either side of the structure and the chosen parameters and representation of the structure. Initially, however, although the volume calculation took into account the dimensions of the hydraulic structure, the momentum did not, and was calculated based on the EFDC internal solution which assumes the volume was added to the entire depth and width of the cell. An update to the momentum calculation replaced the cell depth and width with the flow-through area of the hydraulic structure, ensuring the conservation of momentum. A measurable effect was seen on the velocities and wake persistence of the turbine cells when modelling a Severn Barrage. This could potentially have the impact of worsening recirculation effects and their associated problems, particularly in tidal lagoon proposals where the basin size is much smaller.

Extending the momentum investigation to 3D by increasing the number of vertical layers to 5, enabled the vertical velocity profile of the turbine wake to be assessed. The corrected momentum representation was applied, and the turbine simulated in the 2nd of 5 layers, where the 1st is in contact with the bed. The vertical velocity profile showed elevated velocities in the 2nd layer immediately downstream of the turbine. The velocity profile returned to a more typical profile between 300 - 400 m downstream of the turbine, suggesting that the wake may persist to that distance.

The results of the 3D and 2D models of the Severn Barrage were compared, assessing the differences in water levels and energy generated. The results were near identical, indicating that in the case of the Severn Barrage it is sufficient to perform the hydraulic modelling in 2D, unless looking at the vertical velocity profile of the turbine induced wake.

8.1.2 2D models in lagoon scheme optimisation

The Bridgwater Bay Lagoon was one of the shortlisted schemes in the 2010 DECC study on tidal power development in the Severn Estuary. A prospective design was presented, with 144 turbines housed in two locations along a lagoon wall from Hinkley Point to Brean Down.

The SEM was used to determine likely minimum water depths along the proposed lagoon line, and demonstrated that depth would be a major constraint to the housing of turbines in the southern of the two sites. A stretch of 5.5 km at the northern turbine housing site location had sufficient minimum depth to ensure the turbines would always be submerged.

The SEM was refined to give cell sizes of 15 x 15 m in the vicinity of Bridgwater Bay. To demonstrate the applicability of the EFDC model to aid optimisation of tidal lagoons, 13 model scenarios were created, varying the number of turbines in the 5.5 km northern site. The turbine quantity varied from 60 to 360, with the aim of comparing the peak power, total energy, average generating time and tidal range preservation of each scenario.

The results showed that there is a diminishing return on peak power with each additional turbine, particularly after around 200 turbines where the peak power did not increase.

Somewhat counter intuitively, total energy output of the lagoon was maximised with just 120 turbines. One might expect a similar diminishing (but positive) return with each additional turbine, however, the results demonstrated that additional turbines may in fact reduce total energy output. This is because with fewer turbines, the generating cycles are operated at a higher head difference, increasing the power output of each turbine sufficiently that the lower installed capacity is mitigated. Additionally, with fewer turbines the number of generating hours per cycle is increased, as the lagoon is emptied or filled more quickly with greater numbers of turbines.

The tidal range within the lagoon is best preserved with the maximum number of turbines. The maximum number of turbines allows the most exchange of volume between the lagoon and the estuary, minimising intertidal loss.

In the design process for a lagoon, the developer will need to minimise environmental damage, while maximising energy output and minimising cost. Various options would be available from a design perspective to keep turbine numbers low while maintaining the tidal range within the lagoon, including sluice gates and pumping. Both of these options would have to be integrated into a suite of designs for a formal design process, and the study demonstrates the capability of the 2D model to assist in this procedure.

8.1.3 Water quality modelling

The EFDC model has been chosen for this study partly due to its capacity to simulate sediment and water quality. Prior to this research, the SEM had not been used to simulate water quality processes in the Severn Estuary.

Phosphate concentrations are of particular concern in many estuaries, due to the heavy nutrient loading associated with intensive land use in coastal areas and the combination of marine and freshwater sources. Phosphate is known to be strongly sediment associated, and less readily available to algae uptake when adsorbed rather than dissolved. In assessing the eutrophication potential of an estuary, it is therefore important to include a representation of the phosphate-sediment interaction.

Data on the phosphate loadings from wastewater treatment works and Severn Estuary tributaries were provided by the Environment Agency and Natural Resources Wales, allowing the simulation of total phosphate levels in the SEM. With very limited field data on phosphate concentrations, it was not possible to validate or calibrate the model, other than to demonstrate that the model predictions were within the same range as the field data.

Simulating total phosphate only, and assuming it was all in a dissolved phase, overestimated the concentrations in the Severn Estuary. In order to improve the prediction of dissolved phosphate levels, suspended sediment was also modelled, and their relationship defined using a partition coefficient. The limited literature on phosphate partition coefficients suggested a value of 0.5 L/g. The suspended sediment concentrations were validated and calibrated at two sites for which the Environment Agency provided field data.

Modelling dissolved phosphate levels with sediment interaction roughly halved the predicted concentrations, bringing them much closer in line with the field data.

Experimental work in the Severn Estuary defined a relationship between salinity and the partition coefficient of phosphate. This had not been implemented into a hydraulic model before, and provided a second method of partitioning the phases of phosphate to compare with the value obtained from current literature. The salinity-linked partition coefficient increased as salinity decreased, suggested to be due to less competition for sorption sites with seawater anions. The salinity-linked partition coefficient varied spatially and temporally throughout the model run, but generally within the range of 0.5 - 0.7 L/g. The raised partition coefficient in the upper estuary, where salinity is lower, reduced the proportion of phosphate in the dissolved phase, further bringing the model predictions in line with observed field data.

The important conclusions of the water quality research are that it is difficult to accurately predict dissolved phosphate without associating sediment, and the likely outcome is the overprediction of the eutrophication potential of the modelled estuary. Including suspended sediment and a constant K_d in the simulation hugely improved the prediction, despite large uncertainty around the value of K_d . Some of the uncertainty in the K_d value was removed by implementing an empirically derived relationship between salinity and the partition coefficient, developed from field data collected in the Severn Estuary.

The tidal renewable proposals modelled as part of this research project would likely impact suspended sediment levels in the Severn Estuary. The EFDC SEM is now sufficiently developed that it could be used to determine the impacts of tidal renewable proposals on not only the hydrodynamics in the estuary, but also the suspended sediment levels, salinity and dissolved phosphate concentrations, using an empirically derived partition coefficient.

8.2 Recommendations for future work

The thesis addressed several of the shortcomings in tidal renewable and water quality modelling, however, several areas of interest were left unexplored due to data, time and computational restraints.

Over the duration of the research, commercial and government interest has increased focus on tidal lagoon proposals, with several different locations suggested including Swansea, Cardiff, Bridgwater, Colwyn Bay, West Cumbria and others internationally. There is the suggestion that a fleet of

tidal lagoons could be operated around Wales, generating energy holistically due to the difference in time timings. Although there has been some limited research into the combined effects of tidal lagoons in the Severn Estuary or in North Wales, the updated CSM has the potential to model the entire network, demonstrating energy output timings and any potential interactions.

The huge benefit of flood protection offered by tidal lagoons could be quantified using the updated SEM, and a 2D extension to represent, for example, the River Parrett feeding into Bridgwater Bay. Using the lagoon to maintain a low water level in the bay despite a tidal storm surge applied at the open boundary would enable the demonstration of the increased conveyance offered by the river, reducing flood extents and depths in the Somerset Levels.

The updated momentum calculations indicated a potential for higher velocities and turbine wakes persisting further than previously modelled. Recirculation effects would be worsened by faster, longer turbine wakes, particularly in tidal lagoons where the basin is clearly smaller than upstream of the barrage. Using the updated momentum calculation, and the calibrated suspended sediment module in the SEM, the potential effects of the recirculation on sediment deposition within tidal lagoons could be assessed, in both 2 and 3 dimensions.

A further outcome of the faster velocities and longer wakes associated with the updated momentum calculation is the potential for tidal stream devices to take advantage of the energy. A 3D simulation of the Severn Barrage,

with tidal stream turbines strategically placed to extract energy from the fast-moving wake could demonstrate even higher energy potential in the Severn Estuary.

Although the refined SEM was shown to be a useful tool in lagoon design optimisation, multiple additional scenarios would need to be considered to aid the development process. This would include sluicing, pumping, and potentially different lagoon wall lines or dredging to accommodate other turbine housing sites. A comprehensive suite of design options could help to reduce potential environmental impacts of the operation of a tidal lagoon, while increasing energy output and reducing wasted capacity and cost.

The water quality research within this thesis provides a platform from which the effects of the Severn Barrage and tidal lagoons on salinity, sediment and phosphate levels can be assessed. Before the results could be considered sufficiently conclusive to incorporate the barrage module to the water quality study, further field data would need to be acquired to validate the model.

Last, but not least, with increasingly complex simulations, larger domains and higher resolution modelling, the computational demands on the serial EFDC code are becoming prohibitive, with the refined SEM model taking upwards of 60 hours to run a 7-day simulation. If the sediment and water quality modules were to be introduced, or 3D modelling at that resolution required, the modelling times would be impractical. Incorporating the refinements to the EFDC model made in this thesis to the OpenMP version of EFDC would significantly reduce model runtimes, enabling further

complexity and detail to further improve the hydro-environmental modelling of marine renewable energy devices.

Chapter 9

References

Abdulgawad, F. (2010) 'Field and laboratory investigations of the adsorption of nitrogen compounds on estuarine based sediments', *Cardiff University*, PhD(March).

Ahmadian, R. and Falconer, R. A. (2012) 'Assessment of array shape of tidal stream turbines on hydro-environmental impacts and power output', *Renewable Energy*, 44, pp. 318-327. doi: 10.1016/j.renene.2012.01.106.

Ahmadian, R., Falconer, R. A. and Bockelmann-Evans, B. (2014) 'Comparison of hydro-environmental impacts for ebb-only and two-way generation for a Severn Barrage', *Computers and Geosciences*, 71(C), pp. 11-19. doi: 10.1016/j.cageo.2014.05.006.

Ahmadian, R., Falconer, R. and Bockelmann-Evans, B. (2012) 'Far-field modelling of the hydro-environmental impact of tidal stream turbines', *Renewable Energy*, 38(1), pp. 107-116. doi: 10.1016/j.renene.2011.07.005.

Ahmadian, R., Falconer, R. and Lin, B. (2010) 'Hydro-environmental modeling of proposed Severn barrage, UK', *Proceedings of the ICE - Energy*, 163(3), pp. 107-117. doi: 10.1680/ener.2010.163.3.107.

Ahmadian, R., Olbert, A. I., Hartnett, M. and Falconer, R. A. (2014) 'Sea level rise in the Severn Estuary and Bristol Channel and impacts of a Severn Barrage', *Computers and Geosciences*, 66, pp. 94-105. doi: 10.1016/j.cageo.2013.12.011.

Alcrudo, F. (2002) 'A state of the art review on mathematical modelling of flood propagation', *EC contract EVG1-CT-2001-00037 IMPACT investigation of extreme flood processes and uncertainty: Proceedings of the first*

IMPACT project workshop, Wallingford, UK, May 2002 (CD-ROM), pp. 1-22.
Available at: http://www.impact-project.net/cd/papers/print/008_pr_02-05-16_IMPACT_Alcrudo.pdf.

Alcrudo, F. (2004) 'Mathematical modeling techniques for flood propagation in urban areas', *Buscar*, pp. 1-34.

Anderson, D. M., Glibert, P. M. and Burkholder, J. M. (2002) 'Harmful algal blooms and eutrophication: Nutrient sources, composition, and consequences', *Estuaries*, 25(4 B), pp. 704-726. doi: 10.1007/BF02804901.

Anderson, J. D. and Wendt, J. (1995) *Computational fluid dynamics*. Springer.

Andre, H. (1978) 'Ten Years of Experience at the "La Rance" Tidal Power Plant', *Ocean Management*, 4(4), pp. 165-178. doi: 10.1016/0302-184X(78)90023-9.

Angeloudis, A., Ahmadian, R., Falconer, R. A. and Bockelmann-Evans, B. (2016) 'Numerical model simulations for optimisation of tidal lagoon schemes', *Applied Energy*. Elsevier Ltd, 165, pp. 522-536. doi: 10.1016/j.apenergy.2015.12.079.

Angeloudis, A. and Falconer, R. A. (2016) 'Sensitivity of tidal lagoon and barrage hydrodynamic impacts and energy outputs to operational characteristics', *Renewable Energy*. Elsevier Ltd. doi: 10.1016/j.renene.2016.08.033.

Angeloudis, A., Falconer, R. A., Bray, S. and Ahmadian, R. (2016) 'Representation and operation of tidal energy impoundments in a coastal

hydrodynamic model', *Renewable Energy*. Elsevier Ltd, 99, pp. 1103-1115. doi: <http://dx.doi.org/10.1016/j.renene.2016.08.004>.

Atlantis Resources (2017) *MeyGen Phase 1*. Available at: <https://www.atlantisresourcesltd.com/projects/meygen/> (Accessed: 20 March 2018).

Bae, Y. H., Kim, K. O. and Choi, B. H. (2010) 'Lake Sihwa tidal power plant project', *Ocean Engineering*, 37(5-6), pp. 454-463. doi: 10.1016/j.oceaneng.2010.01.015.

Baker, C. (1991) 'Tidal power', *Energy Policy*, 19(8), pp. 792-797. doi: 10.1016/0301-4215(91)90049-T.

Baker, C. (2006) 'Tidal Power', *The Institute of Engineering and Technology*, p. 250.

Baker, C. and Leach, P. (2006) 'Tidal Lagoon Power Generation Scheme in Swansea Bay', (April).

Bathe, K.-J. and Wilson, E. L. (1976) *Numerical methods in finite element analysis*. Prentice-Hall Englewood Cliffs, NJ.

Bernshtein, L. B. (1972) 'Kislava Guba Experimental Tidal Power Plant and Problem of the Use of Tidal Energy', in Gray, T. J. and Gashus, O. K. (eds) *Tidal Power: Proceedings of an International Conference on the Utilization of Tidal Power held May 24--29, 1970, at the Atlantic Industrial Research Institute, Nova Scotia Technical College, Halifax, Nova Scotia*. Boston, MA: Springer US, pp. 215-238. doi: 10.1007/978-1-4613-4592-3_6.

Black & Veatch (2005) 'Phase II - UK Tidal Stream Energy Resource Assessment', *Black & Veatch, London*, 44(0), p. 14. Available at: <http://scholar.google.com/scholar?hl=en&btnG=Search&q=intitle:UK+Tidal+Stream+Energy+Resource+Assessment#7>.

Blunden, L. S. and Bahaj, A. S. (2006) 'Initial evaluation of tidal stream energy resources at Portland Bill, UK', *Renewable Energy*, 31(2), pp. 121-132. doi: 10.1016/j.renene.2005.08.016.

Bockelmann-Evans, B. N., Schnauder, I., Fenrich, E. K., Falconer, R. A., Fenrich, E. K. and Schnauder, I. (2007) 'Development of a catchment-wide nutrient model', *Water Management*, 160(March), pp. 35-42. doi: 10.1680/wama.2007.160.1.35.

Brammer, J., Roger, A. F., Christopher, E. and Reza, A. (2014) 'Physical and numerical modelling of the Severn Barrage', *Science China Technological Sciences*, 57(8), pp. 1471-1481. doi: 10.1007/s11431-014-5602-5.

Bray, S. (2009) *Water Quality Impact of Nutrient Adsorption in Sediment of the Severn Estuary*. University of Cardiff.

Bray, S., Ahmadian, R. and Falconer, R. A. (2014) 'Refinements to turbine representation in modelling the Severn Barrage', in. 3rd European IAHR Congress. Available at: <http://webpages.fe.up.pt/iahr2014/>.

Bray, S., Ahmadian, R. and Falconer, R. A. (2015) 'Sensitivity study of modelling of Severn Barrage performance', *Renewable Energies Offshore*. CRC Press, p. 147.

Bray, S., Ahmadian, R. and Falconer, R. A. (2016) 'Impact of representation

of hydraulic structures in modelling a Severn barrage’, *Computers and Geosciences*. Elsevier, 89, pp. 96-106. doi: 10.1016/j.cageo.2016.01.010.

British Hydro (2008) *Sihwa Tidal - Turbines and generators for the world’s largest tidal power plant*. Available at: <http://www.british-hydro.org/uploads/1132008110145AM.pdf> (Accessed: 8 March 2017).

British Hydro (2009) *La Rance Tidal Power Plant - 40-year operation feedback - Lessons learnt*. Available at: http://www.british-hydro.org/downloads/La_Rance-BHA-Oct_2009.pdf (Accessed: 7 March 2017).

Bryden, I. G. and Couch, S. J. (2006) ‘ME1—marine energy extraction: tidal resource analysis’, *Renewable Energy*, 31(2), pp. 133-139. doi: 10.1016/j.renene.2005.08.012.

Bui, T. (2010) ‘Explicit and Implicit Methods In Solving Differential Equations’, *Honors Scholar Theses, University of Connecticut*, (Paper 119), p. 48.

CAA (2017) *Power for the Future, Canadian Electricity Association*. Available at: <http://powerforthefuture.ca/project/annapolis-tidal-station-2/> (Accessed: 8 March 2017).

Casulli, V. (1990) ‘Semi-implicit finite difference methods for the two-dimensional shallow water equations’, *Journal of Computational Physics*. Elsevier, 86(1), pp. 56-74.

Chaineux, M. C. and Charlier, R. H. (2008) ‘Women’s tidal power plant Forty candles for Kislava Guba TPP’, *Renewable and Sustainable Energy Reviews*,

pp. 2508-2517. doi: 10.1016/j.rser.2007.03.013.

Charlier, R. H. (2007) 'Forty candles for the Rance River TPP tides provide renewable and sustainable power generation', *Renewable and Sustainable Energy Reviews*, pp. 2032-2057. doi: 10.1016/j.rser.2006.03.015.

Charlier, R. H., Chaineux, M.-C., Finkl, C. W. and Thys, A. C. (2012) 'Power from Arctic waters', *International Congress of Polar Science*, (42), pp. 93-102.

Chaunkun, W. (2009) 'History, Current state and Prospect of the Development of Ocean Energy in China', *Proceedings of international ocean energy symposium*.

Cho, Y.-S., Lee, J. W. and Jeong, W. (2012) 'The Construction of a Tidal Power Plant at Sihwa Lake, Korea', *Energy Sources, Part A: Recovery, Utilization, and Environmental Effects*, 34(14), pp. 1280-1287. doi: 10.1080/15567030903586055.

Choi, B. H., Choi, D. J., Choi, J. C. and Kim, K. O. (2010) 'Construction status of sihwa lake tidal power plant project', in *Proceedings of the 5th International Conference on Asian and Pacific Coasts, APAC 2009*, pp. 45-51. doi: 10.1142/9789814287951_0004.

Clavero, V., García, M., Fernández, J. A. and Niell, F. X. (1993) 'Adsorption-desorption of phosphate and its availability in the sediment of a saline lake (Fuente de Piedra, southern Spain)', *International Journal of Salt Lake Research*. Springer, 2(2), pp. 153-163.

Copping, A., Battey, H., Brown-Saracino, J., Massaua, M. and Smith, C.

(2014) 'An international assessment of the environmental effects of marine energy development', *Ocean and Coastal Management*. Elsevier Ltd, 99(C), pp. 3-13. doi: 10.1016/j.ocecoaman.2014.04.002.

Cornett, A., Cousineau, J. and Nistor, I. (2013) 'Assessment of hydrodynamic impacts from tidal power lagoons in the Bay of Fundy', *International Journal of Marine Energy*, 1, pp. 33-54. doi: 10.1016/j.ijome.2013.05.006.

Correll, D. L. (1998) 'The Role of Phosphorus in the Eutrophication of Receiving Waters: A Review', *Journal of Environment Quality*, 27(2), p. 261. doi: 10.2134/jeq1998.00472425002700020004x.

Courant, R., Friedrichs, K. and Lewy, H. (1967) 'On the partial difference equations of mathematical physics', *IBM journal of Research and Development*. IBM, 11(2), pp. 215-234.

Craig, P. (2017) *Theory Guide For EFDC+*.

DECC (2010a) 'Severn tidal power - Feasibility Study Conclusions and Summary Report', *October*, (October), pp. 1-75. doi: 10.1073/pnas.0703993104.

DECC (2010b) 'STRATEGIC ENVIRONMENTAL ASSESSMENT OF PROPOSALS FOR TIDAL POWER DEVELOPMENT IN THE SEVERN ESTUARY', 1(3).

DECC (2011) 'UK Renewable Energy Roadmap', *Carbon*, 5(July), pp. 293-298. doi: 10.1021/es00108a605.

DECC (2012) *2010 to 2015 government policy: low carbon technologies*. Available at: <https://www.gov.uk/government/publications/2010-to-2015->

government-policy-low-carbon-technologies/2010-to-2015-government-policy-low-carbon-technologies.

DECC (2013a) 'A Severn Barrage?', *House of Commons Energy and Climate Change Committee*, (May).

DECC (2013b) *Wave and tidal energy: part of the UK's energy mix, Low carbon energy*. Available at: <https://www.gov.uk/guidance/wave-and-tidal-energy-part-of-the-uks-energy-mix> (Accessed: 10 March 2017).

DECC (2015a) 'Digest of UK Energy Statistics: Chapter 5 Electricity', in *Digest of UK Energy Statistics*, pp. 113-155. doi: 10.1227/01.NEU.0000028161.91504.4F.

DECC (2015b) *Digest of UK Energy Statistics: Chapter 6 Renewables*.

DECC (2015c) *Tidal Lagoon Swansea Bay - National Infrastructure Planning*. Available at: <https://infrastructure.planninginspectorate.gov.uk/projects/wales/tidal-lagoon-swansea-bay/> (Accessed: 8 March 2017).

DEFRA (2003) 'Energy White Paper - Our energy future - creating a low carbon economy', *Energy Review*, p. 142. Available at: <http://webarchive.nationalarchives.gov.uk/+http://www.berr.gov.uk/files/file10719.pdf>.

Delft (2006) 'Delft3D-RGFGRID: Generation and Manipulation of Curvilinear Grids for FLOW and WAVE', *User Manual*.

Demirbaş, A. (2006) 'Global Renewable Energy Resources', *Energy Sources*,

28(8), pp. 779-792. doi: 10.1080/00908310600718742.

DHI (2014) 'Mike 21 toolbox: User guide', p. 268.

Diersing, N. (2009) 'Phytoplankton blooms: The basics', *Florida Keys National Marine Sanctuary, Key West, Florida, USA*, 2.

DSI (2013) 'Environmental Fluid Dynamics Code (EFDC) Model Description Hydrodynamics Water Quality Sediment Transport Toxics Figure 1 Primary modules of the EFDC model .', (1), pp. 1-12.

DSI (2016) *CVLGrid*. Available at: <http://www.efdc-explorer.com/downloads/cvlgrid.html>.

DTI (2003) *Our energy future - creating a low carbon economy*. Available at: <https://www.gov.uk/government/publications/our-energy-future-creating-a-low-carbon-economy>.

Electric-Power (2015) *Sihwa Lake Tidal Power Plant, Gyeonggi Province*. Available at: <http://www.powermag.com/sihwa-lake-tidal-power-plant-yeonggi-province-south-korea/?pagenum=1> (Accessed: 8 March 2017).

Ben Elghali, S. E., Benbouzid, M. E. H. and Charpentier, J. F. (2007) 'Marine tidal current electric power generation technology: State of the art and current status', *Proceedings of IEEE International Electric Machines and Drives Conference, IEMDC 2007*, 2, pp. 1407-1412. doi: 10.1109/IEMDC.2007.383635.

Environment Agency (2017) *Environment Agency Flood Map for Planning*. Available at: <https://flood-warning-information.service.gov.uk/warnings>.

-
- Fairley, I., Ahmadian, R., Falconer, R. A., Willis, M. R. and Masters, I. (2014) 'The effects of a Severn Barrage on wave conditions in the Bristol Channel', *Renewable Energy*. Elsevier Ltd, 68, pp. 428-442. doi: 10.1016/j.renene.2014.02.023.
- Fairley, I., Evans, P., Wooldridge, C., Willis, M. and Masters, I. (2013) 'Evaluation of tidal stream resource in a potential array area via direct measurements', *Renewable Energy*, 57, pp. 70-78. doi: 10.1016/j.renene.2013.01.024.
- Falconer, R. A., Xia, J., Lin, B. and Ahmadian, R. (2009) 'The Severn Barrage and other tidal energy options: Hydrodynamic and power output modeling', *Science in China, Series E: Technological Sciences*, 52(11), pp. 3413-3424. doi: 10.1007/s11431-009-0366-z.
- Fallon, D., Hartnett, M., Olbert, A. and Nash, S. (2014) 'The effects of array configuration on the hydro-environmental impacts of tidal turbines', *Renewable Energy*. Elsevier Ltd, 64, pp. 10-25. doi: 10.1016/j.renene.2013.10.035.
- Ferziger, J. H. and Peric, M. (2002) *Computational Methods for Fluid Dynamics*, Vasa. doi: 10.1016/S0898-1221(03)90046-0.
- Foxon, T. J., Gross, R., Chase, A., Howes, J., Arnall, A. and Anderson, D. (2005) 'UK innovation systems for new and renewable energy technologies: Drivers, barriers and systems failures', *Energy Policy*, 33(16), pp. 2123-2137. doi: 10.1016/j.enpol.2004.04.011.
- Fraenkel, P. L. (2002) 'Power from marine currents', *Proceedings of the I*

MECH E Part A Journal of Power and Energy, 216(1), pp. 1-14. doi: 10.1243/095765002760024791.

Fraenkel, P. L. (2006) 'Tidal current energy technologies', *Ibis*, 148(SUPPL. 1), pp. 145-151. doi: 10.1111/j.1474-919X.2006.00518.x.

Frau, J. P. (1993) 'Tidal energy: Promising projects la rance, a succesful Industrial-scale experiment', *IEEE Transactions on Energy Conversion*, 8(3), pp. 552-558. doi: 10.1109/60.257073.

Frid, C., Andonegi, E., Depestele, J., Judd, A., Rihan, D., Rogers, S. I. and Kenchington, E. (2012) 'The environmental interactions of tidal and wave energy generation devices', *Environmental Impact Assessment Review*, pp. 133-139. doi: 10.1016/j.eiar.2011.06.002.

Galperin, B., Kantha, L. H., Hassid, S. and Rosati A (1988) 'A Quasi-Equilibrium Turbulent Energy-Model for Geophysical Flows', *Journal Of The Atmospheric Sciences*, 45(1), pp. 55-62. Available at: http://www.gfdl.noaa.gov/bibliography/related_files/bg8801.pdf%5Cnpapers2://publication/uuid/E240DC81-6657-431B-8780-B7404273350A.

Gao, G., Falconer, R. A. and Lin, B. (2013) 'Modeling effects of a tidal barrage on water quality indicator distribution in the Severn Estuary', *Frontiers of Environmental Science and Engineering*, 7(2), pp. 211-218. doi: 10.1007/s11783-012-0464-1.

Goldwag, E. and Potts, R. (1989) '5. Energy production', in *Developments in tidal energy*, pp. 75-91. doi: 10.1680/dite.15715.0007.

Hammons, T. J. (1993) 'Tidal Power', *Proceedings of the IEEE*, 81(3), pp.

419-433. doi: 10.1109/5.241486.

Hammons, T. J. (2008) 'Energy Potential of the Oceans in Europe and North America: Tidal, Wave, Currents, Otec and Offshore Wind', *International Journal of Power and Energy Systems*, 28(4), pp. 416-428. doi: 10.2316/Journal.203.2008.4.203-4142.

Hamrick, J. M. (1992) *A three-dimensional environmental fluid dynamics computer code: Theoretical and computational aspects*. Virginia Institute of Marine Science, College of William and Mary.

Hamrick, J. M. and Wu, T. S. (1997) 'Computational design and optimization of the EFDC/HEM3D surface water hydrodynamic and eutrophication models', in *Next generation environmental models and computational methods*. Society for Industrial and Applied Mathematics, Philadelphia, PA, pp. 143-161.

Hartnett, M. and Nash, S. (2004) 'Modelling nutrient and chlorophyll_a dynamics in an Irish brackish waterbody', *Environmental Modelling and Software*, 19(1), pp. 47-56. doi: 10.1016/S1364-8152(03)00109-9.

Hendry, C. (2016) 'The role of tidal lagoons final report', (December).

Holligan, P. M. and Boois, H. de (1993) 'Land ocean interactions in the coastal zone (LOICZ). Science plan', *Global Change Report (Sweden)*. IGBP Secretariat.

IHA (2016) *Technology case study: Sihwa Lake tidal power station*. Available at: <https://www.hydropower.org/blog/technology-case-study-sihwa-lake-tidal-power-station> (Accessed: 7 March 2017).

IRF (2013) 'SMARTtide: a unique tidal energy modelling tool', *Innovation & Research*, (95), pp. 1-8.

Ji, Z.-G. (2017) *Hydrodynamics and water quality: modeling rivers, lakes, and estuaries*. John Wiley & Sons.

De Jonge, V. N., Elliott, M. and Orive, E. (2002) 'Causes, historical development, effects and future challenges of a common environmental problem: Eutrophication', *Hydrobiologia*, 475-476, pp. 1-19. doi: 10.1023/A:1020366418295.

Kadiri, M., Ahmadian, R., Bockelmann-Evans, B., Falconer, R. A. and Kay, D. (2014) 'An assessment of the impacts of a tidal renewable energy scheme on the eutrophication potential of the Severn Estuary, UK', *Computers and Geosciences*, 71, pp. 3-140. doi: 10.1016/j.cageo.2014.07.018.

Kadiri, M., Ahmadian, R., Bockelmann-Evans, B., Rauen, W. and Falconer, R. (2012) 'A review of the potential water quality impacts of tidal renewable energy systems', *Renewable and Sustainable Energy Reviews*, pp. 329-341. doi: 10.1016/j.rser.2011.07.160.

Kadiri, M. and Bockelmann-Evans, B. (2012) 'Water Quality Model Development for Estuaries: a Combined Numerical and Experimental Approach', *Researchgate.Net*. Available at: http://www.researchgate.net/publication/233863983_WATER_QUALITY_MODEL_DEVELOPMENT_FOR_ESTUARIES_A_COMBINED_NUMERICAL_AND_EXPERIMENTAL_APPROACH/file/79e4150c60de8d8df1.pdf.

Kemp, W. M., Wetzel, R. L., Boynton, W. R., D'Ella, C. F. and Stevenson, J.

C. (1981) 'Nitrogen cycling and estuarine interfaces: some current concepts and research directions'.

Kerr, D. (2007) 'Marine energy', *Philosophical Transactions of the Royal Society A. Mathematical, Physical, and Engineering Sciences*, 365(1853), pp. 971-92. doi: 10.1098/rsta.2006.1959.

Khan, M. J., Bhuyan, G., Iqbal, M. T. and Quaicoe, J. E. (2009) 'Hydrokinetic energy conversion systems and assessment of horizontal and vertical axis turbines for river and tidal applications: A technology status review', *Applied Energy*. Elsevier Ltd, 86(10), pp. 1823-1835. doi: 10.1016/j.apenergy.2009.02.017.

Kim, G., Lee, M. E., Lee, K. S., Park, J. S., Jeong, W. M., Kang, S. K., Soh, J. G. and Kim, H. (2012) 'An overview of ocean renewable energy resources in Korea', *Renewable and Sustainable Energy Reviews*. Elsevier Ltd, 16(4), pp. 2278-2288. doi: 10.1016/j.rser.2012.01.040.

Kirby, R. and Parker, W. R. (1983) 'Distribution and behavior of fine sediment in the Severn Estuary and Inner Bristol Channel, UK', *Canadian Journal of Fisheries and Aquatic Sciences*. NRC Research Press, 40(S1), pp. s83-s95.

Kirby, R. and Retiere, C. (2009) 'Comparing environmental effects of Rance and Severn barrages', *Proceedings of the Institution of Civil Engineers: Maritime Engineering*, 162(4), pp. 187-196. doi: 10.1680/maen.2009.162.

Knowles, S. and Myatt-Bell, L. (2001) 'The Severn Estuary Strategy: A consensus approach to estuary management', *Ocean and Coastal*

Management. Elsevier, 44(1-2), pp. 135-159. doi: 10.1016/S0964-5691(01)00044-8.

Van Der Kooij, L. A., Van De Meent, D., Van Leeuwen, C. J. and Bruggeman, W. A. (1991) 'Deriving quality criteria for water and sediment from the results of aquatic toxicity tests and product standards: Application of the equilibrium partitioning method', *Water Research*, 25(6), pp. 697-705. doi: 10.1016/0043-1354(91)90045-R.

Lauder, B. E. and Spalding, D. B. (1974) 'The numerical computation of turbulent flows', *Computer Methods in Applied Mechanics and Engineering*, 3(2), pp. 269-289. doi: 10.1016/0045-7825(74)90029-2.

Lax, P. D. and Wendroff, B. (1960) 'Systems of conservation laws', *Communications on Pure and Applied ...* Available at: <http://onlinelibrary.wiley.com/doi/10.1002/cpa.3160130205/abstract>.

Li, D., Wang, S. and Yuan, P. (2010) 'An overview of development of tidal current in China: Energy resource, conversion technology and opportunities', *Renewable and Sustainable Energy Reviews*, pp. 2896-2905. doi: 10.1016/j.rser.2010.06.001.

Lin, B., Yang, L. and Falconer, R. A. (2008) 'Modelling enteric bacteria level in coastal and estuarine waters', *Proceedings of the ICE - Engineering and Computational Mechanics*, 161(4), pp. 179-186. doi: 10.1680/eacm.2008.161.4.179.

Liu, H., Ma, S., Li, W., Gu, H., Lin, Y. and Sun, X. (2011) 'A Review on the Development of Tidal Current Energy in China', *Renewable and Sustainable*

Energy Reviews, 15(2), pp. 1141-1146. doi: 10.1016/j.rser.2010.11.042.

Logan, D. L., Veitch, E., Carson, C., Burrell, K. R., Gould, V., Wagner, E., Logan, D. L., Veitch, E., Carson, C., Burrell, K. R., Gould, V. and Wagner, E. (2007) *A First Course in the Finite Element Method Fourth Edition, Transport*. doi: 10.1016/0022-460X(91)90505-E.

Magnien, R. E., Summers, R. M. and Sellner, K. G. (1992) 'External Nutrient Sources, Internal Nutrient Pools, and Phytoplankton Production in Chesapeake Bay', *Estuaries*, 15(4), p. 497. doi: 10.2307/1352393.

Mattiusi, C. (1997) 'An analysis of finite volume, finite element, and finite difference methods using some concepts from algebraic topology', *Journal of Computational Physics*. Elsevier, 133(2), pp. 289-309.

Mellor, G. L. and Yamada, T. (1982) 'Development of a turbulence closure model for geophysical fluid problems', *Reviews of Geophysics*, pp. 851-875. doi: 10.1029/RG020i004p00851.

Mitchell, C. and Connor, P. (2004) 'Renewable energy policy in the UK 1990-2003', *Energy Policy*, 32(17), pp. 1935-1947. doi: 10.1016/j.enpol.2004.03.016.

Mueller, M. and Wallace, R. (2008) 'Enabling Science and Technology for Marine Renewable Energy', *Energy Policy*, 36(12), pp. 4376-4382. doi: 10.1016/j.enpol.2008.09.035.

Nash, J. E. and Sutcliffe, J. V. (1970) 'River flow forecasting through conceptual models part I - A discussion of principles', *Journal of Hydrology*, 10(3), pp. 282-290. doi: 10.1016/0022-1694(70)90255-6.

Nash, S., O'Brien, N., Olbert, A. and Hartnett, M. (2014) 'Modelling the far field hydro-environmental impacts of tidal farms - A focus on tidal regime, inter-tidal zones and flushing', *Computers and Geosciences*. Elsevier, 71, pp. 20-27. doi: 10.1016/j.cageo.2014.02.001.

Nash, S., Olbert, A. I. and Hartnett, M. (2015) 'Towards a low-cost modelling system for optimising the layout of tidal turbine arrays', *Energies*, 8(12), pp. 13521-13539. doi: 10.3390/en81212380.

Nash, S. and Phoenix, A. (2017) 'A review of the current understanding of the hydro-environmental impacts of energy removal by tidal turbines', *Renewable and Sustainable Energy Reviews*, pp. 648-662. doi: 10.1016/j.rser.2017.05.289.

Néelz, S., Pender, G. and Britain, G. (2009) *Desktop review of 2D hydraulic modelling packages*, Environment Agency. doi: 978-1-84911-079-2.

Neelz, S., Pender, G. and Wright, N. G. (2010) *Benchmarking of 2D Hydraulic Modelling Packages protecting and improving the environment in England and, Benchmarking*.

Neill, S. P., Litt, E. J., Couch, S. J. and Davies, A. G. (2009) 'The impact of tidal stream turbines on large-scale sediment dynamics', *Renewable Energy*, 34(12), pp. 2803-2812. doi: 10.1016/j.renene.2009.06.015.

Nixon, S. W. (1995) 'Coastal marine eutrophication: a definition, social causes, and future concerns', *Ophelia*, 41(September), pp. 199-219. doi: 10.1080/00785236.1995.10422044.

NOAA (2017) *Center for Operational Oceanographic Products and Services*.

Available at: <https://www.co-ops.nos.noaa.gov/faq2.html#26> (Accessed: 8 March 2017).

O'donncha, F., James, S. C., O'brien, N. and Ragnoli, E. (2016) 'Parallelisation of hydro-environmental model for simulating marine current devices', *OCEANS 2015 - MTS/IEEE Washington*.

O'Donncha, F., Ragnoli, E. and Suits, F. (2014) 'Parallelisation study of a three-dimensional environmental flow model', *Computers and Geosciences*, pp. 96-103. doi: 10.1016/j.cageo.2013.12.006.

Park, K. and Kuo, A. Y. (1996) 'A multi-step computation scheme: decoupling kinetic processes from physical transport in water quality models', *Water Research*. Elsevier, 30(10), pp. 2255-2264.

Patel, V. C., Rodi, W. and Scheuerer, G. (1985) 'Turbulence models for near-wall and low Reynolds number flows - A review', *AIAA Journal*, 23(9), pp. 1308-1319. doi: 10.2514/3.9086.

Pelc, R. and Fujita, R. M. (2002) 'Renewable energy from the ocean', *Marine Policy*, 26(6), pp. 471-479. doi: 10.1016/S0308-597X(02)00045-3.

Petley, S. and Aggidis, G. (2016) 'Swansea Bay tidal lagoon annual energy estimation', *Ocean Engineering*, 111, pp. 348-357. doi: 10.1016/j.oceaneng.2015.11.022.

Reddy, J. N. (1993) *An introduction to the finite element method*. McGraw-Hill New York.

Redfield, A. C. (1958) 'The Biological Control of Chemical Factors in the

Environment', *American Scientist*, 46(230), pp. 205-221. doi: 10.2307/27828530.

Renewable Energy Policy Network for the 21st Century (REN21) (2016) *Renewables 2016: global status report*. doi: ISBN 978-3-9818107-0-7.

Retiere, C. (1994) 'Tidal power and the aquatic environment of La Rance', *Biological Journal of the Linnean Society*, 51(1-2), pp. 25-36. doi: 10.1111/j.1095-8312.1994.tb00941.x.

Roache, P. J. (1998) 'Fundamentals of computational fluid dynamics(Book)', *Albuquerque, NM: Hermosa Publishers, 1998*.

Rodi, W. (1993) *Turbulence models and their application in hydraulics*. CRC Press.

Rourke, F. O., Boyle, F. and Reynolds, A. (2010) 'Tidal energy update 2009', *Applied Energy*, 87(2), pp. 398-409. doi: 10.1016/j.apenergy.2009.08.014.

Ryther, J. H. and Dunstan, W. M. (1971) 'Nitrogen, Phosphorus, and Eutrophication in the Coastal Marine Environment', *Science*, 171(3975), pp. 1008-1013. doi: 10.1126/science.171.3975.1008.

SBC (1981) 'Tidal power from the Severn Estuary', *Severn Barrage Committee - Her Majesty's Stationery Office, Energy Pap(2)*.

SDC (2007) 'Turning the Tide: Tidal Power in the UK', *Sustainable Development Commission*, (51), p. 16. doi: 10.1038/nbt1010-999.

Sellner, K. G., Doucette, G. J. and Kirkpatrick, G. J. (2003) 'Harmful algal blooms: Causes, impacts and detection', *Journal of Industrial Microbiology*

-
- and Biotechnology*, pp. 383-406. doi: 10.1007/s10295-003-0074-9.
- Severn Estuary Partnership (2001) *Strategy for the Severn Estuary*.
- Sibley, T. H. and Myttenaere, C. (1986) 'Application of distribution coefficients to radiological assessment models'.
- SMARTtide (2013) 'SMARTtide Launch', (May).
- Southeast National Marine Renewable Energy Centre (2017) *Ocean Energy Industry*. Available at: <http://coet.fau.edu/ocean-energy/ocean-energy-industry.html>.
- Stapleton, C. M., Wyer, M. D., Kay, D., Bradford, M., Humphrey, N., Wilkinson, J., Lin, B., Yang, Y., Falconer, R. A., Watkins, J. and Francis, C. A. (2007) *Fate and transport of particles in estuaries - Volume IV: Numerical modelling for bathing water enterococci estimation in the Severn estuary*, Environment Agency Science Report.
- Stephens, C. V. (1986) 'A three-dimensional model for tides and salinity in the Bristol Channel', *Continental Shelf Research*, 6(4), pp. 531-560. doi: 10.1016/0278-4343(86)90022-1.
- STPG (1989) 'The Severn Barrage Project: General Report', *Energy Paper Number 57*, Department of Energy, HMSO.
- Tetra Tech (2007) 'The Environmental Fluid Dynamics Code Theory and Computation - Volume 2: Sediment and Contaminant Transport and Fate', 2(June), p. 96.
- The Crown Estate (2012) 'UK Wave and Tidal Key Resource Areas Project -

Summary Report', (February), p. 10. Available at: <http://www.thecrownstate.co.uk/media/5478/uk-wave-and-tidal-key-resource-areas-technological-report.pdf>.

Tidal Lagoon Power, T. (2015) *Harnessing the power of our tides*. Available at: <http://www.tidallagoonpower.com/projects/swansea-bay/> (Accessed: 8 March 2017).

TUFLOW (2016) *Parallelisation of TufLOW Classic*. Available at: <https://www.tufLOW.com/forum/index.php?/topic/1574-parallelisation-of-tufLOW-classic/> (Accessed: 16 September 2017).

Uncles, R. J. (1984) 'Hydrodynamics of the Bristol channel', *Marine Pollution Bulletin*. Elsevier, 15(2), pp. 47-53.

Uncles, R. J. (2010) 'Physical properties and processes in the Bristol Channel and Severn Estuary', *Marine Pollution Bulletin*, 61(1-3), pp. 5-20. doi: 10.1016/j.marpolbul.2009.12.010.

United Nations Environment Programme, U. (2010) *Why Is Eutrophication Such a Serious Pollution Problem?, Lakes and Reservoirs*.

University of Bristol (1981) 'Preliminary model tests of sluice caissons', *Department of Energy*.

US-EPA (2006a) 'Environmental Fluid Dynamics Code (EFDC) Reference List', *Water Resources*, (April). doi: 10.1029/2001WR001121.Ji.

US-EPA (2006b) *Exposure Assessment Models*. Available at: <https://www.epa.gov/exposure-assessment-models/efdc> (Accessed: 19

September 2017).

Versteeg, H. K. and Malalasekera, W. (2007) *An introduction to computational fluid dynamics: the finite volume method*. Pearson Education.

Vollenweider, R. A. and others (1971) *Scientific fundamentals of the eutrophication of lakes and flowing waters, with particular reference to nitrogen and phosphorus as factors in eutrophication*. Organisation for economic co-operation and development Paris.

WalesOnline (2016) *The Swansea Bay tidal lagoon: What is it?* Available at: <http://www.walesonline.co.uk/business/business-news/swansea-bay-tidal-lagoon-what-11999320>.

Walkington, I. and Burrows, R. (2009) 'Modelling tidal stream power potential', *Applied Ocean Research*, 31(4), pp. 239-245. doi: 10.1016/j.apor.2009.10.007.

Wang, S., Yuan, P., Li, D. and Jiao, Y. (2011) 'An overview of ocean renewable energy in China', *Renewable and Sustainable Energy Reviews*, 15(1), pp. 91-111. doi: 10.1016/j.rser.2010.09.040.

Wang, X. (2011) 'Development and Application of an Integrated Hydro-environmental Model for Predicting the Distribution of Nutrients in Estuarine and Coastal Waters'.

Warren, I. R. and Bach, H. (1992) 'MIKE 21: a modelling system for estuaries, coastal waters and seas', *Environmental Software*. Elsevier, 7(4), pp. 229-240.

Waters, S. and Aggidis, G. (2016) 'Tidal range technologies and state of the art in review', *Renewable and Sustainable Energy Reviews*. Elsevier, 59, pp. 514-529. doi: 10.1016/j.rser.2015.12.347.

Whitton, B. A. (1975) *River ecology*. Univ of California Press.

Wolf, J., Walkington, I. a, Holt, J. and Burrows, R. (2009) 'Environmental impacts of tidal power schemes', *Proceedings of the ICE Maritime Engineering*, 162(4), pp. 165-177. doi: 10.1680/maen.2009.162.4.165.

Xia, J., Falconer, R. A. and Lin, B. (2010a) 'Hydrodynamic impact of a tidal barrage in the Severn Estuary, UK', *Renewable Energy*, 35(7), pp. 1455-1468. doi: 10.1016/j.renene.2009.12.009.

Xia, J., Falconer, R. A. and Lin, B. (2010b) 'Impact of different operating modes for a Severn Barrage on the tidal power and flood inundation in the Severn Estuary, UK', *Applied Energy*, 87(7), pp. 2374-2391. doi: 10.1016/j.apenergy.2009.11.024.

Xia, J., Falconer, R. A. and Lin, B. (2010c) 'Impact of different tidal renewable energy projects on the hydrodynamic processes in the Severn Estuary, UK', *Ocean Modelling*, 32(1-2), pp. 86-104. doi: 10.1016/j.ocemod.2009.11.002.

Xia, J., Falconer, R. A. and Lin, B. (2010) 'Numerical model assessment of tidal stream energy resources in the Severn Estuary, UK', *Proceedings of the Institution of Mechanical Engineers, Part A: Journal of Power and Energy*, 224(7), pp. 969-983. doi: 10.1243/09576509JPE938.

Xia, J., Falconer, R. A., Lin, B. and Tan, G. (2012) 'Estimation of annual

energy output from a tidal barrage using two different methods’, *Applied Energy*, 93, pp. 327-336. doi: 10.1016/j.apenergy.2011.12.049.

Zhang, J. Z. and Huang, X. L. (2011) ‘Effect of temperature and salinity on phosphate sorption on marine sediments’, *Environmental Science and Technology*, 45(16), pp. 6831-6837. doi: 10.1021/es200867p.

Zhou, J., Falconer, R. A. and Lin, B. (2014) ‘Refinements to the EFDC model for predicting the hydro-environmental impacts of a barrage across the Severn Estuary’, *Renewable Energy*, 62, pp. 490-505. doi: 10.1016/j.renene.2013.08.012.

Zhou, J., Pan, S. and Falconer, R. A. (2014a) ‘Effects of open boundary location on the far-field hydrodynamics of a Severn Barrage’, *Ocean Modelling*, 73, pp. 19-29. doi: 10.1016/j.ocemod.2013.10.006.

Zhou, J., Pan, S. and Falconer, R. A. (2014b) ‘Optimization modelling of the impacts of a Severn Barrage for a two-way generation scheme using a Continental Shelf model’, *Renewable Energy*, 72, pp. 415-427. doi: 10.1016/j.renene.2014.07.036.

Zienkiewicz, O. C., Taylor, R. L. and Zhu, J. Z. (2013) ‘The Finite Element Method: its Basis and Fundamentals’, *The Finite Element Method: its Basis and Fundamentals*, pp. 493-543. doi: 10.1016/B978-1-85617-633-0.00015-0.

Zienkiewicz, O. C., Taylor, R. L., Zienkiewicz, O. C. and Taylor, R. L. (1977) *The finite element method*. McGraw-hill London.